ION TRANSPORT CHARACTERISTICS OF FUEL CELL MEMBRANES

by

Yaobang Wu

A dissertation submitted to the Graduate Faculty in
Physics in partial fulfillment of the requirements
for the degree of Doctor of Philosophy,
The City University of New York

1998

This manuscript has been read and accepted for the Graduate Faculty in Physics in Satisfaction of the dissertation requirement for the degree of Doctor of Philosophy.

12/5/97
Date

Professor Steve G. Greenbaum, Chair of Examining Committee

12/10/97
Date

Professor Louis Celenza, Executive Officer

Professor John J. Fontanella

Professor Robert A. Marino

Professor Micha Tomkiewicz

Doctor Thomas A. Zawodzinski, Jr.

Supervisory Committee

The City University of New York

Abstract

ION TRANSPORT CHARACTERISTICS
OF FUEL CELL MEMBRANES
by
Yaobang Wu

Advisor: Professor Steve G. Greenbaum
Doctor Thomas A. Zawodzinski, Jr.

Perfluorosulfonic Acid (PFSA) membranes are the most important polymer electrolytes for polymer electrolyte fuel cells (PEFCs) application. In this thesis, experimental studies of the transport properties of the PFSA membranes under various conditions have been carried out. Water uptake into the membranes at 30°C and 80°C was determined. Protonic conductivity of the membranes for immersed and partially hydrated samples at elevated temperatures was measured using an AC impedance method. Activation energies extracted from the conductivity temperature dependence suggested that there are two distinct proton transport mechanisms, depending on H_2O content. A low water content, diffusional motion of H_3O^+ molecules is the dominant proton transport mechanism, while the proton hopping mechanism is more significant at high water content. Electro-osmotic drag coefficients for the partially hydrated membranes at 80°C were measured using a concentration cell. The drag coefficients is similar for several membrane samples over a quite wide range of water content. ^1H, ^2H and ^{19}F NMR relaxation measurements were carried out at various pressures (up to 0.25 GPa) for several membranes with various water contents. The water diffusion coefficients in the

membranes at elevated temperatures was measured by means of NMR pulsed-field gradient spin-echo method. Some transport parameters for the membranes in contact with methanol/water mixtures were determined. One of the main results is that both water and methanol diffusion coefficients in the membranes are practically the same over a wide methanol concentration (1m-16m).

ACKNOWLEDGMENTS

I would like to give grateful thanks to my advisor, Professor Steve G. Greenbaum, for his special advice which was invaluable to this thesis work. He was always available when I needed him, with enthusiasm, patience and encouragement.

I take this opportunity of expressing my deep appreciation to Dr. Thomas A. Zawodzinski, Jr., my co-advisor, for his kind and generous advice when I was performing this research at Los Alamos National Laboratory under his supervision. His guidance and assistance were critical to this thesis work.

I also wish to thank Professor John J. Fontanella, Professor Robert A. Marino, and Professor Micha Tomkievicz for sitting on my supervisory committee.

This work was partially supported by US Department of Energy.

Table of Contents

List of Tables

List of Figures

Chapter 1. Introduction

Zero emission power systems for portable power and electric vehicles are attracting increasing attention.[1-3] Polymer electrolyte fuel cell using perfuorosulfonic acid (PFSA) membranes as the electrolyte is one of the most promising candidates.[1-3] Improved understanding of the ion transport properties are important not only for fundamental studies of the membranes but also for practical aspects of fuel cell application. The transport properties of PFSA membranes have been studied by numerous groups using a variety of methods. However, to date, there is a relatively small amount of data reported at elevated temperatures. Since the polymer electrolyte fuel cells perform at about 80°C, the ion transport properties in the membranes at elevated temperatures have particular importance. The main motivation of this thesis is to study experimentally the ion transport properties in PFSA membranes at elevated temperatures including membrane conductivities, electro osmotic drag coefficient, and water diffusion coefficients.

1-1. Fuel Cell Background

Since William Grove invented the fuel cell in 1839, fuel cells have been developed for over 150 years.[1-3] A primary reason attracting people to make unremitting efforts over such a long time is the direct energy conversion of chemical to electrical energy in a fuel cell. This allows one to avoid the Carnot's theorem limitation, as in conventional "indirect energy conversion" which has three conversion stages, chemical to heat, heat to mechanical, then mechanical to electrical energy. Hence, the efficiency of the fuel cell as a device converting chemical energy to electricity can be much higher than of the indirect energy conversion. In the past a few decades, fuel cell technology, particularly in Polymer

Electrolyte Fuel Cells (PEFCs), has made significant progress. PEFCs have benefited from substantial progress in the polymer electrolytes and in high catalyst utilization. This study focuses on progress in polymer electrolytes.

1-1-1. Polymer Electrolyte Fuel Cells (PEFCs)

Polymer electrolyte Fuel Cells (PEFCs) are a relatively young member of the fuel cell family since their first use was about four decades ago. PEFCs are promising power sources for use in the next generation, non-polluting automobile. The most important class of polymer electrolytes currently used in PEFCs is the perfluorosulfonic acid (PFSA) membranes which are a type of ion-exchange membranes. Some advantages of PEFCs using a PFSA ionomer membrane are: 1) no free corrosive liquid in the cell and minimal material corrosion problems, 2) easily fabricated cell, and 3) demonstrated long life.[1, 3, 4] PFSA ionomer membranes have exhibited high performance in the application of fuel cells since they have high chemical stability and high H^+ transport. This thesis will focus on extending the understanding of the transport properties and related behavior of PFSA ionomer membranes under various conditions. Factors affecting transport will be probed to explore the mechanisms of transport in PFSA ionomer membranes.

A typical polymer electrolyte fuel cell single cell consists of a polymer electrolyte membrane sandwiched between catalyzed gas diffusion electrodes.[5] The cross section of such a single cell is shown schematically in Figure 1.1. The membrane-electrode assembly is the electrochemical heart of system. On the anode, hydrogen gas is catalytically dissociated (*i.e.* oxidized) according to the reaction

$$H_2 \rightarrow 2H^+ + 2e^- \qquad (1.1)$$

The hydrogen ions pass through the polymer electrolyte to the cathode of the cell. There they are combined catalytically with oxygen and electrons from the adjacent cell to form water, according to the reaction

$$4H^+ + O_2 + 4e^- \rightarrow 2H_2O \qquad (1.2)$$

The transport properties of PFSA membranes are of central importance in the application of these materials as fuel cell electrolytes. To optimize their performance, the state of hydration of these materials is a crucial factor that must be controlled. If the electrolyte is too dry, its conductivity falls, resulting in reduced cell performance. An excess of water in the fuel cell can lead to cathode flooding problems, also resulting in less than optimal performance.[6-10]

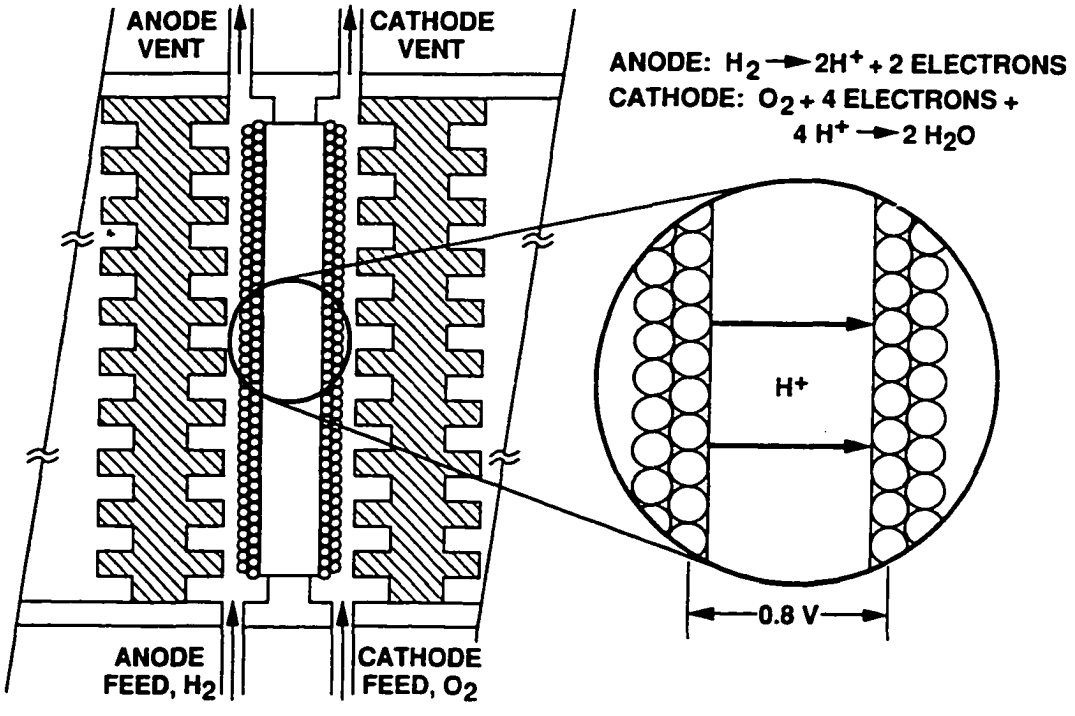

Figure 1.1 Schematic cross section of a polymer electrolyte fuel cell. (reproduced from [5])

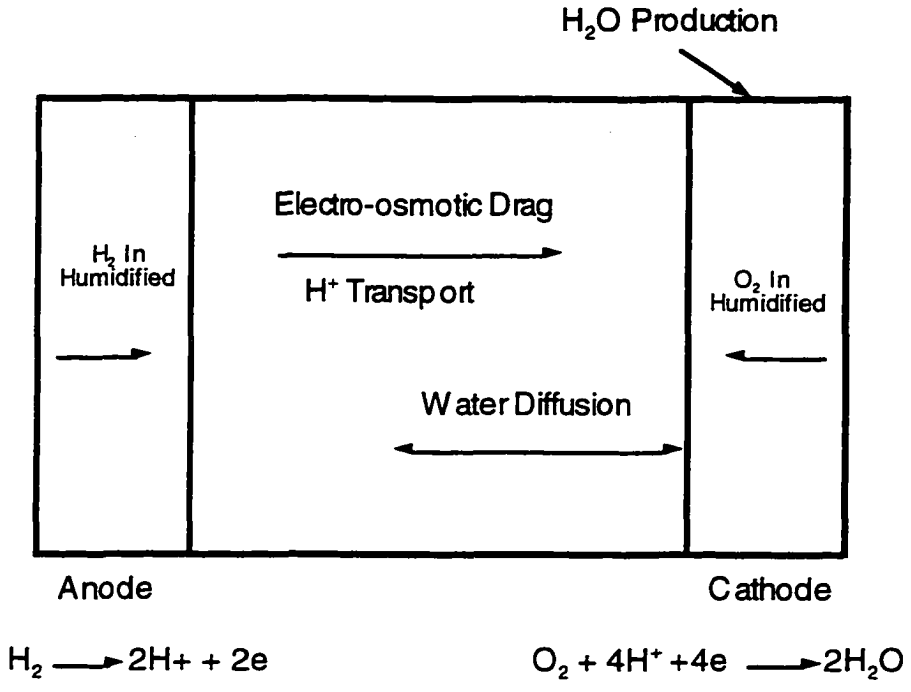

Figure 1.2 Schematic of fuel cell illustrating modes of water transport, uptake into fuel cell. (reproduced from [7])

As shown schematically in Figure 1.2, both the anode (compartment) and cathode are sites for water introduction into the fuel cell. At the anode of the membrane-electrode assembly, where the oxidation reaction occurs, the humidified gas, *i.e.* hydrogen gas, enters the gas diffusion electrode, so that water is carried into the fuel cell. The cathode, at which the reduction reaction occurs, is the other water source. Water in the membranes is transported by two main mechanisms: 1) Electro-osmotic drag of water by protons transported from anode to cathode; 2)

Back-diffusion of water from cathode to anode. These two mechanisms create two offsetting trends of water distribution in the membranes: electro-osmotic drag and the oxidation reaction tend to create an excess of water around the cathode, while back-diffusion tends to flatten the water concentration profile in the membrane.[8]

1-1-2. Direct Methanol Fuel Cells (DMFCs)

Direct methanol fuel cells (DMFCs) have been for the last 30 years, and still are the fuel cell researcher's dream. Methanol is an ideal fuel for the application of fuel cells in electric vehicles since it is the simplest organic liquid fuel. It is relatively cheap and easily transported and converted into energy. DMFCs using liquid methanol in the cell without reforming (breaking down methanol into hydrogen) have been extensively studied since such a mode of operation eliminates the reformer, which is necessary for indirect methanol fuel cells. This significantly reduces the size and mass of a system suitable for automobile use. The potential advantages of the methanol liquid-feed fuel cell over cells designed for gas-feed may be summarized as follows: 1) elimination of fuel vaporizer and its associated heat source and controls; 2) elimination of complex humidification and thermal management systems; 3) dual-purpose use of the liquid methanol/water as fuel and as an efficient stack coolant; 4) significantly lower system size, weight and temperature than existing fuel cell systems.[1]

A DMFC single cell, with a similar structure to PEFCs', is fed with liquid methanol/water mixtures (typically 1M methanol concentration) at the anode, with the reaction:

$$CH_3OH + H_2O \rightarrow CO_2 + 6H^+ + 6e^- \qquad (1.3)$$

On cathode, fed with oxygen gas or air, the reaction is

$$O_2 + 4H^+ + 4e^- \rightarrow 2H_2O \qquad (1.4)$$

The overall cell reaction is

$$2CH_3OH + 3O_2 \rightarrow 2CO_2 + 4H_2O \qquad (1.5)$$

A schematic presentation of transport modes of methanol and water in DMFCs is shown in Figure 1.3. Unfortunately, there are significant difficulties encountered which limit the performance of the DMFC. These problems may be summarized as: 1) methanol cross-over from anode to cathode causing "chemical short circuits" (directly oxidized at cathode) introducing further inefficiency; 2) poor methanol oxidation kinetics at the anode; 3) currently used electrode with high platinum content is easily poisoned both by impurities and more seriously by products of the anodic reaction itself; 4) mixed potentials at both electrodes leading to a significant reduction in efficiency.

This thesis will include some experimental studies in the transport parameters for DMFCs, carried out *ex situ* regarding Nafion® 117 under conditions of liquid feed of methanol. This will aid in extending understanding the behaviors of methanol cross-over through the PFSA membranes under various conditions.

1-2. Perfluorosulfonic Acid (PFSA) Membrane

1-2-1. A Brief Review of PFSA Membranes

Ion-exchange membranes, usually including many ionizable groups (fixed and mobile) in their polymeric structure, are widely used in electrochemical cells. W.T. Grubb may have been the first person using an ion-exchange membrane as an "electrolyte" in electrochemical cells in 1959.[12] Since then, extensive research and development programs have been undertaken.[1-3, 13-15] An ion-exchange membrane with good performance for fuel cells must meet a combination of requirements: high protonic conductivity, extremely low electronic conductivity, low permeation of undissociated fuel, adequate chemical and thermal stability, and

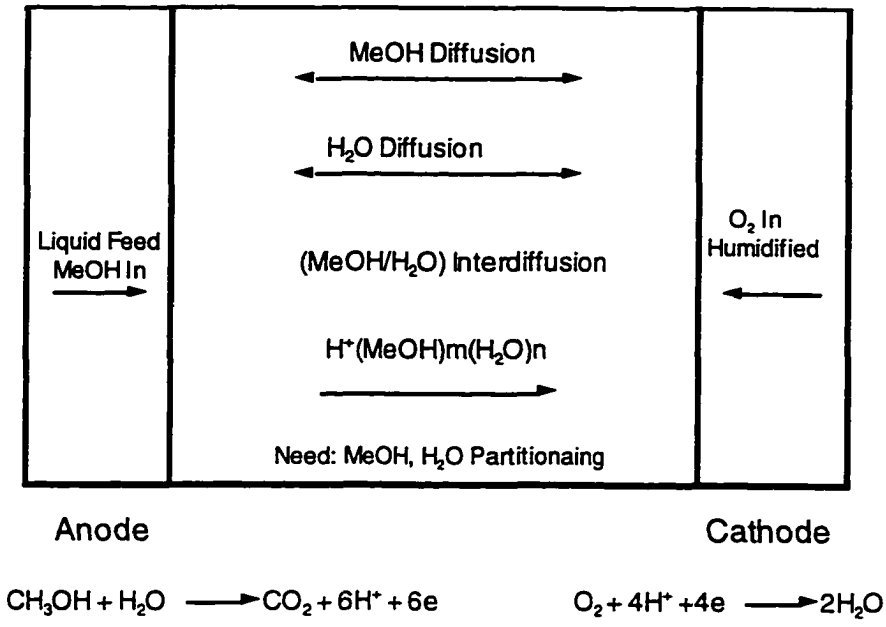

Figure 1.3 Schematic of direct methanol fuel cell illustrating modes of water/methanol transport, uptake into fuel cell. (reproduced from [11])

reasonable mechanical properties including sufficient mechanical strength under operating condition and a defined swelling behavior in the presence of water. In fact, one has to make a compromise because of conflicts among these requirements, *e.g.* low resistance suggests that membrane be thin; low permeability and sufficient mechanical strength requires that it be sufficiently thick. Some PFSA membranes, such as Nafion® which was manufactured by E.I. du Pont de Nemours and Co., and other related PFSA membranes, such as Dow Membrane (Dow) and Membrane C (C) developed by Dow Company and Chlorine Engineering (Japan), respectively, are the most attractive candidates for fuel cells which come close to fulfilling these requirements. Nafion membranes were developed during the middle 1960's, and have been available in various forms for study since the early 1980's.[16-18] PFSA membranes have shown considerable promise with respect to their performance characteristics. However, the present cost of these membranes, up to a few hundred dollars per square meter, becomes one of the major concerns in PEFC application. In addition, the PFSA membranes have been used in a great variety of electrochemical applications.[19]

1-2-2. The Chemical Structure of PFSA Membranes

The sole electrolyte in the most common present-day PEFCs is the hydrated perfluorosulfonate ionomer membranes, currently sold commercially by DuPont under the Nafion® trade name or available as experimental membranes such as Dow and Membrane C manufactured by other companies. In contrast to conventional ion-exchange membranes, there is no cross-linking in these perfluorinated membranes. Structurally, Nafion consists of a backbone of tetrafluoroethylene with pendent side chains of perfluorinated vinyl ethers which terminate in sulfonic acid groups. The general formulas of Nafion, Dow and Membrane C in acid form

are shown in Figure 1.4. For commercial materials, *m* is usually equal to one and *n* varies from about 5 to 11. The amount of ionic groups in these membranes is conventionally expressed in terms of the equivalent weight (EW) of acid polymer per SO_3H group, in a range of about 800 to 1500 grams of dry hydrogen ion form polymer per mole of exchange sites. For example, Nafion 117, EW=1100, has a thickness of about 7 mil (1 in = 1000 mil); Nafion 105, EW=1000, has a thickness of about 5 mil. Other PFSA membranes include the Dow membrane, EW=800 with thickness about 4 mil and Membrane C, EW=900 with thickness 6 mil. Membrane C is structurally identical to Nafion, while the Dow membrane has a shorter side-chain, missing the (F-C-CF_3) group. These membranes are permeable

O-CF_2

to one kind of ion while resisting the direct flow of liquids and transport of ions of opposite charge.[19]

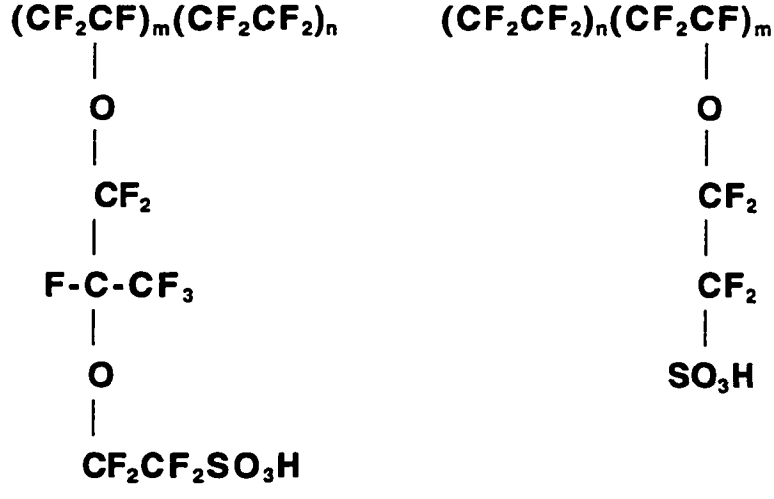

Nafion 117 (EW=1100) Membrane C (EW=900)

Nafion 105 (EW=1000) Dow Membrane (EW=800)

Figure 1.4 The general formulas of Nafion, Dow and Membrane C in acid form.

1-2-3. Structure Models of PFSA Membranes

PFSA membranes are essentially characterized by an extremely high hydrophobicity of the perfluorinated backbone with extremely high hydrophilicity of the sulfonic acid group SO_3H. The existence of ion clustering in perfluorinated sulfonate ionomers was first reported by R.S. Yeo and A. Eisenberg in 1975.[20] Several structural models of Nafion have been proposed which are based on various transport and spectroscopic properties of the polymer.[21-25] Although a detailed picture which is quantitatively consistent with all the experimental observations has not been yet completed, the ionic cluster-network model which was proposed by T.D. Gierke[21] is usually accepted, and such ionic clustering dominates the transport properties in these PFSA membranes.

Ionic clustering in PFSA membranes has been suggested by a variety of techniques including mechanical and dielectric relaxations, nuclear magnetic resonance (NMR) spectroscopy, infrared (IR) spectroscopy, electron microscopy, X-Ray experiments and transport experiments. The most direct evidence may come from the small angle X-Ray experiments by T.D. Gierke *et al.*.[21] Since Gierke proposed a cluster network model in 1977,[26] the concept of ion clustering has been adopted in this model. The clusters are assumed to be approximately spherical and the cluster size has been calculated from solvent absorption data, *e.g.* for sodium form Nafion 1200 and a water content of 9%, the cluster diameter is about 3 nm. These clusters are interconnected by short, narrow channels in the fluorocarbon backbone network. The diameter of these channels is about 1 nm estimated from hydraulic permeability data.[21] Gierke considered that Bragg spacing could represent the distance between clusters which is about 5 nm from SAXS data. W.Y. Hsu and T.D. Gierke[23] proposed a semi-phenomenological elastic theory for ionic clustering. They derived an expression which describes the experimental variation in cluster diameter with cation form, equivalent weight, and

water content, and that short channels connecting adjacent clusters are thermodynamically stable. However M. Falk[27] suggested, based on infrared data, that the hydrated ion clusters are much smaller than the estimation by T.D. Gierke, and highly nonspherical in shape. K.A. Mauritz and A.J. Hopfinger[22] presented a general formalism to describe the structural organization of Nafion membranes under different physicochemical conditions. This model semiquantitatively reproduces water absorption, polymer density, and the number of water molecules per exchange site in these polymers. Based on a series of investigations, M. Pineri *et al.* derived a three-phase model in which fluorocarbon crystallites, ionic hydrophilic clusters, and an amorphous hydrophobic region of lower ionic content coexist.[25] H.L. Yeager and A. Steck[28] proposed a structural model which correlates various spectroscopic and ionic diffusional results. A schematic diagram of the model in Figure 1.5 for the Na-form of Nafion indicates three regions: region A consists of fluorocarbon backbone material, some of which is in a microcrystalline form, as detected by Pineri *et al.*[29] The interfacial region B contains the pendant side chains, a smaller amount of water, some sulfonate exchange sites which have not been incorporated into clusters, and a corresponding fraction of counterions. Ion clusters form region C, in which the majority of sulfonate exchange sites, counterions, and sorbed water exist.

However, the cluster network model described above is still controversial now rather than a comprehensive and universally accepted theory regarding Nafion structure model. Motton Litt proposed another Nafion structure model which crystallizes in a lamellar morphology.[30] This model attempts to avoid the conflict, with the concepts of polymer physics, encountered by the Yeager and Steck model. The major difficulties of the latter is that due to the crystalline matrix the membrane is not supposed to be completely reversible in dimensional changes with each swelling and deswelling. Since the Litt model provides a simpler

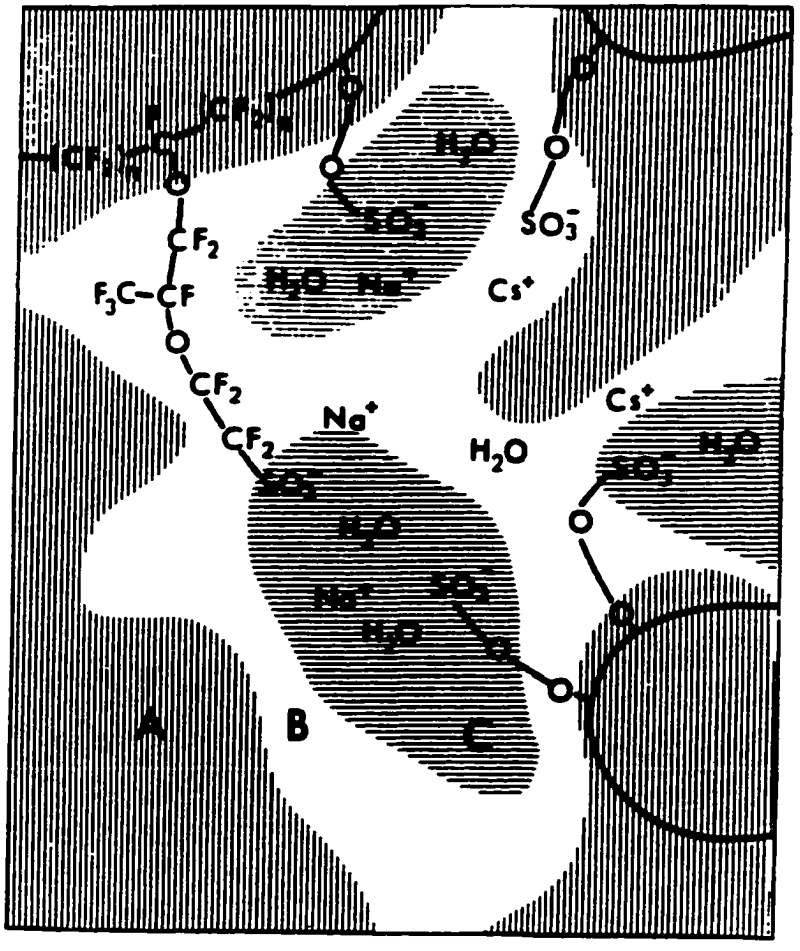

Figure 1.5 Three region structural model for Nafion (Na-form): A, fluorocarbon; B, interfacial zone; C, ionic clusters. (reprocuced from [28])

rationalization of the data available than does the Yeager and Steck model, it might be paid attention to in the future.

1-2-4. Water in PFSA Membranes

The general picture regarding water in PFSA membranes is that a part of water is associated with the sulfonic acid groups, part forms water clusters, while still another part, probably, might interact weakly with the polymer backbone.[27, 31] The analysis of the state of water in PFSA membranes by means of various techniques is the most common way to study the interactions of water with ions and polymers as well as the structure of polymers, such as thermodynamic studies of the interaction between water and perfluorosulfonated polymer,[31] water mobility by neutron quasielastic scattering (NQES).[32]

Pineri *et al.* studied the thermodynamic properties of the interaction between water and perfluorosulfonated polymer.[31] Two well defined hydration regimes were observed. The first regime corresponds to the solvation of ions as λ<4-6, where λ is defined as the H_2O/SO_3^- ratio, and the obseved decrease in the absolute value of the interaction molar energy for further water sorption may involve a deformation of the hydrophobic matrix. These authors observed a similar behavior by using NMR[33] and Mossbauer[34] techniques. The studies of water mobility in a water soaked Nafion membrane by neutron quasielastic scattering (NQES)[32] indicate that on a scale of *ca.* 10 angstrom, the water molecules move practically as freely as in bulk water, but their long-range motion is much more hindered.

M. Fujimura *et al.*[35] found that water present in small quantities tends to be preferentially absorbed into the ionic phase and the ion clusters in Nafion do not fall apart with water saturation. M. Falk[27] observed evidence for two environments of sorbed water in Nafion from infrared spectroscopic studies. The

first environment seems to be aqueous in nature. It is much less strongly hydrogen bonded than water in aqueous salt solutions. In the second environment, the water molecules are not hydrogen bonded and appear to be exposed mainly to fluorocarbon. He also concluded that about three quarters of the water is in the ion cluster from infrared data.

N. Sinvashinsky and G.B. Tanny[36] indicated that the water in the first environment behaves as a liquid which is significantly different in its physical properties from those of bulk water.

Yeo and Eisenberg[37] observed in their dielectric relaxation study of Nafion two dielectric peaks of different energy absorption level. Both of these peaks are highly sensitive to the presence of water in membranes.

T. A. Zawodzinski *et al.*[6-10] have reported a series of investigations on the properties of the PFSA membranes exposed to water vapor phase and liquid water under various conditions. The properties of the PFSA membranes exposed to water can be summarized as follows:

1. The equivalent weight of the PFSA membranes influences water uptake into the PFSAs. The membranes with lower equivalent weights take up more water on a weight percentage basis than with higher equivalent weights.

2. For the membranes exposed to water vapor phase. *a*) there are two regions in the membrane isopiestic absorption for water vapor phase under various water activities. The sorption curves exhibit a relatively small change in water content over the range of water activity 0.15-0.75 (Region *i*), and a much more rapid change at water activity above 0.75 (Region *ii*). Region *i* corresponds to uptake of water of solvation of the proton and sulfonate ions. Region *ii* corresponds to water involved in polymer swelling. *b*) the amount of water absorbed into Nafion 117 is a function of temperature. In Region *i*), there is a

relatively small change of water sorption over the range of temperatures 30°C-80°C, and higher water content at 30°C than at 80°C.

3. Membrane water uptake is sensitive to different phase of water. The water content of the membranes in equilibrium with saturated water vapor (a_w=1)is not the same as the water content of a similarly prepared membrane in contact with liquid water.

4. Water absorption is depended on the history of membrane treatment. It was observed that water absorption into Nafion 117 from liquid water is independent of temperature over the range of temperature 27°C-94°C if no thermal treatment, *e.g.* λ =21 without temperature influence. However, If the membrane was dried at 105°C before rehydration, water content increases with increasing temperature.

1-2-5. A Brief Literature Review of Studies of Transport Properties of PFSA Membranes

There is no question that water content in the membrane is crucial to the performance of the fuel cells since optimizing performance of PFSA membranes requires maintaining appropriate water content in the membranes for maximum conductivity of the membranes. The water uptake behaviors of PFSA membranes have been studied extensively. The most measurements were carried out by simply weighting the samples,[6-10, 27, 33, 35, 37, 38, 39, 40, 41, 42, 43, 44] as well as ^{1}H NMR technique.[45, 46]

The common problem in water uptake measurements is that many different reference states of dry membrane have been chosen by many different workers as mentioned in Chapter 3 of this thesis. Some workers reported the water uptake data for several Nafion membranes immersed in liquid water: LaConti *et al.*[47] Nafion

120 λ=18.7; Pineri *et al.*[33] Nafion 120 λ=13.3; Eisman,[48] Yeo[49] reported similar results for Nafion 117 at 100°C, λ=19. Eisman determined water uptake of Dow membrane with 850EW and 950 EW at 100°C. Hinatsu *et al.* measured water uptake of Nafion membranes (1200EW and 1100EW) in acid form at 25°C, and reported respectively 1200EW λ=15 and 1100EW λ=22.6.

Since water uptake from the vapor phase is the normal mode of water supply to PEFCs, and PEFCs usually work at 80°C or more, water uptake data for PFSA membranes exposed to vapor phase water at high temperature is important. Pushpa *et al.*[40] investigated isopiestic sorption for Nafion 117 in contact with water vapor at room temperature as a function of water activity. However, the maximum water uptake, λ value corresponding to a_w=1, was determined by immersing the membrane in liquid water rather than exposing the sample to water vapor at 100% *RH*. The membrane samples were dried at 120°C for 24 hours. The maximum water content (membrane immersed in liquid water) λ is 13.9, which is much lower than 20-22 reported by Zawodzinski *et al.*,[6-10] 22.6 reported by Hinatsu *et al.*,[50] and 21 by Broka *et al.*[51] This variation may not be caused by their different drying method. Sen *et al.*[52] determined water sorption for several Dow Membrane and Nafion 115 exposed to water vapor phase at elevated temperatures. They observed that Dow water uptake is significantly higher than for Nafion. Under 95% *RH*, for both Dow and Nafion, water uptake decreases with increasing temperature over the temperature from 30°C to 100°C by a factor of 2. Hinatsu *et al.* [50] determined water uptake of Nafion membranes from water vapor at 80°C. The water uptake corresponding to a_w=1 for Nafion 117 in λ=10. Zawodzinski *et al.*[6-10] made a series of determinations of water uptake of several

PFSA membranes from liquid water and water vapor as a function of water activity and temperature. The data they reported are displayed in Table 1.1 and Table 1.2.

Table 1.1 Water uptake (H_2O/SO_3H) from liquid water.

Membrane	No thermal treatment rehydration temperature T: 27°C - 94°C	Dried at 105°C rehydration temperature		
		27°C	65°C	80°C
Nafion 117	21	12	14	16
Membrane C	21	11	15	15
Dow Membrane	25	16	23	25

Table 1.2 Liquid *vs.* vapor phase water sorption (for a membrane pretreated by immersion in boiling water).

Membrane	Uptake from:	
	Liquid (H_2O/SO_3H)	Vapor (H_2O/SO_3H)
Nafion 117	21 to 22	14
Membrane C	21 to 22	14
Dow Membrane	24 to 26	14

The protonic conductivity of PFSA membranes directly affects the PEFC's performance. Particularly, the resistivity dominates the ohmic loss in PEFCs. Generally, the conductivity of PFSA membranes is a function of water content and temperature. The conductivity data obtained also could be strongly affected by

pretreatment methods, history of thermal treatment, conductivity cells design, the measurement methods used,[7, 53, 54] and the different thickness adopted by different workers even for the same membrane. Hence, the conductivity data reported by different groups using their own methods exhibit relative weak consistency. Finally, polymer samples have an intrinsically high property variability. Over the last about ten years, many groups have studied the conductivity of PFSA membranes under a variety of conditions.

Rieke and Vanderborgh[55] studied the temperature dependence of the conductivity of Nafion 117 exposed to vapor phase water (100% *RH*) over the range 25°C-100°C using variable frequency AC impedance methods. They used a conductivity cell with two platinum mesh electrodes and the conductivity was determined along the plane of the membrane. At 30°C and 65kHz, σ = 0.06 S/cm (membrane thickness 7.0 mils). In their measurements, the membrane conductivity reached a maximum value at about 70°C, and then exihibited a steep drop with increasing temperature up to 100°C.

Eisman[48] studied several Dow Membranes with different equivalent weight as a function of hydration degree at 30°C. It was observed that there is the expected normal behavior of increasing conductivity with decreasing equivalent weight. Cai *et al.*[56] measured the conductivity of Nafion 1150 EW in equilibrium with NaCl solutions. At 25°C, σ = 0.014 S/cm (membrane thickness 7.87 mils). Gravach *et al.* [57] investigated the conductivity of Nafion 117 membranes, by means of the AC impedance technique using a mercury cell. They determined the variation of the membrane resistance (no conductivity number converted from resistance), over a range of frequency 1Hz-1MHz, as a function of the water content and ionic composition, independently. Verbrugge *et al.* [58] measured the conductivity of Nafion 117 equilibrated with H_2SO_4 for several acid concentrations.

Over the range of the temperature between 20°C-80°C, they used Mercury/mercurous sulfate reference elecrodes in a DC method by means of recording the change in the cell resistivity with and without membrane sample. The conductivity, at 25°C, 1M acid concentration, was about 0.09 S/cm (wet membrane thickness 9.1 mils).

Kreuer *et al.* [59, 60] reported the data of the conductivity measurements for Nafion 117 by means of complex impedance spectroscopy using gold foils as electrodes. At room temperature, the conductivity of Nafion 117 for fully hydrated state (immersed in water), σ = 0.07 S/cm. They found that proton conductivity of Nafion 117 is correlated with water diffusion for low degrees of hydration. With increasing hydration there is an increasing contribution from the Grotthus hopping mechanism (or chanin mechanism, which explains the proton conduction. The proton conducts by a mechanism that does not involve its actual motion through the solution. There is an effective motion of a proton that involves the rearrangement of bonds in a group of water molecules. The conductivity is govened by the rates at which the water molecules can rotate into orientations in which they can accept or donate protons and the rate at whcih the protons tunnel form one end of a hydrogen bond to another, from $O-H\cdots O$ to $O\cdots H-O$.) culminating in an factor of $A=D_\sigma/D_{H2O}$=2.5 for the fully hydrated membraneat room temperature. (see 4-4-2 for more detailed discussions)

J.J. Fontanella *et al.* made a series of investigations on the conductivity of Nafion 117 using complex impedance techniques.[53, 61-65] This work could be summarized as follow: 1) the "standard" two terminal configuration, with gold electrodes in 6 mm diameter, in transverse geometry (across the thickness of the membrane), showed that the bulk conductivity is not measurable until the frequency is in excess of 10^7Hz. For the measurements carried out in longitudinal geometry

(along the membrane surface), at 5kHz, σ = 0.06 S/cm, and at 1MHz, σ = 0.073 S/cm (exposed to 100% *RH* water vapor, membrane thickness 7.08 mils).[53] 2) for Nafion 117 exposed to 50% and 25% *RH*, at room temperature, σ = 0.0080 and 0.0019 S/cm, respectively.[63] 3) In high pressure conductivity measurements,[61, 63-65] several PFSA membranes exhibit activation volume that increase with decreasing membrane water content, and the conductivity decreases as pressure increases (positive activation volume).

In series of papers Zawodzinski *et al.* have reported the conductivity measurement data for various PFSA membranes under different conditions.[6-9] The primary data are shown in Table 1.3.

Table 1.3 The proton conductivity data, reported by T.A. Zawodzinski *et al.*, for various PFSA membranes and conditions. Conductivity unit: S/cm

Temperature	30°C	30°C	80°C
Hydration Status	Immersed	100% *RH* vapor	Immersed
Nafion 117	0.10 (λ=22)	0.06 (λ=14)	0.18
Membrane C	0.12 (λ=22)	0.09 (λ=14)	0.19
Dow Membrane	0.15 (λ=25)	0.12 (λ=14.5)	0.25

It should be noted that, to date, most of the conductivity measurements of PFSA membranes were carried out in a two electrode configuration. However, a

four electrode configuration as reported by Cahan *et al.*,[54] demonstrates significant advantages in determining the proton conductivity of PFSA membranes. In this configuration, two electrodes supply current to the cell, while two additional leads measure the potential directly. Since the current electrodes and voltage electrodes are used separately, the interfacial effect of the electrodes and lead impedance are almost completely eliminated. In addition, DC measurements also yield the same results as AC method by using the four electrodes method.

Electro-osmotic drag—the tendency of a protonic current to concomitantly transport water from anode to cathode is one of main contributions to the water distribution throughout the fuel cell.[10] The movement of water molecules caused by the movement of hydrogen ions reflects the coupling between water molecules and hydrogen ions. The electro-osmotic drag coefficient ξ, *i.e.* the number of waters transported per proton, is thus an important parameter to probe in understanding proton and water transport properties of PFSA membranes. It is of importance both in treating the issue of water balance in a fuel cell and in understanding transport mechanism in polymer membranes. Some groups have carried out the measurements of electro-osmotic drag coefficient for different types of membranes under various conditions using different methods.

Breslau and Miller measured ξ for immersed polystyrenesulfonic acid and the sulfonic acid form of polyethylene-styrene graft copolymer.[66] A drag coefficient of 2.6 H_2O/H^+ was reported. LaConti *et al.* determined ξ for several Nafion membranes with different equivalent weight.[47] They described a linear dependence of ξ on equivalent weight. ξ at $\lambda \approx 20$ (immersed membranes) are 2.5, 2.9, and 3.2 for Nafion 1150EW, 1200EW and 1275EW, respectively. Also it is found that ξ is independent of temperature. However, there was no detailed data

reported regarding water uptake into these membrane. As an example, water uptake of Nafion 1200EW in contact with liquid water (about $\lambda \approx 15$[50]) is significantly low than Nafion 1100EW (about $\lambda \approx 20$-22, see section 4-1). In the LaConti *et al.* work, only $\lambda \approx 20$ for all three membranes was given. Okada *et al.* reported ξ=2.3 H_2O/H^+ for the membrane consisting of crosslinked sulfonated copolymers of vinyl compounds,[67] and ξ=2.6 H_2O/H^+ for Nafion 117 in acid form at λ=22.[68] Fujita obtained ξ=2.3 H_2O/H^+ for fully hydrated Nafion 117.[69]

Fuller and Newman reported their drag measurements for partially hydrated Nafion 117 by using a concentration cell method.[70] For Nafion 117 exposed to saturated vapor at 25°C, they found ξ=1.4 H_2O/H^+, over a range of water activity a_w=0.2-1.0, with a significant decrease starting at λ about 5, by using an exponential function fit to their data. In another word, the data were fitted with an analytic expression rather than the differentiation equation 2.7 directly. Fuller and Newman introduced some assumptions in their data treatment: The potential approach a constant as the activity of water approaches zero; As the concentration of water tends to zero, the transport number must also approach zero, *i.e.* the drag must drop to zero as $\lambda \rightarrow 0$.

Zawodzinski *et al.* made considerable efforts in determining drag for various PFSA membranes.[7, 8, 10] These workers reported drag for several different membranes in contact with liquid water at 30°C with a modified electro-osmosis method[71] and partially hydrated (exposed to vapor water) by using the method developed by Fuller and Newman.[70] It should be noted that in the liquid case the measurement is carried out under conditions of a flat water concentration profile the with membrane exposed to liquid water on both side. This is contrasted

with the experiment in which water concentration gradients could exist in the membrane (*i.g.* an operating fuel cell), and thus back-diffusion could occur. Table 1.4 shows the data reported by Zawodzinski *et al.* In the partially hydrated case, they plotted the results as the cell potential values *vs.* $log_{10}(a_{w,r}/a_{w,l})$, and take the local slope of the curves as the drag coefficient $\xi=\xi[log_{10}(a_{w,r}/a_{w,l})]$. The method to treat data by Zawodzinski *et al.* is different from Fuller and Newman's exponential fit.

Table 1.4 Electro-osmotic drag ($\xi=H_2O/H^+$) data at 30°C for immersed and partially hydrated membrane samples reported by Zawodzinski *et al.*

Membrane	Immersed	Water vapor
Nafion 117	2.5-2.9 (λ=22)	1.03 (λ=2-14)
Membrane C	2.6-4.0 (λ=22)	1.1 (λ=2-14)
Dow Membrane	1.4-2.0 (λ=25)	0.95 (λ=4-14.5)

Molecular motions are associated with volume fluctuations that can be probed directly by employing prssure (rather than temperature) as the thermodynamic variable. Understanding of the proton transport mechanism in PFSA membranes can be greatly facilitated by investigating these volume fluctuations. A collection of studies in high pressure NMR has been included in High Pressure NMR edited by J. Jonas *et al.*.[72] Other high pressure NMR studies include hydrostatic pressure dependence of molecular motions in polycarbonates,[73] and high pressure NMR of molecular motions and glass transition in natural rubber.[74] However, there are limited reports regarding

PFSA membrane study in high pressure NMR. J.J. Fontanella and S.G. Greenbaum *et al.* reported a series of high pressure electrical relaxation,[62, 75] conductivity and NMR investigation for Nafion 117.[61, 62] The workers determined the effect of pressure on the electrical conductivity and deuteron, proton and ^{17}O NMR in acid form Nafion 117 conditioned at various D_2O and water contents. The high pressure NMR measurements were carried out for pressure up to 0.25 GPa. Several conclusions have been obtained: the spin-lattice relaxation T_1 decrease as pressure increase; the trend of increasing activation volume with decreasing water content is maintained in all of the measurements; deuteron and proton NMR show that the activation volume for materials containing significant amounts of water is about 2-3 cm^3/mol. However, ^{17}O NMR results seems difficult to explain.

The author in this work studied the pressure dependence of the proton, deuteron and ^{19}F NMR spin-lattice relaxation time(T_1) in three different molecular weights of acid-form PFSA membranes under various hydration states.

Deuteron NMR is a powerful technique for strudying molecular structure and dynamics of polymers.[76-78] The primary advantage of using Deuteron NMR techniques in studying PFSA membranes is that deuterons represent well-defined nuclear spin labels, because the NMR parameters of ^2H with spin $I=1$ are almost exclusively governed by the quadrupole interaction.[79] Deuterons yield almost unique information about molecular motions in polymers. In particular, rotational motions can be clearly interpreted owing to the nuclear quadrupole moment of the deuteron which dominates the relaxation process. Previous ^2H NMR studies in PFSA membranes have been reported[7, 36, 75] as well as high pressure ^2H NMR.[61, 63, 75]

Water diffusion coefficients in PFSA membranes as well as in liquid water has been extensively studied by means of various techniques, such as rediotracer,

[28, 58, 80, 81] optical spectroscopy,[82] neutron quasielastic scattering, [32] water sorption,[37] NMR,[7-10, 59, 60, 83, 84] and NMR imaging[6] *etc.*.

Verbrugge *et al.* [58, 81, 85, 86] measured proton diffusion coefficient in Nafion 117, 3.5×10^{-6} cm^2/s, using a radio tracer method. Kreuer *et al.*[59, 60] studied diffusion in Nafion 117 by means of an NMR technique. Yeo *et al.*[37] estimated the diffusion coefficient of water in Nafion membranes in various equivalent weight over the temperature range 0-99°C by means of studying the water sorption. Diffusion coefficients from these measurements increased with increasing temperature. The measurements yielded diffusion coefficient of about 10^{-6} cm^2/s with activation energy 4.8 kcal/mol. Yeager *et al.* [28, 87, 88] determined water diffusion coefficient in Nafion 120 using radio-tracer method over the range of temperature 0-40°C. At 25°C, for fully hydrated Nafion 120, diffusion coefficient is 2.65×10^{-6} cm^2/s. Pineri [82] measured the water diffusion coefficient in Nafion membrane by using far infrared spectroscopy. The measurements were carried out under various water vapor pressures. Pineri *et al.* [32] studied water mobility in Nafion 120 using neutron quasielastic scattering techniques. The diffusion coefficient of Nafion 120 is reported in 1.6×10^{-6} cm^2/s with $\lambda=10$ at 25°C.

Zawodzinski *et al.* [6-9] reported water diffusion coefficient for PFSA membranes at room temperature with different equivalent weight under various hydration states using the NMR pulsed gradient technique. The diffusion coefficient is on the order of 10^{-6} cm^2/s for several membranes at this temperature. A significant dependence on water content for the diffusion coefficient was observed.

Chapter 2. Research Methods in This Thesis

2-1. Protonic Conductivity

The membrane protonic conductivity σ in units of S cm^{-1} is expressed in the Equation 2.1.

$$\sigma = G\frac{l}{A} \tag{2.1}$$

G is the reciprocal of the resistance $R(\Omega)$, and is nowadays measured in Siemens, symbol S. A common method of conductivity measurement is the variable frequency method. The current passing through the test cell and voltage across it are both measured as a function of frequency. Typically, the electrolyte is capacitively coupled to the electrodes. The test cell contains capacitive and perhaps also inductive components as well as resistance, R. The total complex impedance is given by

$$Z = R - \frac{j}{\omega C} + j\omega L \tag{2.2}$$

where C is the capacitance and L is the inductance, ω is the angular frequency and j is the imaginary unit. A convenient way to present the data is by means of complex plane representation. The real contributions arise from the resistances and imaginary terms from the capacitance and inductance. The electrolyte resistance can be obtained from the high-frequency intersection with the real-axis. The electrolyte conductivity is then obtained from the measured electrolyte resistance by means of the measured cell constant.

Generally, an electrochemical experiment aims to analyze a transport and reaction mechanism by chemical identification and kinetic characterization of reaction intermediates by measuring a well-defined quantities. The experiment is supposed to disentangle the information between electrochemical process to be

studied and the other effects (*e.g.* interfacial reaction) involved in the experiment. These effects could cause an system error or simply disable the measurement. In the measurement of membrane electrical conductivity (in the radio frequency range, it is impossible to measure the conductivity of an isolated electrolyte. Instead, a test cell has to be used, in which the electrolyte is sandwiched and contacted by a pair of electrodes or by electrodes plus an additional electrolyte. The property thus measured pertains to the whole assembly, *i.e.* to the electrolyte plus the attendant instrument leads, electrodes and interfaces. The measured complex impedance Z_{Total} includes several contributions from membrane charge transfer, mass transport, effect of interface between electrodes and membrane, and effect of leads. Usually, an equivalent circuit is applied for this complex impedance system as shown in Figure 2.1,

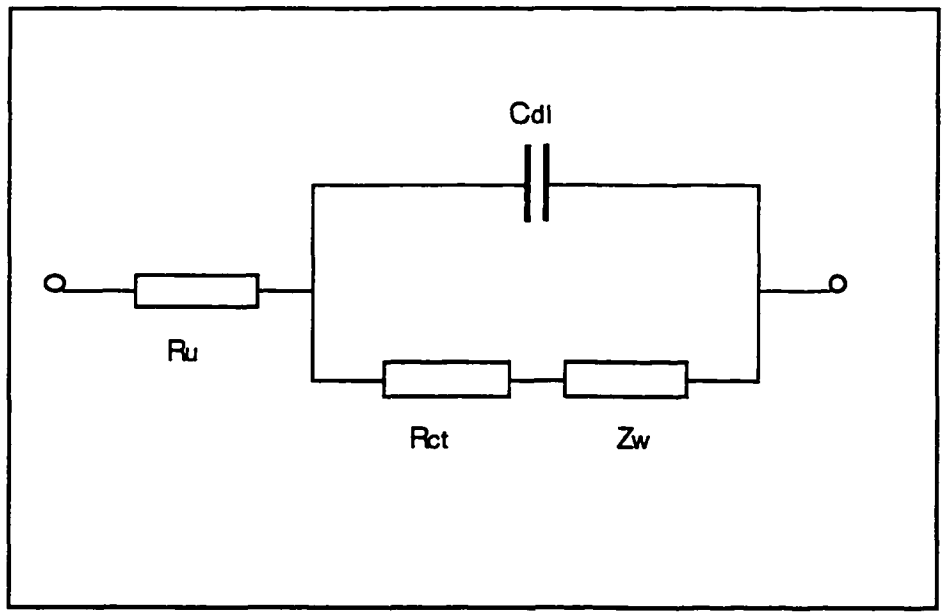

Figure 2.1 Equivalent circuit of an electrochemical cell

where R_u, uncompensated membrane resistance, is connected in series to a parallel circuit , which takes into account all the effects considered, including a charge transfer resistance (R_{ct}), a mass transport component (Warburg impedance, Z_w) and a double layer capacitance (C_{dl}). Here the lead effects could be minimized if the lead connections between all the parts are designed appropriately. The mass transport components particularly dominate at low frequency, while the charge transfer resistance dominates at high frequency. Therefore the main problem in the measurement could be the interfacial effect (C_{dl} or R_{ct}) if the measurement is carried out at a too low frequency, or if geometry is such that R_u is small. Thus measurements should be made at high frequency. It will not only reduce C_{dl} effect, but also the Warburg impedance. Hence, properly designing electrical conductivity cell for reducing the interface effect to a minimum is extremely important.

The electrical conductivity measurements were carried out with a 2-point AC impedance technique. In order to minimize interfacial effect, the measurement was arranged along the membrane film rather than across the thickness of it. It should be understood that the measurement in such a cell design is the bulk conductance of the membranes rather than a surface conductance. J. J. Fontanella *et al.* reported when "standard" two terminal measurements are made across the thickness of the membrane film, it is necessary to use frequencies in excess of 10^7 Hz in order to observe the bulk conductivity of the sample.[53]

Equation 2.1 could be rewritten in

$$\sigma = \frac{1}{R_e}\frac{l}{tw} = \frac{C}{R_e t} \qquad (2.3)$$

where C, t and R_e are the cell constant , membrane thickness and resistance of the membrane, respectively. R_e is determined with the AC impedance method, and t and C are measured with a micrometer.

In this thesis work, conductivity of several different membranes were measured at elevated temperatures under various conditions, exposed to water vapor phase (100% relative humidity), immersed in water, and water/methanol mixtures.

2-2. Electro-Osmotic Drag Coefficient

The electro-osmotic drag coefficient ξ

$$\xi = \frac{N_0}{N_+} \tag{2.4}$$

is defined as the number of water molecules transported per proton.

An ingenious method to obtain electro-osmotic drag coefficient which allows equilibration of membrane with water vapor phases was developed by Fuller and Newman.[70] This method measures the potential difference between two reversible H^+/H_2 electrodes on each side of the membrane. This potential difference is due to the generation of water activity gradient between two sides of the membrane. The primary advantage is to enable one to measure the drag coefficient over the full range of membrane water content.

Transport properties can be obtrained from electrochemical cells with a single electrolyte of varying concentration.[89] The electro-osmotic drag coefficient ξ in an proton conducting membrane can be obtained by using the concentration cell below:

$$\underset{a}{Pt,H_2(g)\,|Membrane,H_2O(g),a_{w,l}\,|Junction\ region\,|Membrane,H_2O(g),a_{w,r}\,|Pt,\ H_2(g)}\ \underset{b}{}$$

We can derive the relation between the cell potential and electro-osmotic drag coefficient from analyzing the junction region. A gradient in chemical potential

of water exists in the junction region, and diffusion occurs. Since charge (H^+ in our case) transported across the junction does not contribute to the change of the electrochemical free energy in the cell[90], the only change in the electrochemical free energy is caused by dragging water molecules with the protonic current. The electrochemical free energy difference between a and b is given by[70]

$$\Delta\mu = F\Delta\Phi = \int_b^a \xi \frac{d\mu_{H_2O}}{dx} dx \qquad (2.5)$$

where F is faraday constant, ξ is electro-osmotic drag coefficient, and differentiation gives

$$\xi = F\frac{d(\Delta\Phi)}{d\mu_{H_2O}^{\ a}} \qquad (2.6)$$

This means that we can hold the water activity constant on the right side (*b*) and vary the activity of water on the left side (a). Equation 2.6 then gives the value of ξ at this water activity (water activity a is defined as $a = \frac{p}{p^*}$, where p and p* are solution vapor pressure and pure water vapor pressure, respectively).

At equilibrium, the chemical potential of water is the same in the vapor phase and in the membrane. Equation 2.6 becomes

$$\xi(a_{w,r}) = \frac{F}{RT}\left[\frac{d(\Delta\Phi)}{d\ln(a_{w,r}/a_{w,l})}\right] \qquad (2.7)$$

If we keep $a_{w,l}$ constant and measure $\Delta\Phi$, this differential equation will determine the relation between ξ and $a_{w,r}$. The local slope of a plot of normalized potential (in the form $F\Delta\Phi/RT$) *vs.* the logarithm of the ratio of water activity is the electro-osmotic coefficient $\xi = \xi(a_{w,r})$. Since we know $\lambda(a_{w,r})$, we then know $\xi(\lambda)$.

2-3. NMR Measurements

2-3-1. Fundamental Principles of NMR

1. The NMR Phenomenon

In 1946 two research groups, that of Bloch *et al.* and that of Purcell *et al.*, independently observed nuclear magnetic resonance (NMR) signals for the first time.[91, 92] Since then NMR spectroscopy has developed into an indispensable, powerful tool for scientists.

According to a basic principle of quantum mechanics, a magnetic moment of a nucleus is associated with its spin angular momentum. The associated magnetic moment μ of a nucleus with spin $\boldsymbol{I}$, is given by

$$\mu = \gamma\hbar\boldsymbol{I} \tag{2.8}$$

where γ is called gyromagnetic ratio, and $\hbar$ is Planck's constant h divided by 2π. The Hamiltonian, H, of the magnetic moment μ in an applied magnetic field is

$$H = \mu \cdot \boldsymbol{H}_o \tag{2.9}$$

Taking the field to be $\boldsymbol{H}_o$ along the z-direction, the Hamiltonian can be written as

$$H = -\gamma\hbar|\boldsymbol{H}_0|I_z \tag{2.10}$$

and the allowed energies are

$$E = -\gamma\hbar|\boldsymbol{H}_0|m \qquad m = I, I-1, \ldots, -I \tag{2.11}$$

The energy levels are equally spaced with the gap between adjacent ones of:

$$\Delta E = \gamma\hbar|\boldsymbol{H}_0| \tag{2.12}$$

A transition between two levels could be induced by applying a radio-frequency (*rf*) magnetic field $\boldsymbol{H}_x$ which is perpendicular to the static applied field $\boldsymbol{H}_o$

$$\boldsymbol{H}_x = \boldsymbol{e}_x 2H_x \cos\omega t \qquad |\boldsymbol{H}_x| << |\boldsymbol{H}_o| \tag{2.13}$$

and related perturbing Hamiltonian is

$$H_{pert} = -\mu \cdot \boldsymbol{H}_x \tag{2.14}$$

Applying time-dependent perturbation theory, the transition rate is

$$P_{mm'} = \gamma^2 |H_x|^2 |< m|I_x|m' >|^2 \delta(\nu_{mm'} - \nu) \qquad (2.15)$$

where

$$\nu_{mm'} = \frac{\Delta E_{mm'}}{h} = \frac{\gamma |H_0| |m' - m|}{2\pi} \qquad (2.16)$$

Therefore, we reach the following conclusions:

1) The transition rate is proportional to γ^2 and $|H_x|^2$.

2) H_x must be perpendicular to H_o. Otherwise, no transition occurs due to the condition $< m|I_z|m' >= \gamma\hbar\delta_{mm'}$.

3) From the transition matrix $< m|I_x|m' >$, only transitions occur when $|m' - m| = 1$, and then $2\pi\nu_{mm'} = \gamma H_o$, which is the condition the applied *rf* should satisfy in order to induce transitions. Rewritten as the well-known resonance condition:

$$\omega_o = \gamma |H_0|, \qquad (2.17)$$

where ω_o is called the Larmor frequency.

2. Pulse Fourier Transform Methods

In 1957, Lowe and Norberg[93] rigorously proved that in the high temperature approximation (a normally fulfilled condition), the frequency spectrum obtained by the continuous wave (*cw*) irradiation method and the time-domain free induction decay (FID) are Fourier transforms of each other, whatever the system, gas, liquid or solid. However, in the *cw* slow passage technique, the irradiated frequency is swept slowly through the range of interest, while recording the frequency response. The main inefficiency of this method is that it is time consuming. In 1966, Ernst and Anderson pointed out the potential for great efficiency in using Fourier transform pulse NMR to enhance the sensitivity of the

NMR experiment, or conversely, to greatly reduce the acquisition time needed to reach a given signal-to-noise ratio.[94] It was shown by Ernst[95] that the signal-to-noise ratio increases with $\sqrt{n}$, where n is the number of scans. In the time domain, a *rf* pulse is responded to by a spin system, with the response called the free induction decay (FID). The output signal in time domain is Fourier transformed to yield the spectrum in frequency domain. Assuming the FID signal *f(t)* is an exponential decay function:

$$f(t) = A_0 e^{-\frac{t}{T_2^*}} \tag{2.18}$$

where T_2^* is a characteristic time constant. The spectral lineshape is its Fourier transform, the well-known Lorenz function:

$$F(\omega) = \int_{-\infty}^{+\infty} f(t) e^{-i\omega t} dt = v - iu \tag{2.19}$$

where

$$v = \frac{A_0 T_2^*}{1 + \omega^2 T_2^{*2}} \qquad , \qquad u = \frac{A_0 T_2^{*2} \omega}{1 + \omega^2 T_2^{*2}} \tag{2.20}$$

Where v is the absorption spectrum and u is the dispersion spectrum. The magnitude spectrum is

$$M = \sqrt{v^2 + u^2} \tag{2.21}$$

The linewidth Δv for a Lorentzian absorption spectrum v is

$$\Delta v = \frac{1}{\pi T_2^*} \tag{2.22}$$

3. Relaxation

The equilibrium magnetization M_0 of the sample is aligned along the applied magnetic field(conventionally assumed to be the z axis). This net magnetization M_0 is a direct result of the difference of spin energies between the states. After

disturbing the equilibrium spin system with an *rf* pulse, the system must tend to return to equilibrium by giving up energy and thus returning to the lower level state. A spin in a higher energy state can make a transition to the lower energy state via spontaneous emission or stimulated emission. The probability of spontaneous emission at radio frequency is too small to be significant (the probability of spontaneous emission A_{spon} is $A_{spon.} \propto \omega_{kk}^3$.). Thus, all NMR transitions are stimulated. In order to realize a stimulated emission, there must be an interaction between the spins and the surroundings, or "lattice", leading to a transfer of the excess energy from the spin system to the lattice. The process by which the spins in an upper energy state return to a lower energy state is called relaxation. There are two kinds of interaction typically influencing the nuclear spins: a time-varying magnetic field interacting with the nuclear magnetic dipole moments and a time-varying electric field gradient (EFG) interacting with the electric quadrupole moment of the nucleus for nuclei with spin>1/2. Since the nuclear spin-lattice relaxation processes usually depend on the existence of molecular motion to generate a randomly varying magnetic field or EFG, we can obtain valuable information about these motions from the relaxation rates. These could be nearly free molecular rotations and translations in liquids and gases as well as hindered rotations and translations in solids but not vibrations since the vibration frequency is so much higher than the usual Larmor frequencies.

A vector representation for the NMR phenomenon is beneficial in giving us a vivid physical picture. A macroscopic magnetization $\boldsymbol{M}$ is defined as

$$\boldsymbol{M} = \sum \mu_i \tag{2.23}$$

i.e. the sum of all the individual nuclear (or molecular) magnetic moments per unit volume. The dynamic equation of the motion of $\boldsymbol{M}$ in an external field $\boldsymbol{H}$ is given by

$$\frac{d\boldsymbol{M}}{dt} = \gamma \boldsymbol{M} \times \boldsymbol{H}, \tag{2.24}$$

referred to as the Bloch equations. $\boldsymbol{M}$ will precess about the direction of $\boldsymbol{H}$ and Equation 2.24 can be solved in a rotating frame (x', y', z') rotating with frequency ω with respect to the laboratory frame (X, Y, Z). The transformed equation is

$$\frac{d\boldsymbol{M}}{dt}\Big|_{rot} = \frac{d\boldsymbol{M}}{dt}\Big|_{lab} - \omega \times \boldsymbol{M} = \gamma \boldsymbol{M} \times \boldsymbol{H} - \omega \times \boldsymbol{M} = \gamma \boldsymbol{M} \times (\boldsymbol{H} + \frac{\omega}{\gamma}) \tag{2.25}$$

Suppose $\boldsymbol{H}$ consists of a static field $\boldsymbol{H_0}$ in Z direction and an *rf* field $\boldsymbol{H_1}$ in the X direction in the form $\boldsymbol{H} = |\boldsymbol{H_z}|\boldsymbol{e_z} + 2|\boldsymbol{H_x}|\cos \omega t \boldsymbol{e_x}$. Taking the direction of z' to coincide with the Z direction, and decomposing $\boldsymbol{H_1} = (2|\boldsymbol{H_1}|\cos \omega t, 0)$ into two counter-rotating vectors, $\boldsymbol{H_L}$ and $\boldsymbol{H_R}$, in xy plane,

$\boldsymbol{H_1} = \boldsymbol{H_L} + \boldsymbol{H_R} = (|\boldsymbol{H_1}|\cos \omega t, -|\boldsymbol{H_1}|\sin \omega t) + (|\boldsymbol{H_1}|\cos \omega t, |\boldsymbol{H_1}|\sin \omega t)$, then in the rotating frame, component $\boldsymbol{H_L}$ is static with amplitude of H_1 while the other is rotating at 2ω which can be ignored. Equation 2.25 becomes

$$\frac{d\boldsymbol{M}}{dt}\Big|_{rot} = \gamma \boldsymbol{M} \times [(\boldsymbol{H_0} + \frac{\omega}{\gamma})\boldsymbol{e_{z'}} + \boldsymbol{H_1}\boldsymbol{e_{x'}}] = \boldsymbol{M} \times \gamma \boldsymbol{H_{eff}} \tag{2.26}$$

When $\omega = -\gamma|\boldsymbol{H_0}|$, then $\boldsymbol{H_{eff}} = |\boldsymbol{H_1}|\boldsymbol{e_x}$, a static field aligned on x axis (Note, $\boldsymbol{M}$ will also precesses about the x' axis with frequency $\gamma|\boldsymbol{H_1}|$). This makes the $\boldsymbol{M}$ tip in the longitudinal direction. The tipping angle θ of $\boldsymbol{M}$ is given by

$$\theta = \gamma|\boldsymbol{H_1}|t_p \tag{2.27}$$

where t_p is the duration of $\boldsymbol{H_1}$. If t_p is a 90° pulse (θ =90°), as illustrated in Figure 2.2, the $\boldsymbol{M}$ will align in the xy plane and precess about Z axis with Larmor frequency ω_0 in the laboratory frame. If the spin system was placed into an *rf* coil, then a small voltage will be induced in the coil. This voltage is the NMR signal.

The induced voltage is a measure of the magnetization in the horizontal plane after the *rf* pulse and will decay due to spin-spin interaction and inhomogeneity of the static field H_0. We call it the free induction decay (FID) since

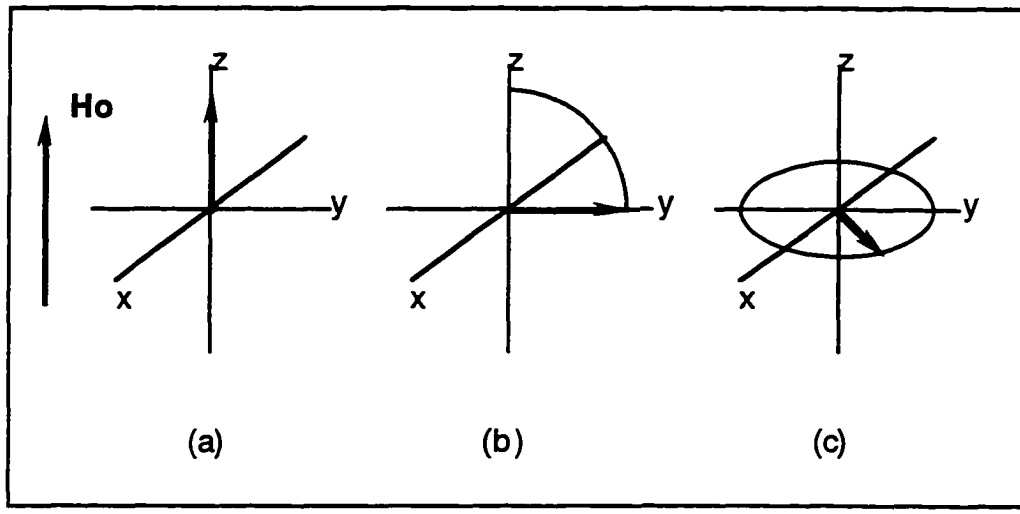

Figure 2.2 Effect of *rf* pulse, a) Initially, M is a aligned along H_0; b) At the end of 90° pulse applied on x axis, M lies in y axis; c) After pulse, M precesses in XY plane at Larmor frequency.

the spins are precessing freely without the *rf* field. The FID can be Fourier transformed from the time domain to frequency domain to obtain the absorption spectrum.

Basically, there are two different relaxation mechanism: spin-lattice relaxation and spin-spin relaxation. Figure 2.3 is a vector diagram describing the process of both relaxations, in z direction and xy plane, respectively. The spin-lattice relaxation is often termed longitudinal relaxation in z direction and involves

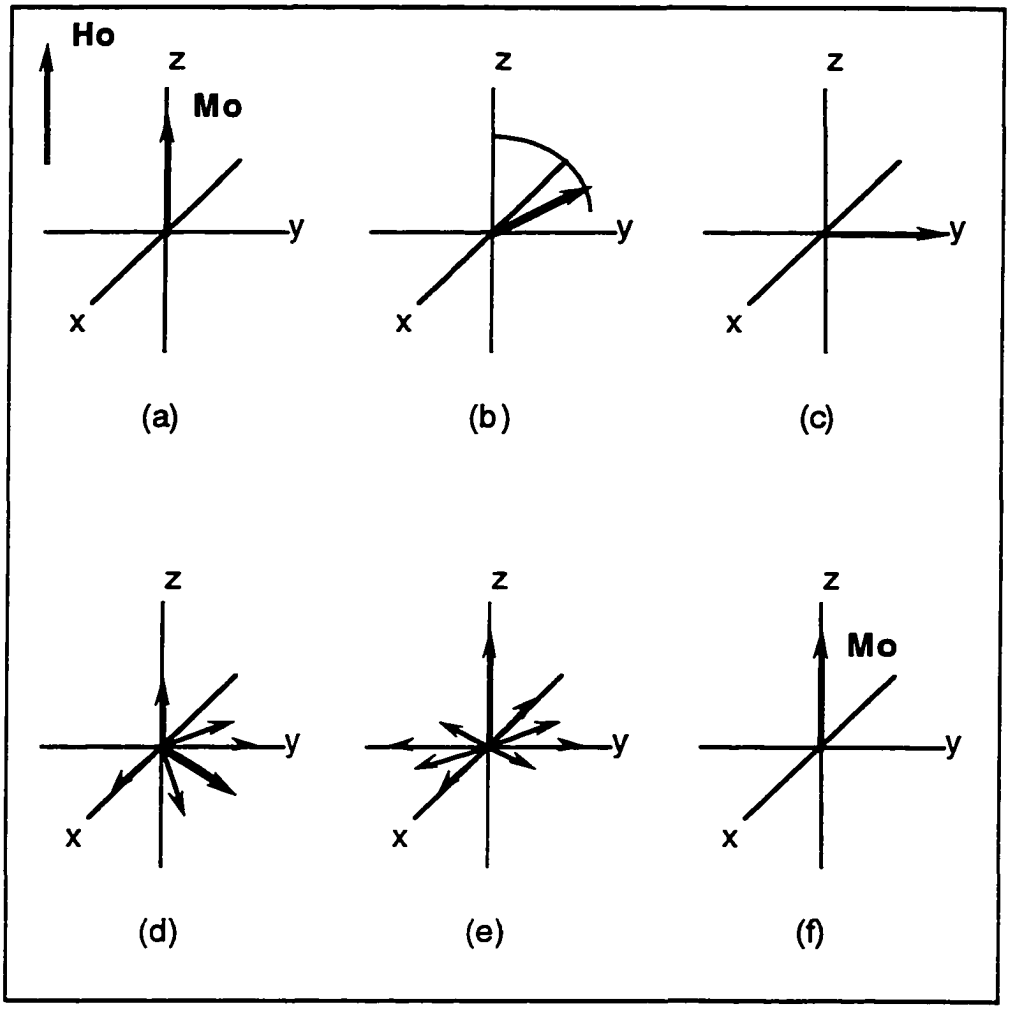

Figure 2.3 Diagrams describing relaxations: a) The net M_o is aligned with H_o; b) & c) A 90° *rf* field H_1 tips M_o to *y* axis; d) & e) The spins begin to relax in the *xy* plane spin-spin (T_2) process and in *z* direction by spin-lattice (T_1) process; f) the equilibrium M_o is reestablished along H_o.

changes in energy and the components of nuclear moments along the z direction of the applied magnetic field. The spin-lattice relaxation time T_1 is a measure of the rate of transfer of energy between spins and lattice. The spin-spin relaxation, also termed transverse relaxation, causes components of the xy magnetization to fan out or dephase. The spin-spin relaxation does not necessarily require any change in energy, so the rate of spin-spin relaxation, in xy plane, may be faster than the rate of spin-lattice in z axis, relaxation. The time constant T_2 intrinsically characters the exchange process of the spin system.

2-3-2. High Pressure NMR Measurements

Temperature dependence of the parameters in NMR studies for solid electrolytes has been studied extensively. However, pressure is one of the essential thermodynamic variables which determine the state of a system, and has been considered much less than temperature in most experimental studies. Measuring NMR parameters at elevated pressure can provide a wealth of additional information. In some case pressure is found to be a complementary variable to temperature, in other cases pressure is the essential variable.[63,96] High pressure studies of ionic conductivity as well as NMR studies in solids have demonstrated that pressure is a useful complementary thermodynamic variable to temperature in trying to understand the mechanisms of ionic conduction and ion diffusion. [61, 63-65, 93] Since many macroscopic properties of solid polymers are a direct result of diffusion of ions, molecular motions of polymer chains and segments, experimental and theoretical efforts to elucidate the dynamics of motion affected by pressure in polymeric materials are of great basic and practical significance. The mechanical motions necessarily produce volume fluctuations that can be probed by changing the pressure. The parameter A related to various motional processes,

which could be a relaxation rate ($1/T_1$ or $1/T_2$), conductivity σ, or diffusion D, can be generally expressed in Arrhenius equation:

$$A = A_0 e^{-\frac{G}{RT}} \tag{2.28}$$

where G is the Gibbs free energy, R is the gas constant. We may break G down into temperature and pressure derivatives near any point on the equilibrium surface, by writing

$$G = Q - ST + pV \tag{2.29}$$

with

$$S = -(\frac{\delta G}{\delta T})_p, \quad V = -(\frac{\delta G}{\delta p})_T \tag{2.30}$$

thus we have

$$\Delta V = V = -RT[\frac{\delta(\ln T_1)}{\delta p}]_T \tag{2.31}$$

ΔV is the activation volume for a spin-lattice relaxation process. It need not be related directly to any physical volume. It may be regarded as the pressure dependence of the activation energy.

This thesis work includes high pressure proton, deuteron and Fluorine-19 NMR measurements on PFSA membranes. The spin-lattice relaxation time T_1 was measured as a function of static hydraulic pressure over a range of 1 bar - 2.5 kbar. Activation volumes were extracted from the T_1 pressure dependence.

2-3-3. Self-Diffusion Coefficient

Self-diffusion is the net result of the thermal motion-induced random-walk process experienced by particles or molecules within a medium, consider molecules undergoing free Brownian motion. The system is assumed to be an isotropic and

homogeneous without flux and thermal or concentration gradient. The motion with mean (a time average) square displacements over time t is defined by the Einstein relation

$$\langle r^2 \rangle = 6Dt \tag{2.32}$$

where D is the molecular self-diffusion coefficient. The Einstein relation is assumed under the condition that the conditional probability of finding a molecule, $P(\mathbf{r}_0,\mathbf{r},t)$ of initial position $\mathbf{r}_o$ at a position $\mathbf{r}$ after some time t is:

$$P(r_0,r,t) = (4\pi Dt)^{-\frac{3}{2}} e^{-\frac{(r-r_0)^2}{4Dt}} \tag{2.33}$$

The single parameter D, the self-diffusion coefficient, characterizes this radial distribution completely.

For a system in which a flux occurs in the presence of a concentration gradient, diffusion is described by Fick's law:

$$J = -D^* \frac{dC}{dx} \tag{2.34}$$

where D^* is the diffusion coefficient with flux or concentration gradient; J, the flux; C, the concentration of the diffusing species.

In membranes the real situation is that a water concentration (and thus activity) gradient exists and the diffusion of water is driven by a chemical potential gradient. Equation 2.34 is pertinent to a "dilute" solution situation, *i.e.* one in which no variation in activity coefficient with composition is present. The pulsed-field gradient spin-echo (PGSE) NMR technique (see below) can be used to determine self-diffusion coefficients which depend upon membrane composition, under conditions of negligible chemical potential gradients or the fluxes of other species. The equation below can be used for converting a measured self-diffusion coefficient to a "chemical" diffusion coefficient D^*:

$$D^{*} = \left(\frac{d\ln a}{d\ln C}\right) D \qquad (2.35)$$

where a is the activity (definition see section 2-2) of the diffusing species.[6] This equation essentially accounts for changes in activity coefficient with concentration. In using D^{*} in equation 2.34 for polymeric systems, other effects such as volume changes must also be accounted for.

2-3-3.1 Pulsed-Gradient Spin-Echo (PGSE) NMR

An NMR method of measuring the self-diffusion coefficient was first suggested by Hahn (1950).[97] A precise theoretical treatment of this "constant gradient" NMR method was given by Carr and Purcell (1954).[98] McCall *et al.* (1963)[99] described the pulsed gradient NMR experiment, eliminating the limitations of "constant gradient" arising from spectrometer bandwidth, noise and power output *etc.*. This method was later demonstrated and given a detailed theoretical description by Stejskal and Tanner (1965)).[100] Not only does this method allow a measurement of thetrue self-diffusion of atoms of molecules, but it is both more accurate and, in some ways, much more convenient than conventional techniques of measuring diffusion.

The PGSE experiment is shown in Figure 2.4 in time sequential form. The procedure for using the pulsed-gradient diffusion measurement consists of two *rf* pulses, 90° and 180° *rf* pulse, with identical magnetic field gradient (z direction) pulses of magnitude g, duration δ, and separation Δ applied respectively during the dephasing and rephasing of the echo cycle. Typically, Δ is set from 5 ms to as much as a few hundred milliseconds, δ a few milliseconds. In this method, two pulsed-gradient with duration δ replace the "constant gradient " allowing one to

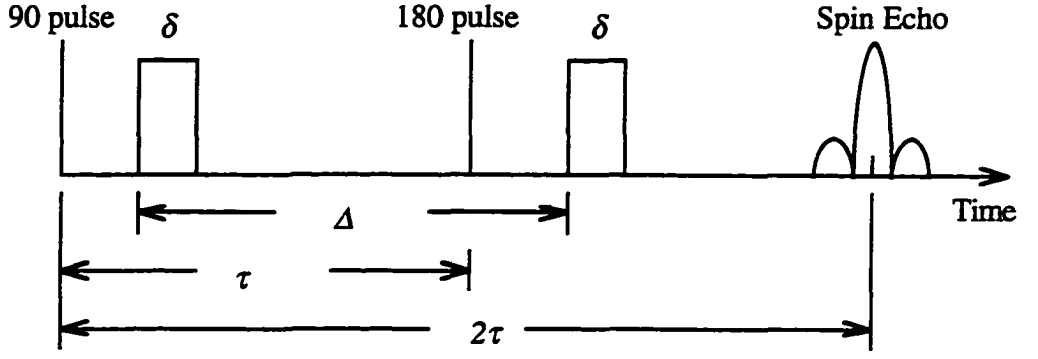

Figure 2.4 PGSE experiment pulse sequence showing the experimental times, δ, Δ, and τ.

produce significant dephasing (*i.e.* detecting with higher sensitivity) without "wide bandwidth" difficulty.

Basically, the experiment is carried out by observing the attenuation of the spin-echo amplitude due to displacement of molecules containing nuclei with magnetic moments in the presence of magnetic field gradients, and inferring the D from the dependence of echo attenuation on field gradient strength (or duration). The first gradient pulse after a 90° *rf* pulse produces a precessional phase shift which depends on the position of each nucleus in the sample. Then the molecules containing the nuclei change position due to diffusing motion during the time between the two gradient pulses. The 180° *rf* pulse inverts all prior phase shifts so that the second gradient pulse has the effect of phase refocusing. However if motion has occurred, the refocusing is incomplete and the attenuation of the spin echo gives a measure of the average of nuclear translations. The two gradient

pulses thus tag and detect, respectively, the initial and subsequent positions of the nuclei over the well defined time interval Δ.

Now, we consider the time-dependent macroscopic nuclear magnetization $M(r,t)$ obeying the equation given by A. Abragam[79]

$$\frac{\partial M(r,t)}{\partial t} = \gamma M \times H(r,t) - \frac{M_x e_x' + M_y e_y'}{T_2} - \frac{M_z - M_0}{T_1} e_z' + D\nabla^2 M \tag{2.37}$$

to compute the result for the case of one 90° pulse followed by a 180° pulse. The behavior of the components of the nuclear magnetization M in the xy plane perpendicular to the applied magnetic field H_0 is represented by M_x+iM_y. H_z is a combination of H_0 and gradient magnetic field G,

$$H_z = H_0 + G \cdot r$$

and $H_x=H_y=0$. Introducing definition

$$M_x + iM_y = \psi e^{-(i\omega_0 + \frac{1}{T_2})t} \tag{2.38}$$

Equation 2.37 is reduced to

$$\frac{\partial \psi}{\partial t} = -i\gamma(G \cdot r)\psi + D\nabla^2 \psi \tag{2.39}$$

Here we assume that G is uniform throughout the sample. $\psi(r.t)$ is independent of T_2 and describes the behavior in a coordinate system rotating with angular velocity $\omega_0=\gamma H_0$ about the z axis and in the same sense as M precesses. D is the diffusion coefficient. Between the 90° pulse (at t=0) and 180° pulse (t=τ), without considering the D term, the solution of Equation 2.39, with boundary condition ψ=A immediately following the 90° pulse, is given by

$$\psi(r,t) = Ae^{-i\gamma r \cdot F} \tag{2.40}$$

where

$$F(t)=\int_0^t G(t')dt' \tag{2.41}$$

After the 180° pulse the phase of ψ is set back by twice the amount which it has advanced. The solution could then be expressed as

$$\psi = Ae^{-i\gamma r\cdot[F+(\xi-1)f]} \tag{2.42}$$

with

$$\xi=+1 \quad for\ 0<t<\tau; \qquad \xi=-1 \quad for\ t>\tau,$$

where

$$f = F(\tau)$$

The solution of Equation 2.39 is assumed to be identical with that shown by Equation 2.42 if A is to be considered a function of t. Therefore, this will yield

$$\frac{dA}{dt} = -\gamma^2 D[F+(\xi-1)F]^2 A \tag{2.43}$$

Integrating between t=0 and t=τ' (echo)

$$ln[\frac{A(\tau')}{A(0)} = -\gamma^2 D[\int_0^{\tau'} F^2 dt - 4f\cdot\int_\tau^{\tau'} F\,dt + 4f^2(\tau'-\tau) \tag{2.44}$$

Since $\psi=A(0)$ immediately following the 90° pulse and $\psi=A(\tau')$ at the peak of the echo, the attenuation factor $R= A(\tau')/A(0)$ represents the effect of diffusion on the echo amplitude. If we specify the gradient G between 2τ as:

g when $t_1<t<t_1+\delta<\tau$, or $t_1+\Delta<t<t_1+\Delta+\delta<2\tau$

0 other times

The attenuation factor R, which attenuates the spin echo signal amplitude due to diffusion, is given by

$$R = e^{-\gamma^2\delta^2 g^2(\Delta-\frac{1}{3}\delta)D} \tag{2.45}$$

the value of gradient g must be known (typically this is calibrated on a well-defined standard sample), as well as the gyromagnetic ratio γ of the specific nuclei under study.

2-3-3.2 Pulsed-Gradient Stimulated Spin-Echo (PGSSE) NMR

Pulsed-gradient stimulated spin-echo (PGSSE)[101], another NMR method for measuring self-diffusion coefficient, was used for determining self-diffusion in the membrane for water/methanol system in this thesis work.

PGSSE, shown in Figure 2.5 , is a pulsed-gradient stimulated spin-echo sequence for diffusion coefficient measurement, consisting of a *rf* pulse sequence of three-90°-pulse which is different from conventional 90°-180° *rf* pulse sequence. It was shown by Hahn[97] that as many as five spin echoes may result from a three-pulse rf sequence. The echo which occurs an interval after the third *rf* pulse equal to that between the first two pulses has been named by him the "stimulated echo". Woessner has given an expression for the echo attenuation by molecular diffusion in a static field gradient for three and four-pulse sequences, including the stimulated echo.[102] Tanner has given expressions for the pulsed-gradient modification of that basic sequence.[101]

In Figure 2.5, five echoes arise from the application of three *rf* pulses including four spin echoes (SE) and the one stimulated echo (STE). Following the second pulse after time τ_1, the first spin echo (SE1) arises from spins that were in the *xy* plane dephasing and refocusing due to the effects of the first and second pulse, respectively. After the first spin echo forms, the spins again dephase and can be refocused with the third *rf* pulse after time τ_2-τ_1(here dephasing time is τ_2-τ_1). If there are spins in the *xy* plane immediately after the second *rf* pulse, they

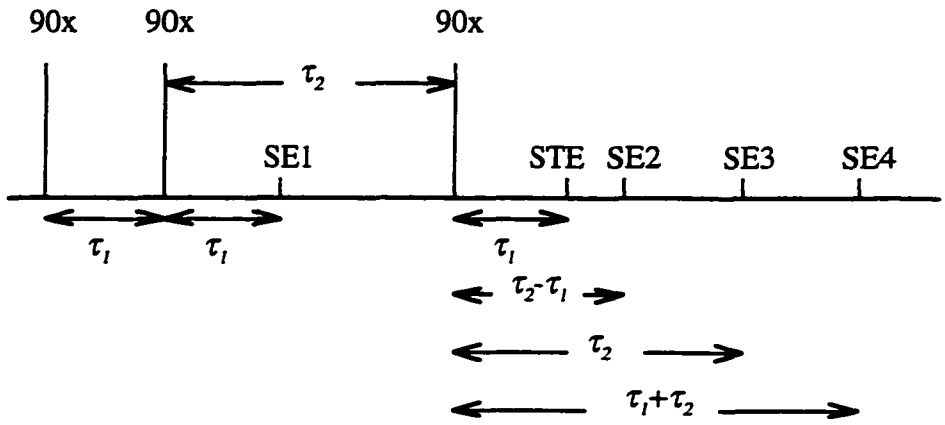

Figure 2.5 Five echoes arise from the application of three *rf* pulses.

could be refocused by the third pulse at a time τ_2 after the third pulse. The fourth spin echo is due to spins in the *xy* plane after the first pulse refocusing with the third pulse a time $\tau_1+\tau_2$ after the third pulse. In the PGSSE method, some magnetic field gradients are applied between the first-second and the second-third 90° pulses to ensure dephasing of the spins after the first pulse and to eliminate the spin echo formation, so that only the stimulated echo is left in the acquisition period.

A simplified vector diagram describing the formation of the stimulated echo is given in Figure 2.6. It gives a useful, intuitive description (however oversimplified) of the general mechanism of stimulated echo formation. A more detailed description can be found in some general references.[97, 102] The first *rf* pulse (*x* direction) creates a *y* component to the magnetization. Assuming that during the first interval (τ_1) the spins totally dephase in the *xy* plane (*i.e.* no net magnetization remains in the *xy* plane). This can be represented by four equal-sized magnetization vectors along the *x*, -*x*, *y*, and -*y* axes labeled *a*, *b*, *c*, and *d*. Note that *a* and *b* have moved by $\pm$ 90^0 during τ_1, *c* has not moved, and *d* has moved

180° (as seen in rotating frame). The second 90° pulse (*x* axis) does not affect the spins along the *x* direction (*a* and *b*); however, it flips the *y* spins (*c*) to *z* and the *-y* spins (*d*) to *-z*. Spins *a* and *b* continue to refocus to form the spin echoes, and will not be considered further here. The third 90° pulse then flips the magnetization vectors *c* and *d* to *-y* and *+y*. Because *c* does not move in this rotating frame, and *d* moves 180° during time τ_1, *c* and *d* refocus for an stimulated echo at a time τ_1 later along the *-y* axis.

Although either a PGSE or a PGSSE could be used, the PGSSE is more useful in extending the range of measurement of diffusion coefficients. The major advantage of PGSSE method is the relaxation attenuation of the stimulated echo has only a T_1 dependence because the middle interval (and hence the time between the diffusion gradients) is limited by T_1 relaxation as Hahn described.[97] Thus, in systems $T_1 >> T_2$, one might be able to lessen the effect of spin-spin relaxation on the signal by increasing Δ (limited by T_1) with a short τ_1. The attenuation of spin-echo in PGSE is affected by both T_1 and T_2. In the PGSSE experiment Equation 2.45 is still valid with the same definition of Δ as in PGSE. Typically, τ_1 and τ_2 were set to 1-5 ms and 10 ms - 1s, respectively, and Δ was 5 ms to a few hundred milliseconds.

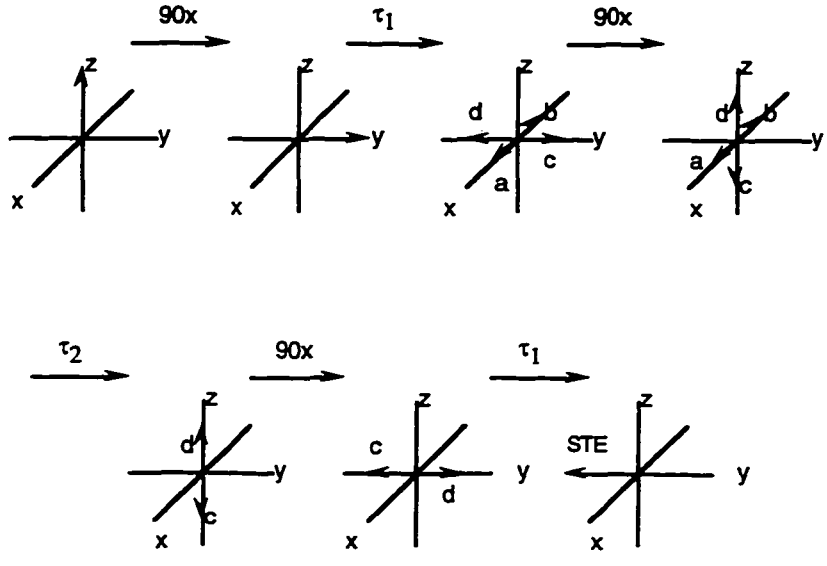

Figure 2.6 Simplified vector diagram describing the formation of a stimulated echo.

Chapter 3. Experiment

3-1. Pretreatment of Samples

Nafion®[Nafion®117 (N117), Nafion®115 (N117), Nafion®105 (N105)], Dow XUS developmental fuel cell membrane, and Membrane C samples were purchased from E. I. du Pont, Dow, and Chlorine Engineers (Japan), respectively. All membranes were pretreated by boiling in 3% H_2O_2, rinsing in boiling water, boiling in 0.5M H_2SO_4, and finally rinsing in boiling water (at least 1 hour for each step).

3-2. Isopiestic Absorption

All the measurements of transport properties were carried out under the conditions of controlled equilibration of the membrane sample. Sufficient time was taken for each membrane sample in environment of known relative humidity for equilibration to be established, and then, the membrane sample was transferred into the appropriate experimental cell before measurements were carried out. These cells were designed to allow continued equilibration of the membrane samples during the measurements. Therefore, water uptake behavior of the membrane must be investigated before carrying out the measurements.

The "absolute" water contents of the membrane is based on water uptake into membrane measured as the difference between hydrated membrane sample and "dry" membrane sample. It is important to understand that selecting a method to dry a membrane sample means selecting a dry reference state of membrane sample. Since using different methods for drying membrane samples could cause poorly comparable results, a dry reference state of membrane sample should be addressed. Different authors used their own methods to dry samples in early studies, in which membrane samples were usually placed in vacuum at various high temperatures for

certain time, such as Nafion dried to constant weight at 160°C,[41] at 170°C,[37] at 220°C for 30 min under 10^{-4} torr pressure,[25, 29, 33] and at 100°C for 18 hours in vacuum.[44] It is difficult to determine relationship of these methods to each other. Bunce *et al.*[45] stated that the absolute water contents in those various arbitrary "standard states" are unknown, they therefore suggested a fixed choice of a reference state, in which the Nafion was dried under vacuum to constant weight at room temperature instead of various high temperature. Zawodzinski *et al.* investigated membrane water uptake using several ways:[9] 1) drying at room temperature for 24 hours under vacuum; 2) treatment 1, followed by 1 hour under vacuum at 105°C; 3) drying at room temperature over P_2O_5; 4) treatment 3, followed by 1 hour under vacuum at 105°C. These workers claimed that the first method results in a membrane water content of $\lambda \approx 1$ (λ is the number of water molecules per sulfonate, see below), as demonstrated by other workers,[33, 45] while the latter results in a "near zero" water content. In this thesis, the forth protocol was used.

Isopiestic sorption of water by the membrane exposed to the water vapor phase was measured by setting the equilibration cell properly as Figure. 3.1. Membrane samples were cut into slivers of dimensions 12 mm × 35 mm and set in a small vessel capped with GORE-TEX which allows water vapor to pass through and blocks liquid water from entering. Two pieces of membranes were set in each vessel for reducing measurement error. Polyethylene mesh (thickness is 0.5 mm) lining separates the membrane samples from the wall of the equilibration vessel thus preventing the membrane samples sticking to the wall of the equilibration vessel. The vessel was placed in a container with a sufficient volume of aqueous LiCl solution of appropriate composition. This design allows the

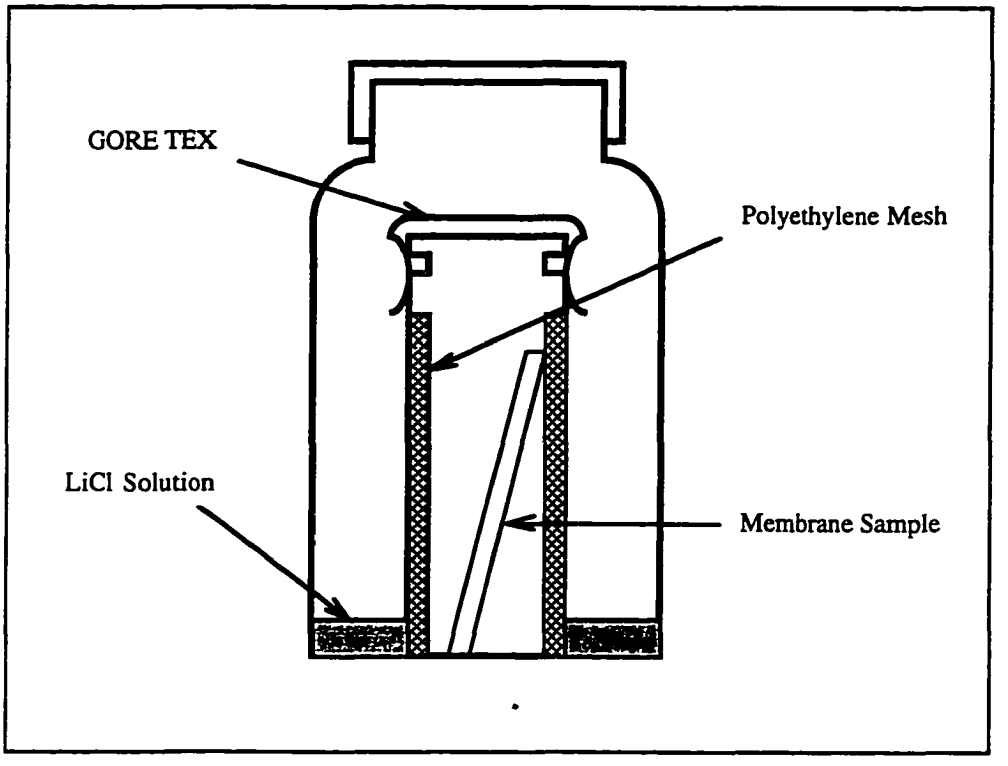

Figure 3.1 Isopiestic absorption of membrane samples exposed to water vapor above aqueous LiCl solutions of known water activity.

membrane to reach equilibrium with water vapor of activity defined by the solution composition without contacting the liquid. Typical equilibration times are on the order of 5 to 10 days. To determine the water uptake in each state of hydration, membrane samples were removed from the equilibration vessel, quickly blotted dry to remove excess surface water, and weighed in a closed vessel. The samples were removed to another vessel, dried in P_2O_5 for about 7 days and then in vacuum oven, about 5×10^{-2} torr, at 105°C for about 6 hours, completely drying the membrane samples. The membranes were then weighed. The water uptake was determined from the difference between wet and dry weights. The calculation of water content absorbed by membrane is based on number of water molecules per sulfonic acid group, *i.e.* water content λ is defined as $\lambda = N(H_2O)/N(SO_3H)$. The water content absorbed by membrane is calculated by the formula

$$\lambda = \frac{Water\% \times EW(g/unit)}{100 \times 18}$$

where

Water % — percentage of water uptake into membrane

EW (g/unit) — membrane equivalent weight per repeat unit in grams

Relatively wide fluctuations, up to 10%, are often observed in spite of careful operating methods. The non-uniform distribution of polymer side chains in the membranes and unequal membrane thickness (normally, 10%) will lead to unequal absorption for several small membrane samples. In order to obtain reliable data, 1) make the samples as large as possible; 2) weight the samples as quick as possible; 3) take a statistical average of several measurements.

3-3. Protonic Conductivity

The conductivity of the membrane as a function of temperature was determined in a specially constructed pressurized (70 psi) "bomb" which was wrapped in heating tape and then insulated. Leads were built into the top of the bomb. Membrane conductivity was determined by using the cell shown in Figure 3.2. The cell was suspended in the high pressure bomb which enables the membrane samples to be exposed to water and various LiCl solutions vapor phase, or immersed in water or various solutions (*e.g.* Methanol solution *etc.*) under various pressures. For obtaining equilibration of the membrane with water controlled relative humidity, the "window" structure was employed. To minimize the effects of electrode contact, all the measurements are carried out along the surface of the membranes. Both electrodes were made of blackened platinum. Temperature was well controlled by a Microprocessor-Based Temperature/Process Controller OMEGA CN76000. The resistivity of membrane was measured using *Schlumberger SI 1260 IMPEDANCE /GAIN-PHASE ANALYZER* as the high frequency (10 kHz) impedance of the system. Both real and imaginary components of the impedance were measured. It has to be ensured that the measurement was free of lead inductance effects. Membrane sample was cut by using template. The cell constant was calculated from the geometry of the cell and the thickness of the membrane sample (the latter was measured with a micrometer).

It should be stressed that some crucial factors will strongly affect the membrane conductivity measurements. 1) Insufficient equilibration time in the experiment could compromise the measurement. Particularly, for the partially hydrated membrane (exposed to vapor phase of liquid solution) and higher temperature, there are serious concerns. Because this is in vapor phase, it is more difficult to obtain water equilibrium than fully hydrate case (membrane immersed in water or solution) due to rather hydrophobic "skin" of the membrane[103]. At high

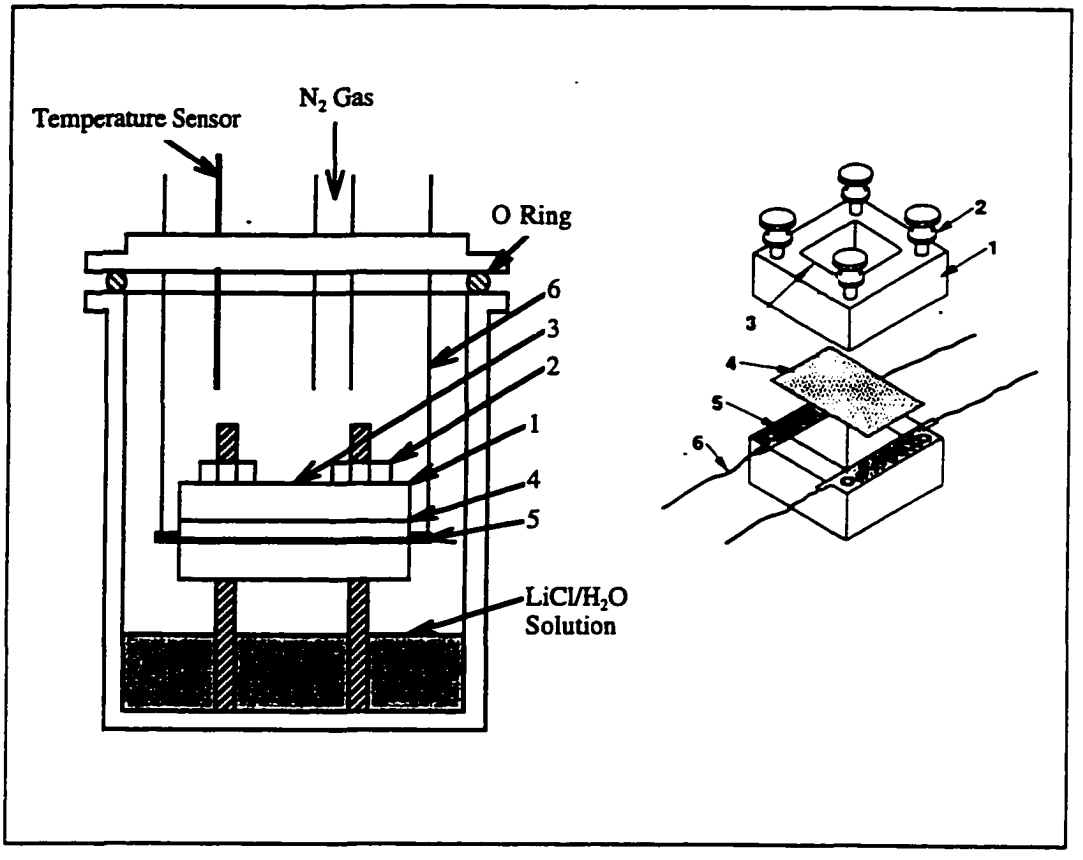

Figure 3.2 Cell used for determination of membrane conductivity: 1) Kel-F Block; 2) screw; 3)"window" area to allow equilibration; 4) membrane sample; 5) blackened Pt foil; 6) Pt lead.

temperature, this effect becomes worse since membranes are more hydrophobic than at low temperature. In this thesis work, the equilibration of the sample usually took 2 hours for the samples immersed in liquid solutions and longer for the exposure of the samples to vapor phases. 2) Since the membrane conductivity is calculated using Equation 2.3 rather than determined directly, the membrane thickness which depends on hydration state and temperature strongly influences the calculation of conductivity ($\Delta\sigma \propto t^{-2}$). Hence, the membrane thickness could be the largest contribution to the deviation of the membrane conductivity. However, more deviation in the measurements could be involved. For certain relative humidity in vapor phase, membrane thickness is different at different temperatures. It should be noted that membrane thickness could not be measured precisely because firstly, membrane thickness varies from batch to batch. Secondly, even for the same batch, there is a small difference at different points along the membrane. Thirdly, for the measurements in which the membrane thickness practically is not able to be measured, thickness correction made could cause more deviation involved in the results.

3-4. Electro-Osmotic Drag Coefficient

The cell for electro-osmotic drag coefficient experiment is essentially the same design as that reported by Fuller and Newman[70]. A schematic cell design is given in Figure 3.3. It consists of two chambers in contact only through the membrane. The two chambers are the reservoirs for the solution of known water activities. One chamber contains a solution close to unit water activity as a reference state. The other chamber is for the solutions of various water activity. The two Pt electrodes are set in both chambers. The strip of membrane sample was

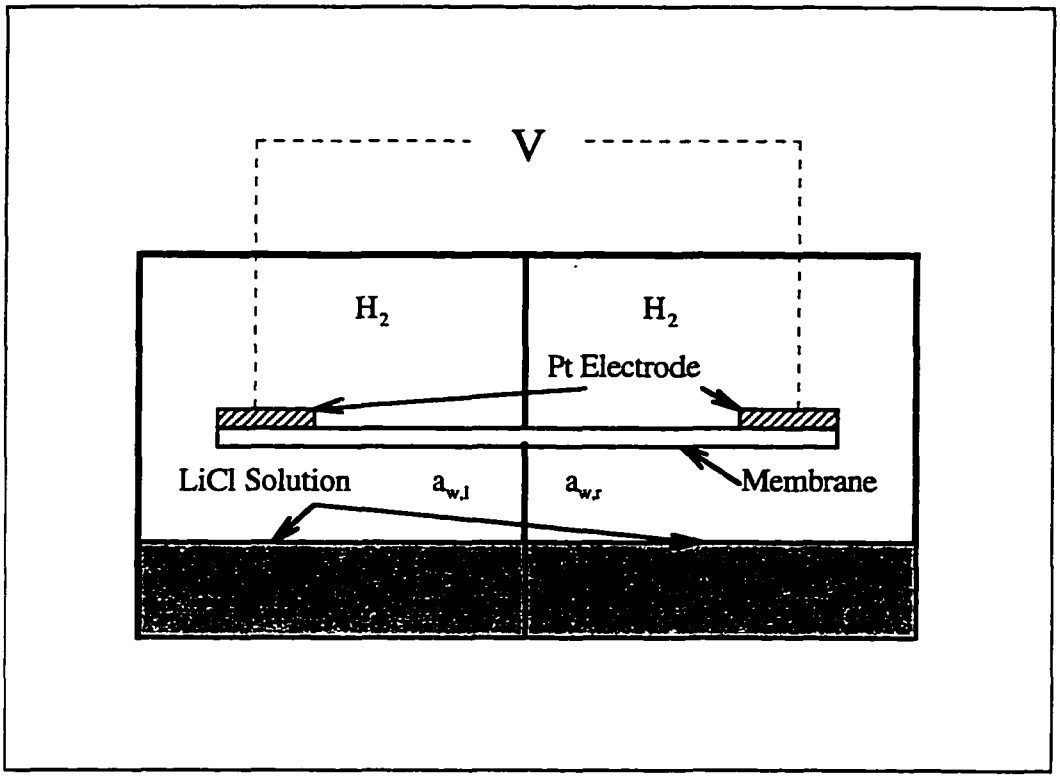

Figure 3.3 Schematic of concentration cell for electro-osmotic drag coefficient measurement. The water activity is controlled with a lithium chloride solution.

cut in dimensions of 10 mm × 75 mm (using a template) and forms a bridge crossing over the center chamber wall from one chamber to the other, and contacts with both Pt electrodes. Humidified hydrogen gas passes through a sparging bottle containing the same solution as is in chamber, and then is inputted into each chamber. The gas flow rate on either side are well equalized by fine-adjust pinvalves and by observing even quantities of bubbles out from both tubes in a sparging bottle. The cell and sparging bottles are thermostated in a water bath and the temperature was well controlled by a Microprocessor-Based Temperature/ Process Controller OMEGA CN76000. Wires making contact with the Pt electrodes are sheathed and isolated from the bath. The cell was sandwiched by two Al plates (top and bottom) of the cell, and sealed by bolts spaced equally around the cell. Silicone rubber gaskets were cut to ensure a good seal around the cell and between chambers.

The potential difference between the electrodes was measured by using a *Hewlett-Packard Model 3468B* digital multimeter with a high impedance input. The potential difference was noted periodically. About 1-2 hours, it achieved a stable value and then recorded.

LiCl solutions were used for the experiment. One chamber (left side in this experiment) holds the solution with fixed water activity, 1 molal (a_w = 0.964), and the other with various water activity, 2-18 molal (a_w = 0.921-0.139). The LiCl solutions were prepared from 18 molal stock LiCl solution made previously. The 7 ml solution was injected using syringes into each chamber. The system was purged by N_2 gas about 30 minutes while raising system temperature. At elevated temperatures, special precautions were taken to avoid condensation of water in the gas feed lines and cell.

3-5. NMR Measurements

3-5-1. NMR Facilities

All the diffusion measurements and part of spin-lattice relaxation measurements were performed on a *Bruker AM-400 NMR* spectrometer using a Bruker microimaging probe equipped with gradient coils of maximum gradient strength 40 gauss/cm, and 10 mm Helmholz coil insert. Previously, gradient pulses were shaped to minimize the effect of eddy currents. The effect of any remaining eddy currents was checked by measuring the signal intensity of a sample of water as a function of time between the end of an applied gradient pulse and the onset of acquisition. The gradient was also previously calibrated by observing the profile of a calibrated water phantom in the presence of gradients covering the range used experimentally. Temperature was controlled by means of the Bruker VT1000 probe temperature controller and calibrated by a Luxtron 1000b fiber optic temperature probe.

All the high pressure NMR measurements and part of spin-lattice relaxation measurements carried out using Novex broad line NMR spectrometer interfaced to a microcomputer and a LeCroy 9400 digital oscilloscope with built in Fourier transform function. The power amplifier of the spectrometer has a maximum output of 1 kilowatt in the frequency range from 10 to 100 MHz. A cryomagnet system with field strength 7.2 tesla superconducting magnet produces the static field. The linewidth broadening of liquid sample due to the field inhomogeneity is about (500-1000) Hz for bulk D_2O in 8 mm tube. Referring to the linewidth of spectra in Nafion sample, this inhmogeneity broadening is negligible. Variable temperature control (±2K) is achieved by regulation the flow rate of N_2 through a copper heat exchanger immersed in liquid N_2. In addition to 7.2 tesla, a Varian electromagnet was utilized for ^1H and ^{19}F measurements at 42 MHz and 39.5 MHz, respectively. The matching network for transmitter and receiver in the probe is

shown in Figure. 3.4. It consist of a matching capacitor C_1, a tuning capacitor C_2, and a solenoid *rf*-coil. Both C_1 and C_2 are high-voltage (2000 V) variable capacitance (0.8-10 pf) capacitors obtained from Polyflon company. The home made coil has 0.5 μH and its quality factor is 250.

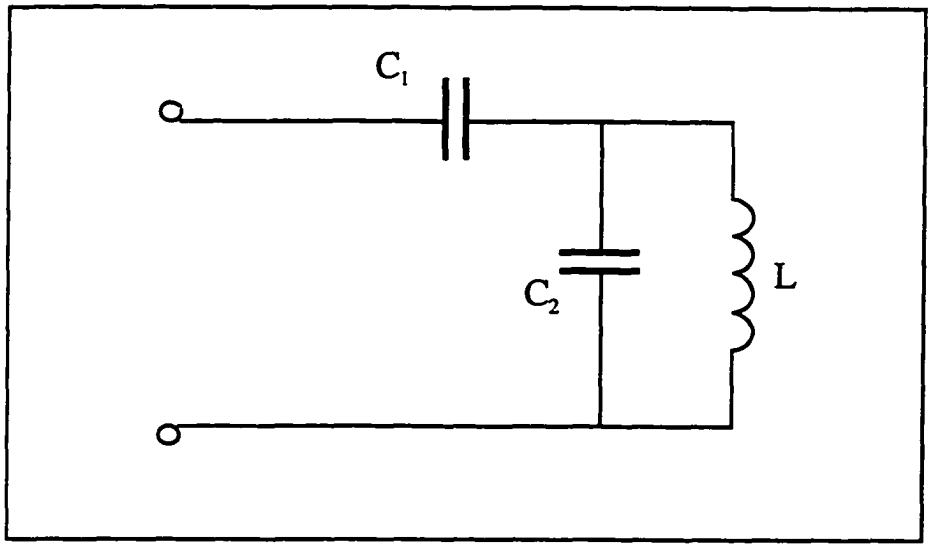

Figure 3.4 The L-C matching network in NMR probe.

3-5-2. High Pressure Measurements

A home-built NMR probe was adapted for use at pressures up to 2.5 kbar. Typical dimension of the solenoidal rf-coils were 7 mm in diameter and 10 mm in length, just large enough to hold the samples. To isolated them form the pressure-transmitting fluid, the samples were tightly sealed by teflon tape for ^{1}H or ^{2}H NMR and a polyurethane sheath for ^{19}F NMR measurements, after determining their water uptake. The teflon tape was checked for absence of proton signal. The coil assembly was housed in a stainless steel cylindrical pressure cell fitted with a plug with two electrical feed-through connections. The insulating material surrounding

the two leads was made from machinable ceramic. The intrinsic capacitance of the plug is very small and has virtually no pressure dependence which leads a good tuning at the elevated pressure. Elevated hydrostatic pressures were achieved using a hydraulic Enerpac 11-4000 manual pump; hydrogen-free Fluorinert FC-77 (3M) and Fluorine-free Spinesstic 22 were employed as the pressure-transmitting fluid for ^{1}H, ^{2}H and ^{19}F measurements, respectively. Pressures were monitored with a Heise 12-inch circular gauge. The structural diagram of high pressure cell and plug is shown in Figure 3.5. ^{1}H and ^{19}F T_1's were measured by inversion recovery at a Larmor frequency of 39 MHz, with a typical inverting pulse width of 10μs. All the T_1 are reported correspond to the decreasing pressure portion of the first cycle, *i.e.* pressure was applied prior to T_1 measurement, then gradually released during the measurements.

3-5-3. Self-Diffusion Coefficient

Water self-diffusion coefficients were measured by both NMR pulsed-gradient spin-echo (PGSE) and pulsed-gradient stimulated spin-echo (PGSSE) techniques. The experiment was carried out using a Bruker AM-400 NMR spectrometer (Detail see 3-5-1). Samples were prepared by several methods due to different types of solutions. 1) The measurements as a function of water content: Slivers of membranes of dimensions 1.5 mm × 15 mm were suspended over different LiCl solutions of known water activity for several days at 30°C. The samples were emersed, blotted quickly to remove the liquid solution on the membrane surface, loaded into 4 mm homemade NMR glass tube with a length of roughly 45 mm within which the equilibration could be maintained, and then sealed with flame. 2) The measurements related to methanol concentration: Slivers of

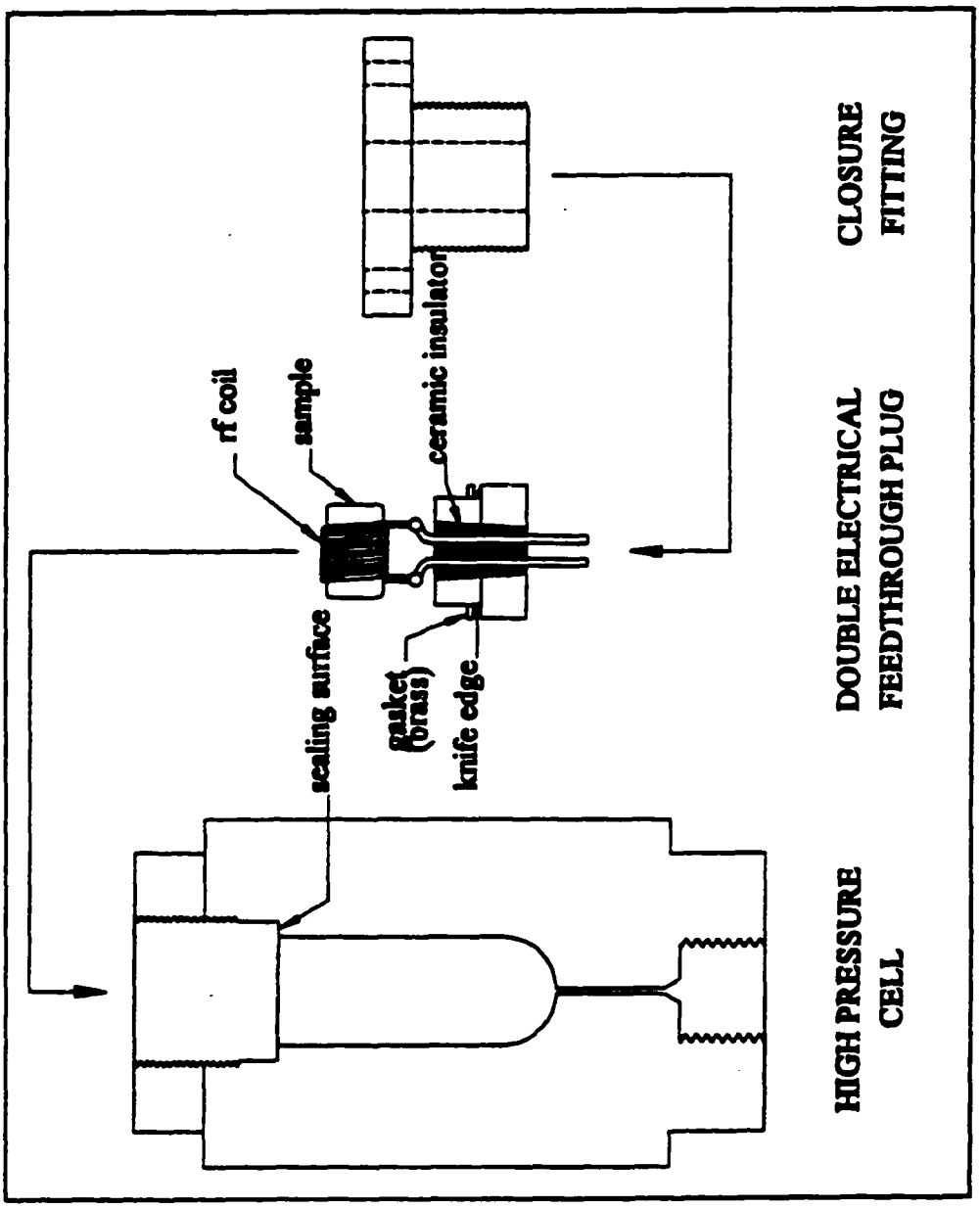

Figure 3.5 Diagram of high pressure cell and plug structure. (reproduced from [104])

membranes of dimensions 8 mm × 15 mm were immersed in several solutions with different methanol concentrations for a few days. The samples were emersed, blotted as quickly as possible to remove the liquid solution on the membrane surface, loaded into 10 mm NMR glass tube, and then sealed with parafilm.

Chapter 4. Results and Discussions

4-1. Water Uptake into PFSA Membranes

In this thesis work, the water uptake measurements for three Nafion membranes immersed in water at room temperature was carried out. The water sorptions at 30°C in units of number of water molecules per sulfonate acid are 20, 15, and 11 for Nafion membrane with 1100, 1200, and 1500 equivalent weight, respectively. The data of Nafion 117 are consistent with Zawodzinski *et al.*[6-9], Broka *et al.*[51] and Hinatsu *et al.*[50] The data for N120 (1200 EW) is in excellent agreement with that of Hinatsu *et al.*(λ=15), [50] but lower than λ=18.7 reported by LaConti *et al.*[47]

The water equilibrium isopiestic absorptions exposed to vapor phase water by Nafion 117, Dow(XUS) membrane and Membrane C from at 80°C were measured. Figure. 4.1.1 shows the isopiestic sorption curves for the three membranes studied at 80°C. Water activities over the range 0.14 to 1.0 can be accessed using LiCl solutions at room temperature.[8, 9] The curve of Nafion 117 is similar to those of Zawodzinski *et al.*[8] and Hinatsu *et al.*[50] The trends of all three curves are similar to ones at 30°C reported by Zawodzinski, Pushpa, and Pineri,[6-9, 33, 40, 105] and also exhibit typical of weakly cross-linked ion-exchangers in general.[106] The value λ=11.3 corresponding to a_w=1.0 is similar to that of Broka *et al.*[51], but slightly higher than λ=10.0 reported by Zawodzinski *et al.*[8] and Hinastu *et al.*[50]

For comparison purpose, water absorption curves of these three membranes exposed to vapor phase water at 80°C and 30°C (the data at 30°C, previously measured by Zawodzinski *et al.* see Ref. (8) are plotted in Figure 4.1.2-4.1.4. Comparing the results in Figure 4.1.2 4.1.4, all three membranes have similar

behaviors of absorption with increasing temperature. In summary: 1) water uptakes at both temperatures (30°C and 80°C) increase with increasing water vapor activity; 2) increase with a steep rise at $a_w \approx 0.75$; 3) water absorption at 80°C is substantially less in the membranes for $a_w > 0.75$; 4) at unit water vapor activity, λ's, at both 30°C and 80°C, are significantly less than the sorption of membrane immersed in liquid water.

The steep rise in water uptake at both 30°C and 80°C which occurs at $a_w \approx 0.75$ may yield the same conclusion as was noted at room temperature[6-9, 40, 105] that water sorption in $a_w < 0.75$ reflects the solvation by ions, and in $a_w > 0.75$ corresponds to membrane swelling. This phenomenon was observed by heat sorption studies,[31] NMR,[33] and Mossbauer Spectroscopy.[34] Clearly, at the higher temperature there is substantially less water in the membrane at equilibrium with high water vapor activity. This was also observed by Zawodzinski *et al.*[8] This could be primarily due to swelling pressure. In general, the amount of water uptake into the membrane is affected by swelling pressure as the membrane begin to swell.[106] The swelling pressure is proportional to the temperature.[106] At low water content, membrane swelling does not occur, therefore the temperature influence on the water sorption is not observed. However, as the membrane swells, and the temperature increases, the membrane must absorb less water to reduce swelling pressure, and balance the system.

An interesting issue is that the values for liquid water uptake are higher than those of saturated water vapor (both conditions corresponding to unit water activity). The explanation for this phenomenon, known as Schroeder's paradox,[107] was discussed by Zawodzinski *et al.*[7, 9] who explained that sorption from the vapor phase involves condensation of water on the strongly hydrophobic, Teflon-like surface of the polymer, and the difficulty in condensing

vapor within the pores of the membrane is a possible reason for lower water uptake from the vapor phase.

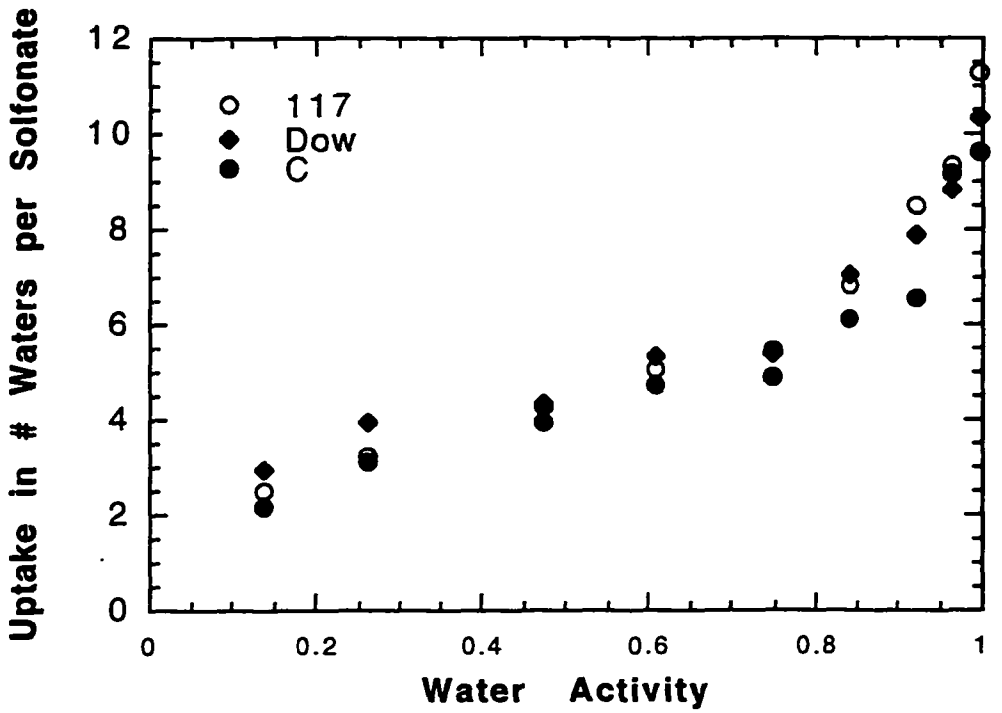

Figure 4.1.1 Isopiestic sorption curves for the three studied membranes at 80°C.

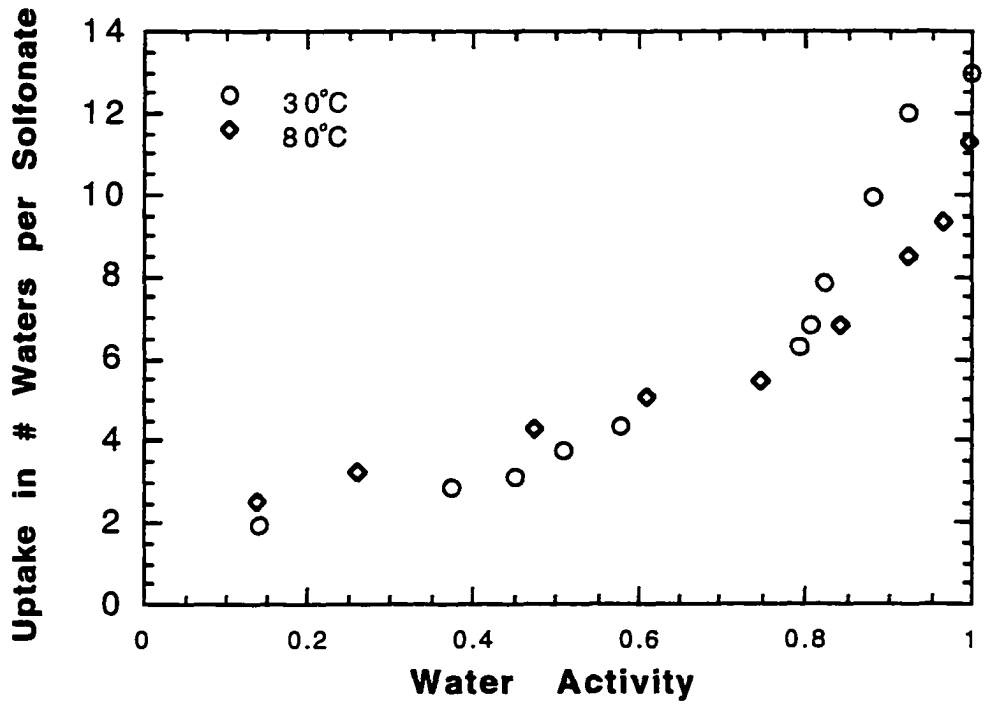

Figure 4.1.2 Comparison of isopiestic sorption curves for Nafion 117 at 30°C and 80°C.

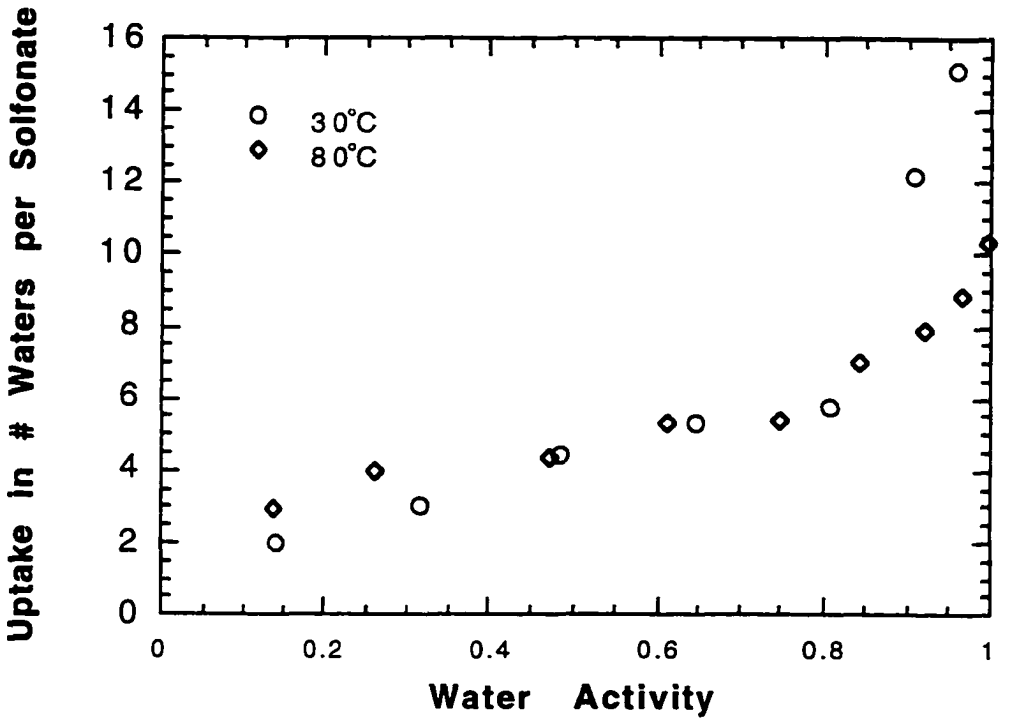

Figure 4.1.3 Comparison of isopiestic sorption curves for Dow (XUS) membrane at 30°C and 80°C.

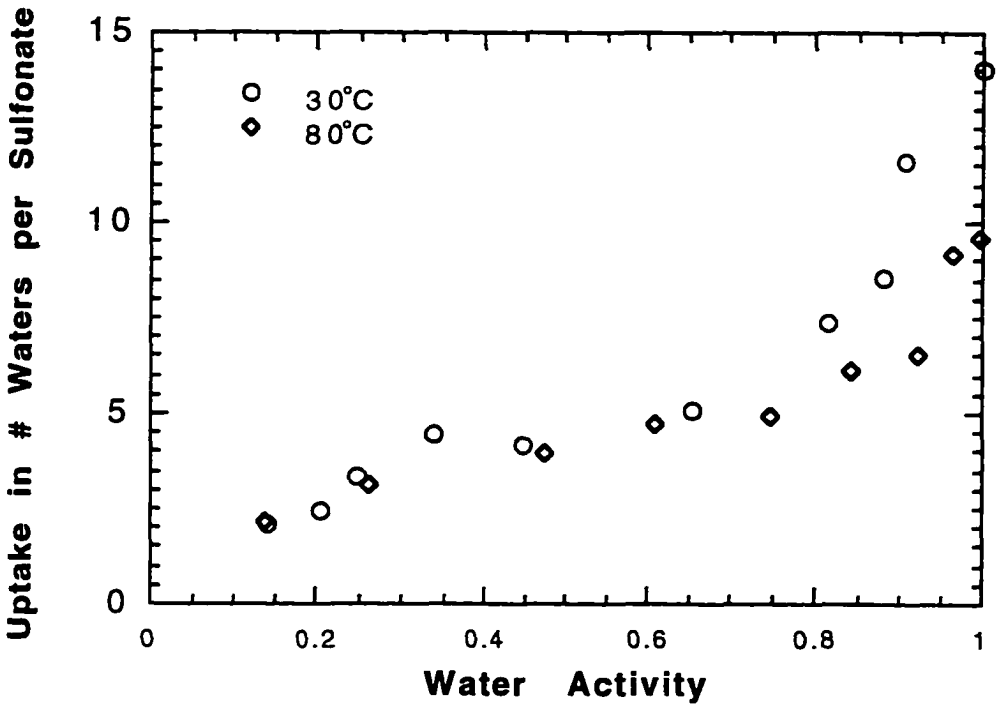

Figure 4.1.4 Comparison of isopiestic sorption curves for Membrane C at 30°C and 80°C.

4-2. Proton Conductivity

Figure 4.2.1 shows the conductivity measurements for three studied membranes, exposed to vapor phase water(100% *RH*), 70 *psi* applied gas pressure, at elevated temperatures 30°C-150°C. The conductivity of all three membranes increases with increasing temperature over the entire range of temperature. The conductivity of Dow is substantially larger than that of two Nafion samples. This is expected since Dow has higher ion exchange capacities and thus larger concentrations of charge carriers than Nafion. The Nafion samples have similar conductivities. This result is also reasonable since N115 and N117 simply are the same materials of different thickness, which confirms negligible contribution of leads and interfaces resistances. This could be checked in this way: Assuming $\sigma_{N117}=\sigma_{N115}$, it is implied that $R_{N117}t_{N117}=R_{N115}t_{N115}$. Where R and t are membrane resistance and thickness, respectively. If the contribution of leads and interface resistances are not negligible, then $(R_{N117}+R')t_{N117}\neq(R_{N115}+R')t_{N115}$, where R' is the interface and lead resistance, will lead to $\sigma_{N117}\neq\sigma_{N115}$. This is contrary to our observation. It is clear that all three curves exhibit non-Arrhenius behavior. This is because the water absorption of PFSA membranes in contact with water vapor in fixed *RH* is a function of temperature. The typical plot of conductivity versus temperature for Dow shown in Figure 4.2.1 deserves more discussion. For fixed water content, λ, it is supposed that there is a linear relation between lnσ and $1/T$, or $\sigma \propto e^{-\frac{E}{kT}}$. The temperature dependence of water uptake of the Dow membrane exposed to constant *RH* vapor phase is shown in Figure 4.2.2. With the membrane exposed to 90% *RH*, the water uptake(λ) by the membrane decreases as temperature is raised from 30°C-80°C then effectively levels off at high

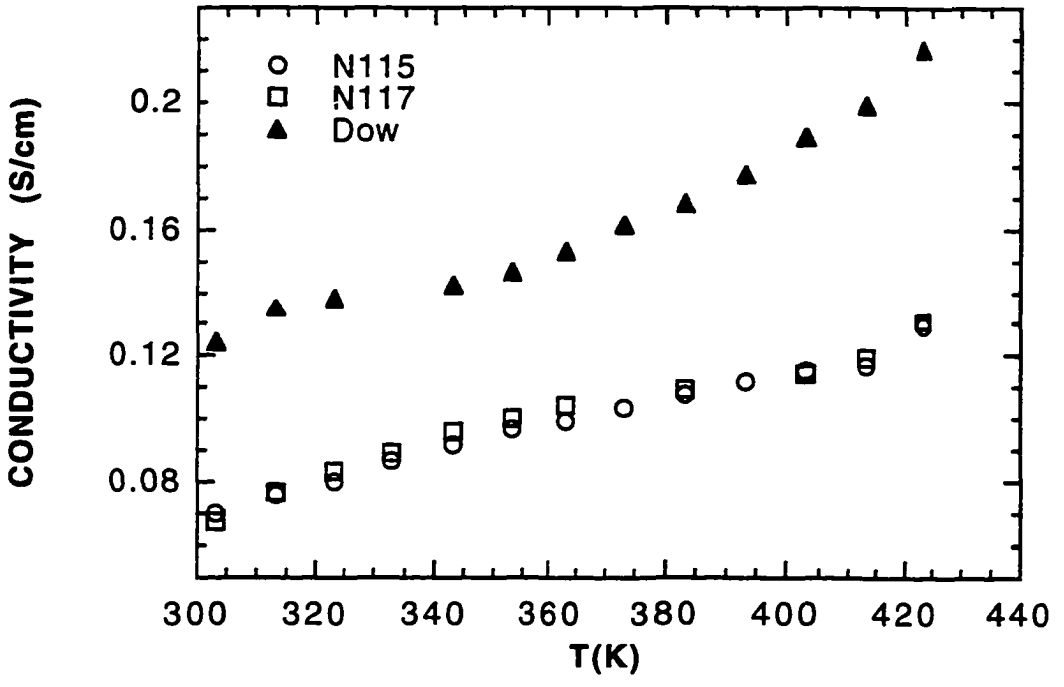

Figure 4.2.1 Conductivities of N117, N115 and Dow in contact with 100% *RH* water vapor at 70 psi as a function of temperature.

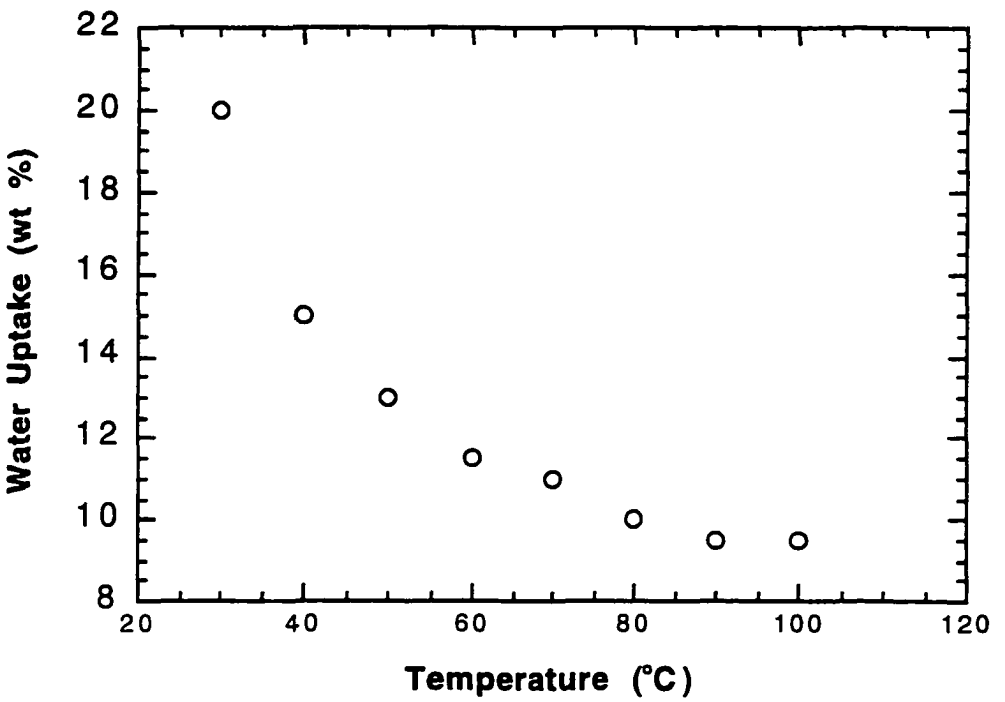

Figure 4.2.2 Temperature dependence of water uptake of Dow membrane exposed to 90% *RH* vapor water. (reproduced from [52])

temperature. Thus, the observed protonic conductivity increases more slowly at low temperature than at high temperature.

The value of conductivity of Nation 117 at 30°C (λ=14 in the presence of saturated water vapor) is 0.068 S/cm, slightly different from previous value, 0.061 S/cm, by T. A. Zawodzinski *et al.*,[8] 0.06 S/cm by Rieke and Vanderborgh[55], and 0.073 S/cm, by J. Fontanella *et al.*[53] This reflects the relative high variability in the membrane conductivity measurements, nevertheless, the conductivity of Nafion 117 under saturated water vapor is around 0.07 S/cm seems an acceptable value according to these independent reports. The conductivity of Dow(XUS) in contact with 100% *RH* water vapor at 30°C is 0.124 S/cm which is higher by a factor of two than A Sen *et al.* data (about 0.06 S/cm).[52] The phenomena reported by Rieke and Vanderborgh [52] has not been observed. In their measurements, membrane conductivity reached a maximum value at about 70°C, and then underwent a steep drop with increasing temperature up to 100°C. One likely explanation is that the membranes in their measurements were not hydrated to steady state condition. This could be caused by insufficient equilibrium time. Rieke *et al.* did not report the waiting time for every temperature increment in their conductivity measurement. It is noted that they reported 60 seconds waited in *IR* measurement (in the same publication). This is much less than the waiting time for the conductivity measurement in this thesis work (two hours is a minimum waiting time observed). In experiments, such as *IR* for determining water content, the hydration method is substantially different from the hydration scheme in the conductivity experiment due to the different steady state. For the conductivity measurements related to partially hydrated membrane, it is much more difficult to obtain water equilibrium than for the fully hydrate case (membrane immersed in water) because of rather hydrophobic "skin" of the membranes.[103] Properly setting the conductivity cell and taking sufficient time for obtaining "real" water

equilibrium in this experiment might be one of the key issues which strongly affects the results.

The conductivities of three Nafion membranes immersed in water at elevated temperatures from 30°C to 80°C are shown in Figure 4.2.3. The value 0.097 S/cm for Nafion 117 at 30°C is in excellent agreement with the value, 0.10 S/cm, reported by Zawodzinski *et al.*[7] The conductivity of Nafion 120 and Nafion 1500 at 30°C are 0.069 S/cm and 0.023 S/cm. The data for Nafion 1500 seems lower by a factor of two than expected. If we assume Grotthus hopping (definition see section 1-2-5 and Ref. [108]) is the primary mechanism, the membrane conductivity is expect to be H^+ conduction and proportion to the water content in membrane. According to the sorption data, Nafion 117 (λ=20-22) and Nafion 120 (about λ=15), the somewhat lower conductivity of the latter membrane is consistent with that expectation. Nafion 1500 deviates from this trend. One argument could be that the pore size of Nafion 1500 is similar to Nafion 117 and Nafion 120 while the polymer chain structure is significantly different from Nafion 117 and Nafion 120. Proton hopping process might occur near the fixed-charge sites. As pointed out by Verbrugge,[58] the central region of the pore may not provide a substantial proton transport pathway. Therefore, the proton transport is more sensitive to the membrane porosity than pore breadth for these membrane. Figure 4.2.4 shows the Arrhenius plot for temperature dependence of the conductivity of three Nafion samples immersed in water. The activation energies for three samples are similar over the temperature range from 30°C to 90°C. This indicates that at high water content (λ>5) the proton transport occurs in the similar environment. A detailed discussion comparing these results with diffusion data is given in section 4-4-2.

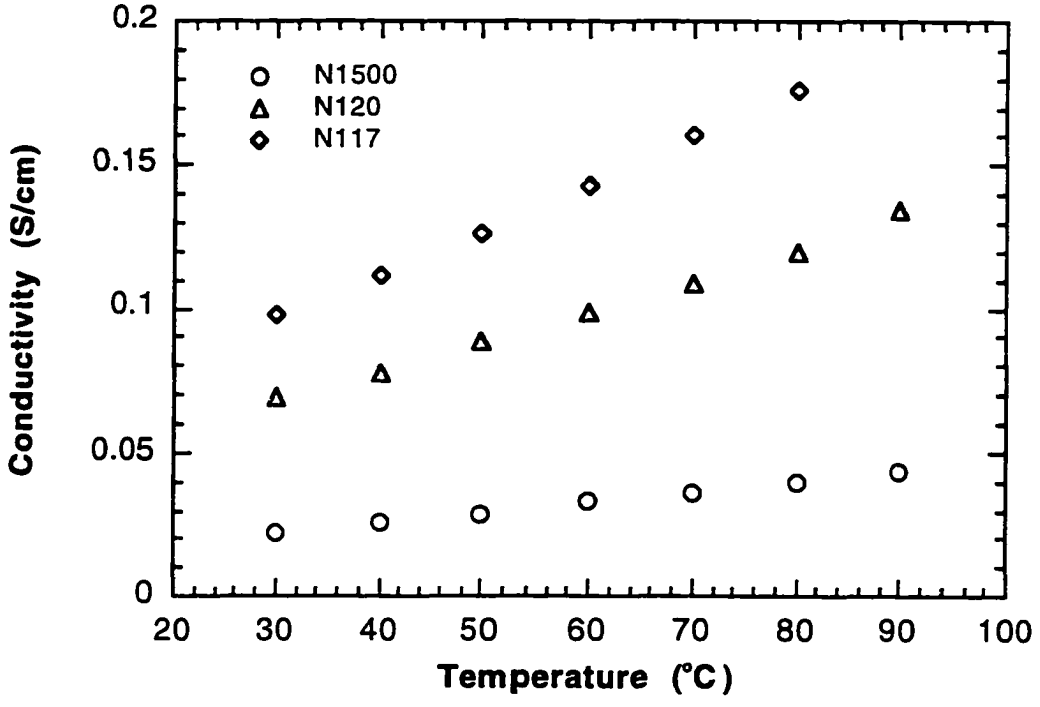

Figure 4.2.3 The conductivity of three Nafion samples immersed in water at elevated temperatures.

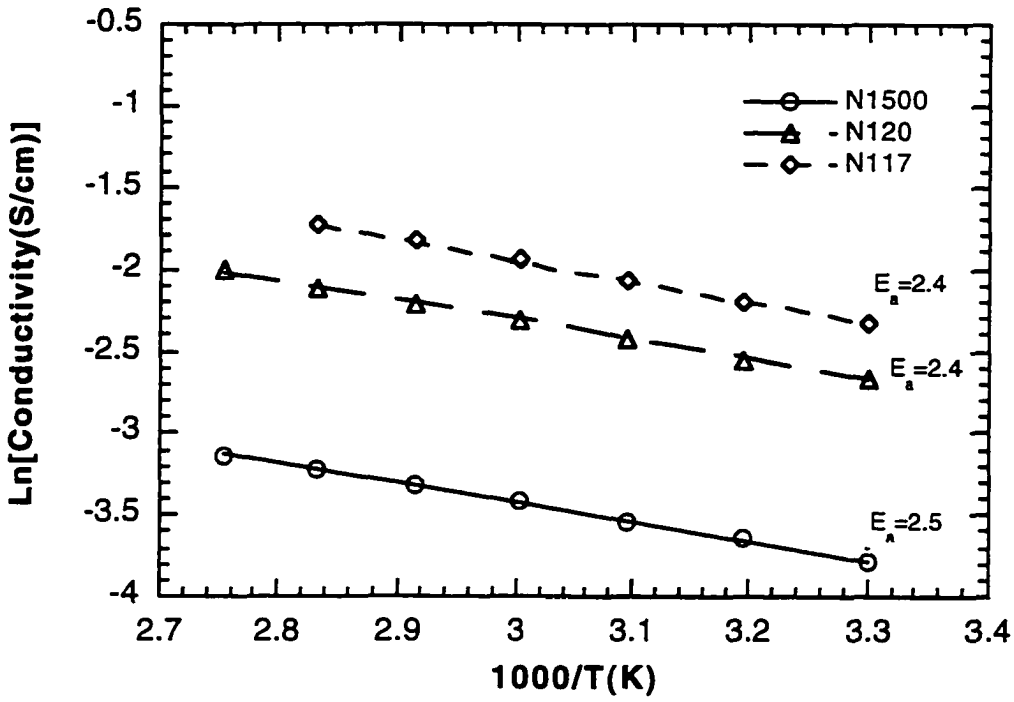

Figure 4.2.4 Arrhenius plot for temperature dependence of the conductivity of three Nafion samples immersed in water. (E_a: kcal/mol)

It is important to know the temperature dependence of the membrane conductivity for a given water content (fixed λ). However, measurements are difficult to make. First of all, according to our experience with water sorption measurements, the water content can be sensitive to details of conditions. Secondly, the membrane hydration state depends on membrane thermal history. Hence, a unique λ for the membrane in the environment with a certain *RH* may not be obtained without matching the thermal history for all the samples. Thirdly, when exposed to water vapor with certain *RH*, the water uptake into the membrane is a function of temperature (see Figure 4.2.2 and discussion following it). In order to extend our knowledge regarding the membrane conductivity *vs.* temperature under the condition of fixed λ, conductivity measurements of membrane at several low water contents were performed. Based on quite a large amount of water uptake data, particularly, data collected by Zawodzinski *et al.* [6-9] and Pushpa *et al.*,[40] at sufficiently low water content (about $\lambda<5$, or 10w% water in Nafion 117), membrane water contents are relatively stable over a certain range of temperature, we are able to analyze some data (at least qualitatively), obtaining the T dependence of conductivity at low water contents and get some insight into membrane transport mechanism. Numerous authors have pointed out the significance of this low λ region in the transport mechanism. Figure 4.2.5 shows the protonic conductivity of a Nafion 117 membrane exposed to vapor phase of water at four different water activities. For a_w=0.474 and a_w=0.610, the conductivities start to decrease significantly at 60°C. This is because the membrane water content decreases significantly with increasing temperature above 60°C. However at a_w=0.260 (λ=3.6±0.6) and a_w=0.139 (λ=2.2±0.2) the membrane conductivities exhibit no significant deviation from Arrhenius behavior over the

temperature range between 30°C and 80°C. The Arrhenius plots of the temperature dependence of Nafion 117 in contact with water vapor at these four water activities are shown in Figure 4.2.6. Activation energies for the four samples decrease with increasing water content. The activation energy changes only slightly for three high water content samples, then shows significant change at low water content. This may imply a distinct proton transport mechanism for this very low water content. (more detailed discussion is deferred until section 4-4-2)

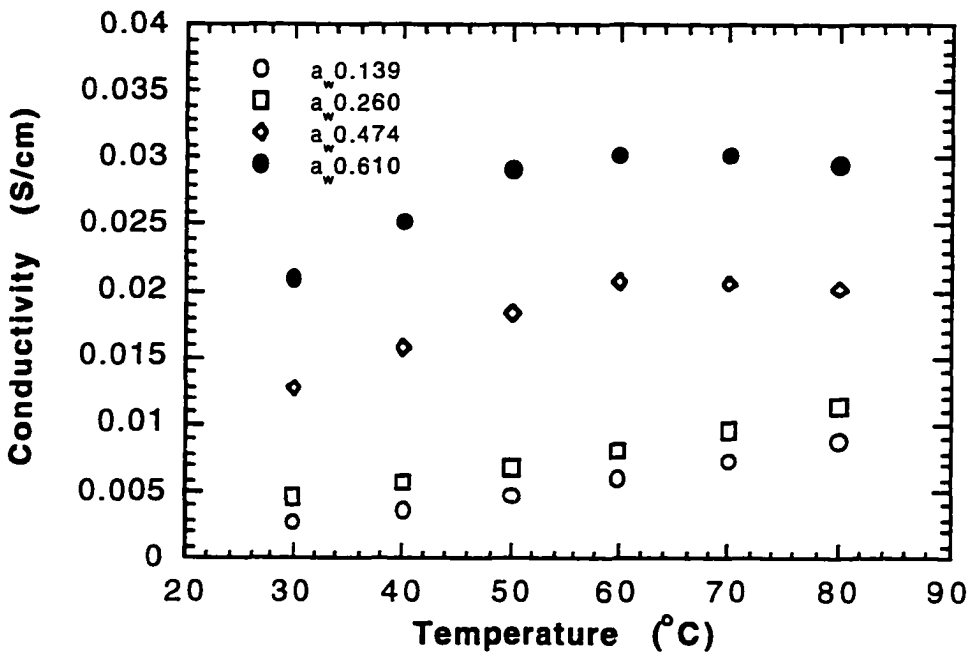

Figure 4.2.5 Temperature dependence of the conductivity of Nafion 117 exposed to vapor phase water at four low water contents.

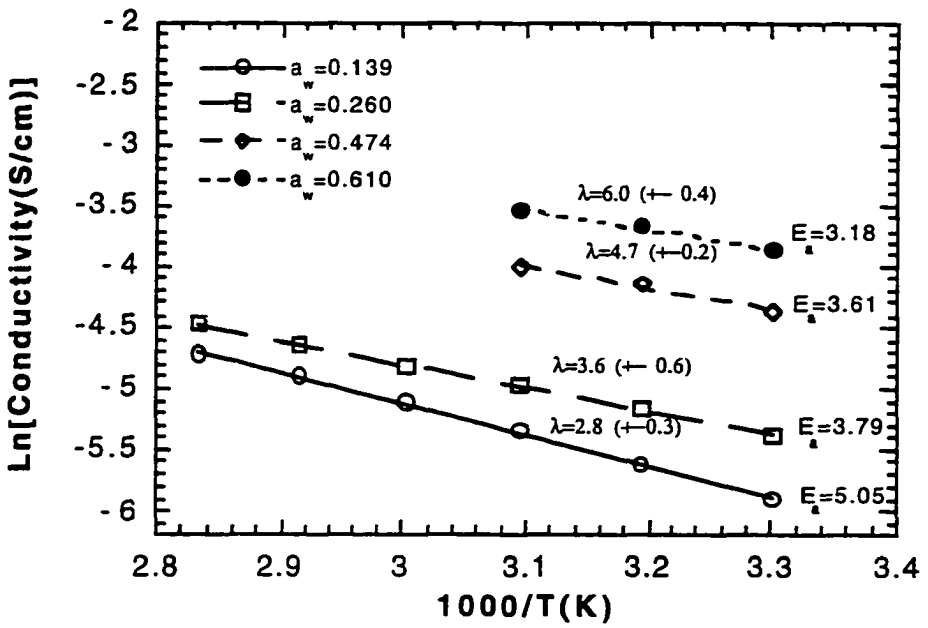

Figure 4.2.6 Arrhenius plot for temperature dependence of the conductivity of Nafion 117 at four low water contents, at 70 psi. (E_a: kcal/mol)

4-3. Electro-Osmotic Drag Coefficient

In this thesis work, the electro-osmotic drag coefficients of several partially hydrated PFSA membranes were measured at 80°C using the same method as by Newman and Zawodzinski *et al.* All the membrane samples were exposed to water vapor phase, over a range of water activity from 0.1 to 1.0 (water content between λ=1.4-10) Figure 4.3 shows cell potential measured *vs.* the water activity ratio. Again, there is a similar result at 30°C as shown by Zawodzinski *et al.*[10] The drag coefficients over the entire range of water activities for all three types of membranes are constant. The fits yield ξ=1.02, 0.98 and 1.09 for Membrane C, Dow Membrane and Nafion 117, respectively.

This seems to be a surprising result. The first, the drag coefficients are practically the same for three different equivalent weights and over the temperature range from 30°C -80°C. This is in contrast to the case of membrane equilibrated with liquid, where Zawodzinski *et al.*[10] observed that the drag coefficient is a function of membrane equivalent weight. This seems reasonable since normally membrane with different equivalent weight absorb different amount of water. Ren *et al.*[109] determined the water drag coefficient for Nafion 117 immersed in water at elevated temperatures over the range from 20°C to 130°C using an electrochemical method. The measured drag coefficients varied over the range from 1.9 to 5.1 as a function of temperature. There is a substantially change in ξ with T shown in their experiment. In contrast, for the vapor equilibrated case, there is no observable difference of the drag coefficient values at 80°C from that at 30°C as shown by Zawodzinski *et al.*[10] That the drag coefficient is not only independent of membrane hydration degree and membrane microstructure, but also temperature (at least in this experiment temperature range) is really beyond our expectation. This obviously conflicts with out physical intuition because such a water-ion

coupling effect should reflect the influence of these factors, at least from the point of view of bonding energy considerations.

Breslau and Miller[66] determined water drag coefficients for various anions and cations, and developed a hydrodynamic model for electro-osmosis in ion-exchange membranes based on the unidirectional flow of macroscopic spheres in a homogeneous bounded medium. In their model, parallel plate pores and cylindrical pores are employed for the membrane pore structure. They also assumed that the ions are partially stripped of their hydration sheaths with the membrane. Most experimental data (excluding the results for H^+) were found to agree with calculated electroosmotic coefficients, which took into account due to ion-solvent interactions, and the molecular size of the ionic sphere. They found a slightly better fit for the proton if one considers proton jumping mechanism and using parallel plate model. The Breslau and Miller model is difficult to use to predict PFSA membrane electroosmotic drag coefficient because of the lack of available data regarding pore sizes in the many of membranes.

One can compare the drag data with the diffusion data. An apparent trend is that the water diffusion coefficients of PFSA strongly depend on the water content in the membranes and the membrane structure, while the drag coefficient does not. It is somewhat surprising that the drag coefficients in the case of the membrane exposed to vapor water are substantially independent of water content. One argument might be that these two parameter (ξ and λ) reflect different transport mechanisms over the different scales of the membrane structure. Zawodzinski *et al.* suggested[10] that one possibility is the electroosmotic drag might be determined by local water structure in the membranes. They consider a reasonable sulfonate/water/proton local structure: the amount of water, roughly 5-6 H_2O/H^+.[8, 110] Directly associated with this structure is the number of waters per sulfonate which are the non-swelling fraction of water in the membrane. In addition, if we

assume ion H_3O^+ as the mobile species exist, the water associated with it in the primary shell is about 3 molecules.[111] Supposing the measured drag coefficient reflects to some extent the amount of water associated with proton transport, it would be then similar for all the vapor phase case.

Essentially, electro-osmotic drag reflects the Coulomb interaction between proton and water molecule in the membranes. Such a electrostatic interaction is strongly affected by the distance between water molecules and ions which could be changed by temperature, membrane swelling condition and membrane microstructure *etc.* If we assume that the interaction scale is about nanometer, 10^{-9} m, such an unscreened, long-range Coulomb interaction is extremely strong between two ions. However, we should consider an electrostatic "screening" effect because of dipole molecules (water) involved in this case. And due to dipole molecules, the electric field becomes screened and decays more rapidly away from them than from a truly isolated ion. At large distances, the decay is very quick with distance, thus making all Coulomb interactions between ions of much shorter range (though still of much longer range than covalent forces).[112] Thus, the scale of the effective interaction between proton and water becomes quite local because of a rapidly decaying Coulomb interaction between them. This screened Coulomb force may explain the electro-osmotic data in both cases - low and high water content in the membrane. Since at low water content, the motion of protons could be mainly contributed by diffusion of protons associated with relatively fixed number of water molecules, the electro-osmotic drag coefficients could be the same over this water content range due to similar local situation and motion mechanism. In contrast, the hopping mechanism determines proton movement at high water content (water in the membrane is more bulk-like) so that effective Coulomb interaction become less local than in the low water content case. Hence, the electro-osmotic drag coefficient for an immersed membrane is substantially higher than that in a partially hydrated

membrane. Note that temperature might not significantly effect the hydration number (the number of water molecules in primary shell), but significantly influences the hopping frequency. That's why the drag coefficient is insensitive to temperature (in the experiments done) for low hydration membranes, while relatively sensitive for high hydration membranes.

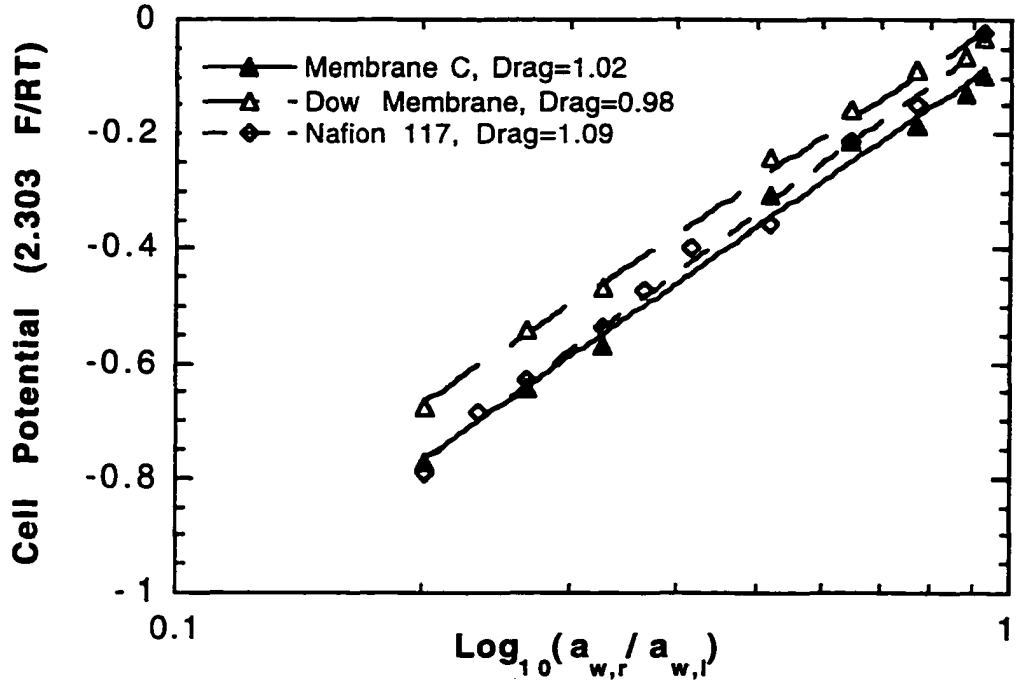

Figure 4.3 Plot of measured potential *vs.* water activity ratio, obtained for three studied membranes in a concentration cell for ξ measurements.

4-4. NMR Measurements

4-4-1. High Pressure NMR

1. Deutron NMR

In this thesis work, deuteron NMR spin-lattice relaxation times (T_1) in three different molecular weights of acid form PFSA membranes conditioned at various levels of relative humidity have been carried out. The measurements were made at room temperature and pressure up to 0.25 GPa. Figure 4.4.1 shows pressure dependence of deuteron T_1 for Nafion 120 with two water contents. Figure 4.4.2 shows pressure dependence of deuteron T_1 for three studied PFSA membranes with similar water contents. Table 4.4.1 lists the activation volumes extracted from the deuteron T_1 pressure dependence. It is clear from the results presented here that the activation volume *vs.* water content curve exhibits two well-defined regions, one for $\lambda<5$ where the activation volume is significantly larger than for $\lambda>5$, and another for $\lambda>5$ where the activation volume is approximately constant at about 3 cm^3/mol. These two regions are correlated with the ability of Nafion to absorb water from the vapor phase.[7] $\lambda<5$ (region *i*) is the region corresponding to solvation of the proton and sulfonate ions, while for $\lambda>5$ (region *ii*) the polymer begins to swell. The results from deuteron NMR seem to support such explanations: 1) the activation volumes yielded in these two regions imply that there might be two distinct transport mechanisms in these two regions. 2) at the high water content $\lambda>5$, the activation volume is the largest for the highest molecular weight membrane. This suggests that, even for high water content, rotational motion, which again is the primary relaxation mechanism, is still influenced by polymer structure.

Table 4.4.1 Activation volumes extracted form the deuteron T_1 pressure dependence. Measurements were made while decreasing the pressure.

	Activation volumes (cm^3/mol)		
λ	Membrane C	Nafion 117	Nafion 120
9.9	2.3±0.2		
12.1		2.6±0.2	
12.0			2.9±0.1
3.6	4.2±0.1		
6.6		2.8±0.7	
4.1			4.0±0.1
3.3		4.6±0.2	

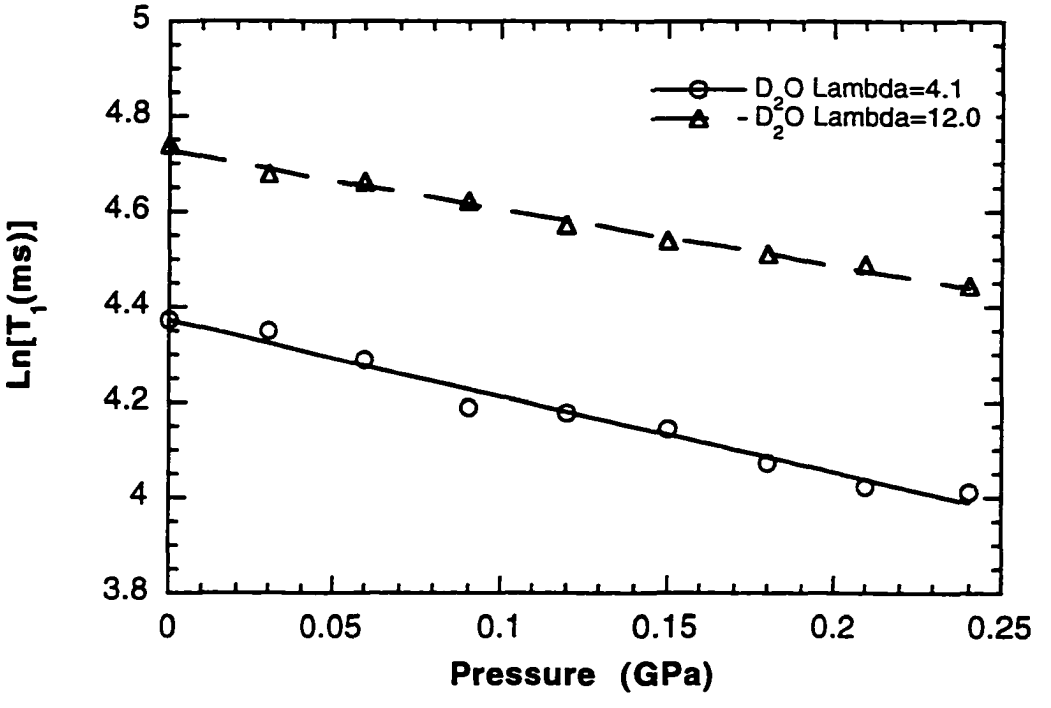

Figure 4.4.1 Pressure dependence of deuteron T_1 for Nafion 120 with λ=12.0 and λ=4.1.)

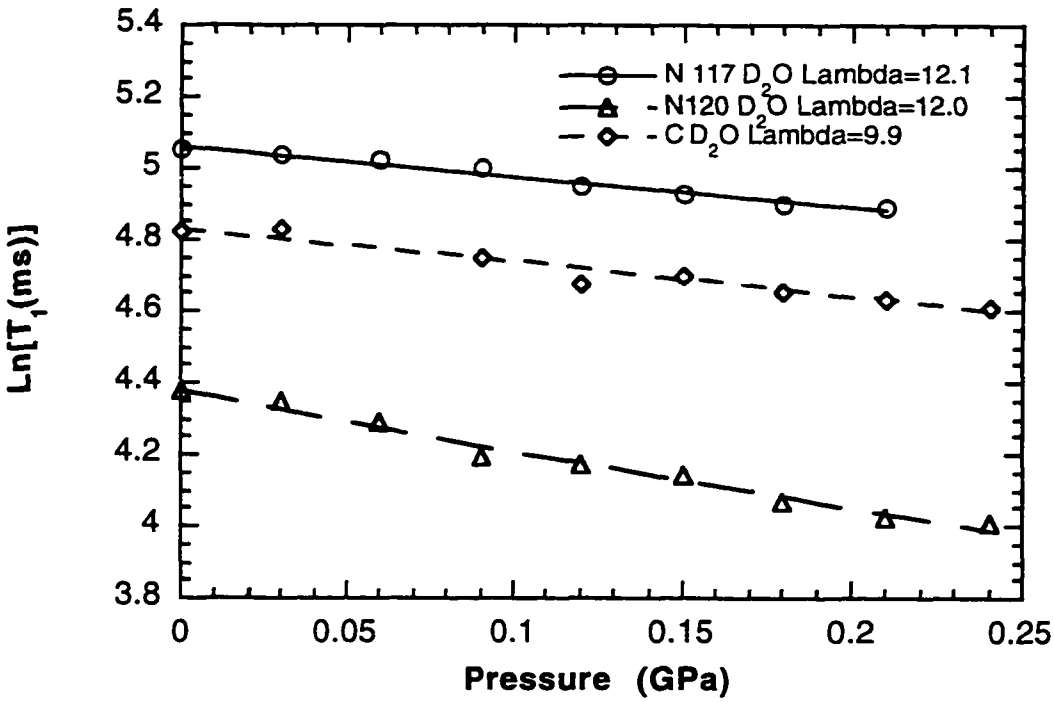

Figure 4.4.2 Pressure dependence of deuteron T_1 for Nafion 120 with λ=12.0, Nafion 117 with λ=12.2, and Membrane C with λ=9.9.

2. Proton and Fluorine-19 NMR

^1H and ^{19}F T_1 measurements have been made, the former as a probe of water molecular motion and the latter reflecting relaxations of the main polymer and pendant chains. The data of ^1H for three studied membranes and several water contents are displayed in Figures from 4.4.3 to 4.4.5. While single, straight-line fits to some of the data (in particular λ=5.6 in Figure 4.4.3, and λ=12 in Figure 4.4.5) are not entirely appropriate, the average slopes are still regarded as meaningful because of the trend of decreasing average slope with increasing water content. Straight-line fits to the data yield activation volumes that are listed in Table 4.4.2. The ^{19}F T_1 measurements for the same three membranes are plotted in Figures from 4.4.6 to 4.4.8. Because of substantial scatter within the very small variation of ^{19}F T_1 *vs.* pressure, the corresponding activation volumes for most of the samples are not regarded as significantly different from zero. Straight-line fits for those samples that exhibit noticeable pressure dependence (Nafion 105 with λ=2.0 and Nafion 117 with λ=2.5 and 13.4) yield activation volumes of about 1.5±0.5 cm^3/mol.

For comparison with the ^1H NMR results for Nafion, T_1 *vs.* pressure data for two different water/H_2SO_4 solutions, corresponding to λ=5 and λ=2 (that is , λ=H_2O/HSO_4^-), are displayed in Figure 4.4.9. Again, because of the small fluctuations of the data about approximately zero slope, the activation volumes for water/H_2SO_4 solutions are regarded as essentially zero, at least in the pressure range employed in this investigation.

For all three membranes, there are two clear trends regarding the ^1H NMR data: 1) T_1 increases with increasing water content; 2) the activation volume increases with decreasing water content. The first observation simply reflects the

decreased water molecular mobility at lower water content, which enhances the relaxation by decreasing τ_c toward the value of ω^{-1}. The second trend could be explained as follows: at low water content, water molecular relaxation requires some assistance from pendant chain motions, thus leading to increased activation volume. The activation volume at high water content, not surprisingly, approaches the value of liquid water (nearly zero in the current pressure range). The addition of H_2SO_4 to water does not appreciably change the activation volume, as indicated in Figure 4.4.9.

The ^{19}F relaxation data exhibit no clear trends, that is, T_1 is approximately independent of both water content and pressure. Given that over 80% of the fluorines reside in the relatively immobile (and, in the current pressure range, imcompressible) PTFE backbone, this result is not entirely unexpected. For the samples that do show a slight pressure dependence, the small and positive activation volumes might indicate restricted polymer motion under pressure.[65]

Table. 4.4.2 Activation volumes extracted from ^1H NMR T_1 pressure dependence. Measurements were made while decreasing the pressure.

wt % H_2O	λ	ΔV (cm^3/mol)
	Nafion 105	
4.0	2.3	5.0±0.2
10.0	5.7	3.6±0.2
27.0	15.4	2.6±0.3
	Nafion 117	
4.0	2.4	4.8±0.4
10.4	6.2	3.5±0.3
20.8	12.3	0.5±1.0
	Nafion 120	
3.0	2.0	4.5±0.4
8.7	5.8	2.8±0.3
18.0	12.0	0.3±1.0

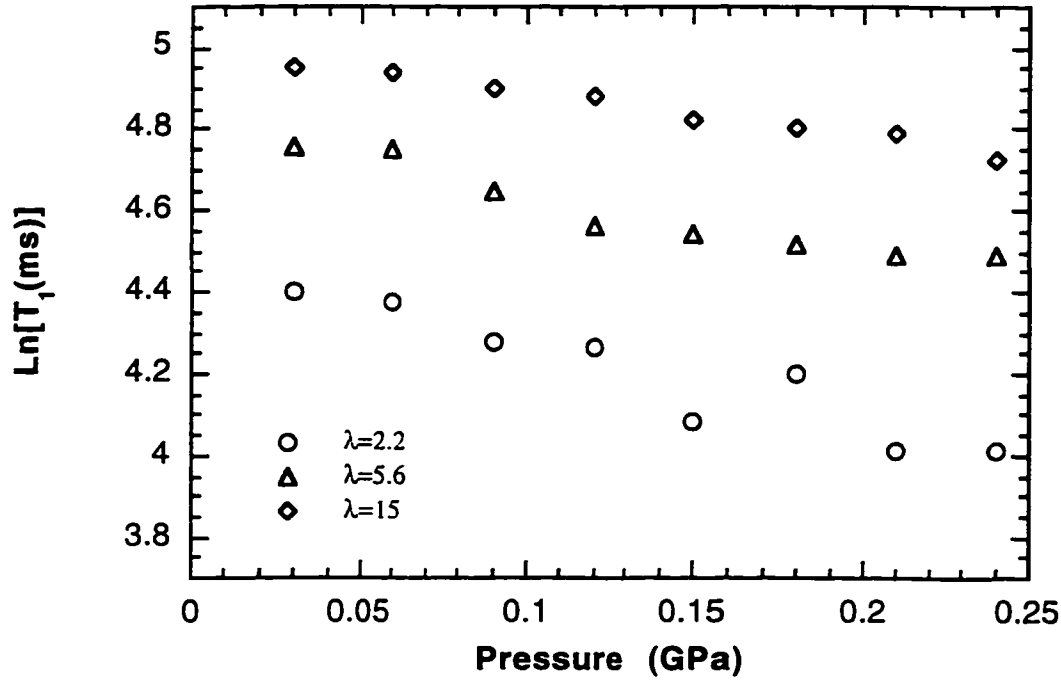

Figure 4.4.3 Proton NMR T_1 *vs.* pressure for Nafion 105 at various water content.

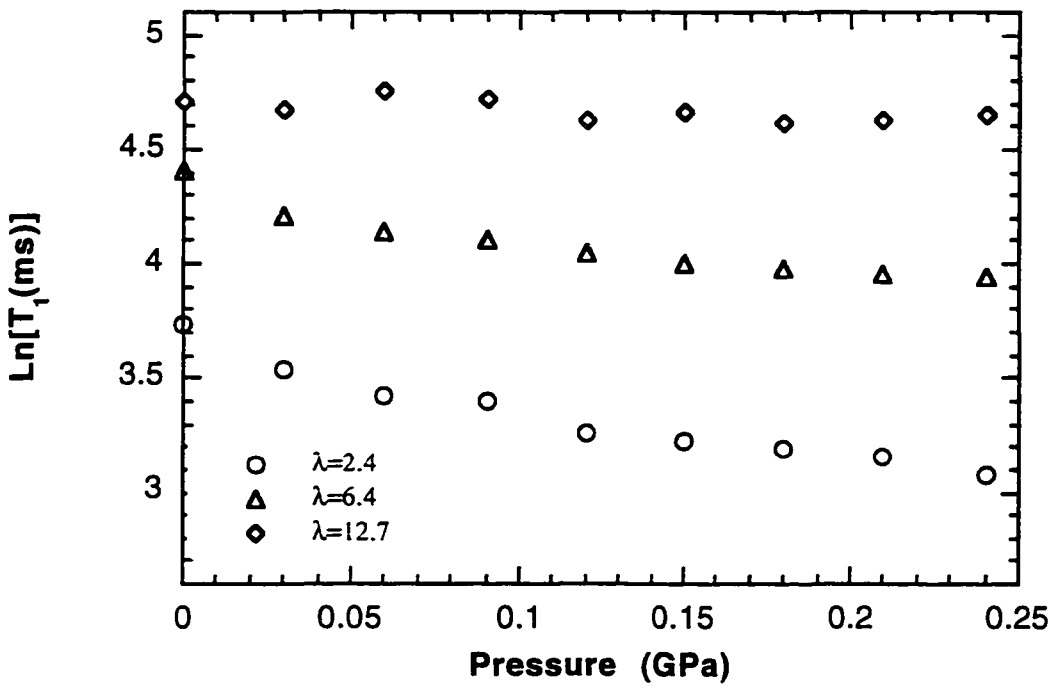

Figure 4.4.4 Proton NMR T_1 *vs.* pressure for Nafion 117 at various water content.

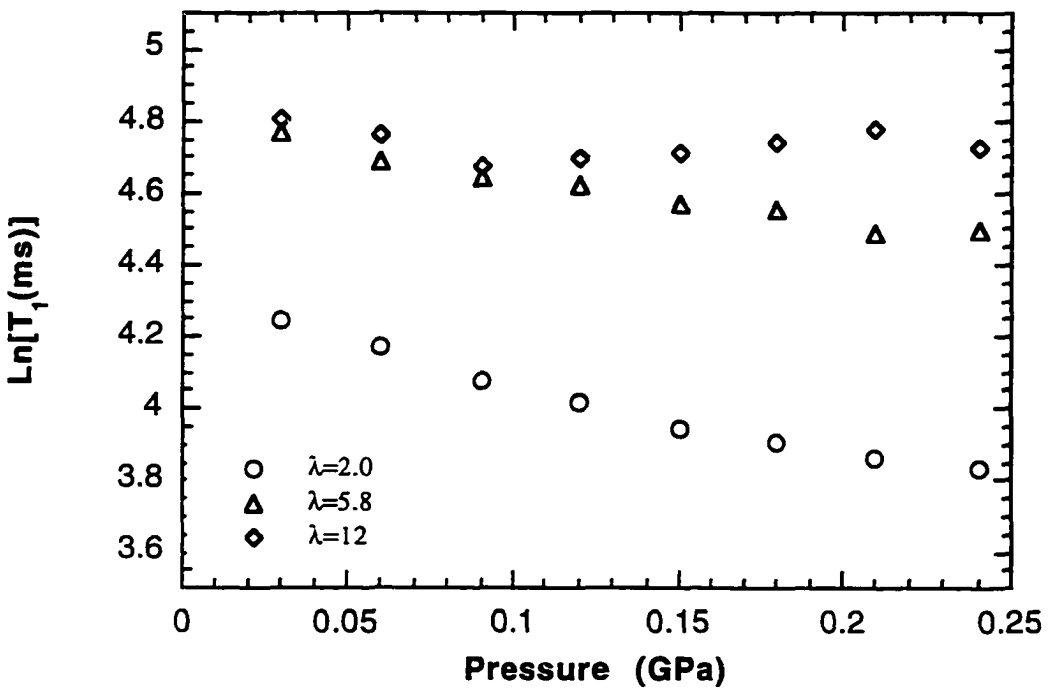

Figure 4.4.5 Proton NMR T_1 *vs.* pressure for Nafion 120 at various water content.

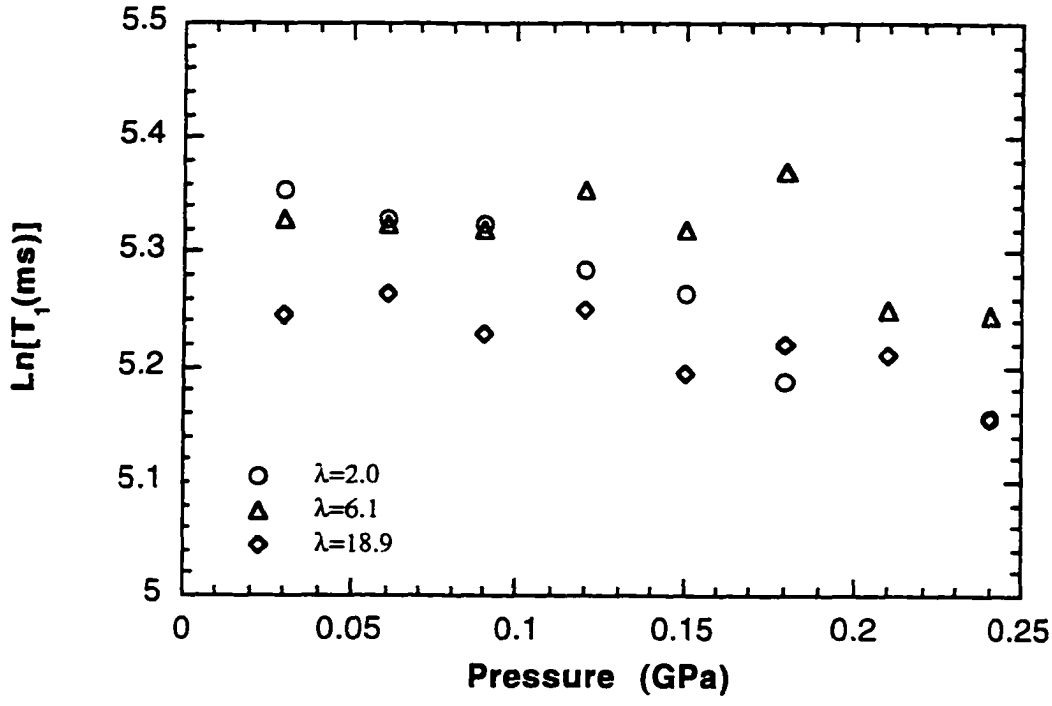

Figure 4.4.6 Fluorine-19 NMR T_1 *vs.* pressure for Nafion 105 at various water content.

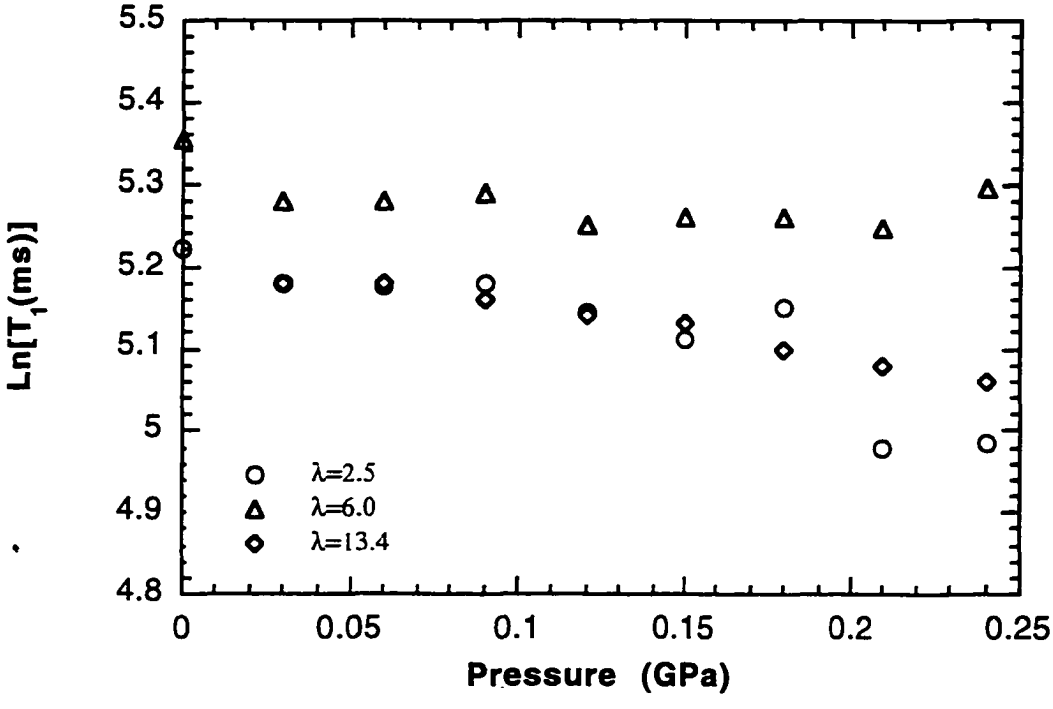

Figure 4.4.7 Fluorine-19 NMR T_1 *vs.* pressure for Nafion 117 at various water content.

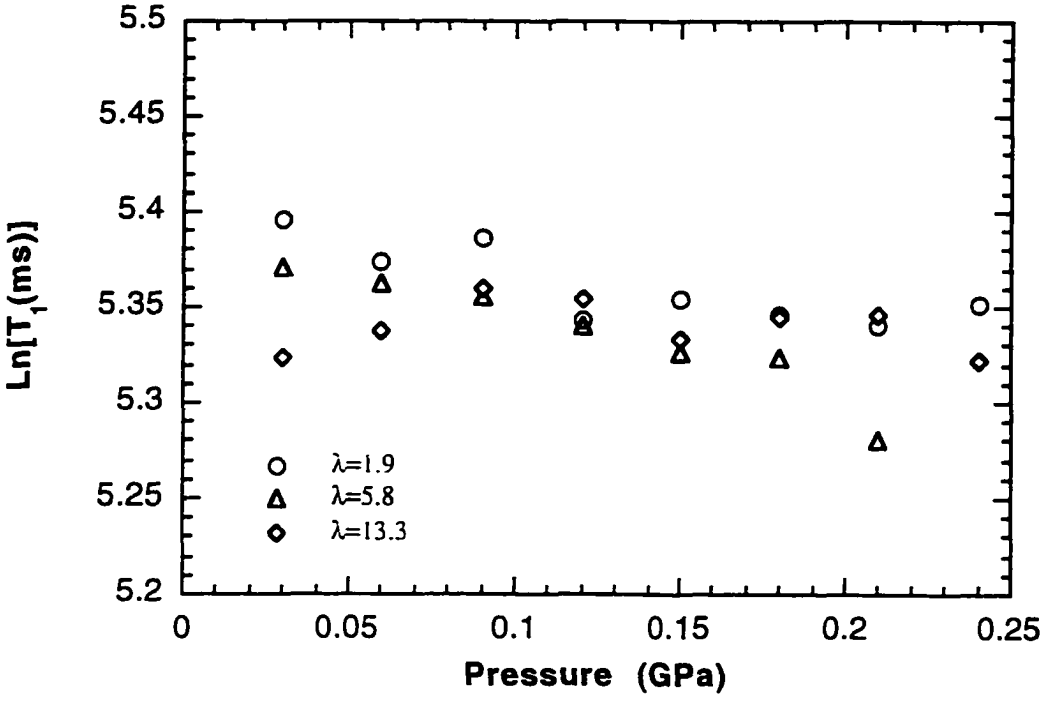

Figure 4.4.8 Fluorine-19 NMR T_1 *vs.* pressure for Nafion 120 at various water content.

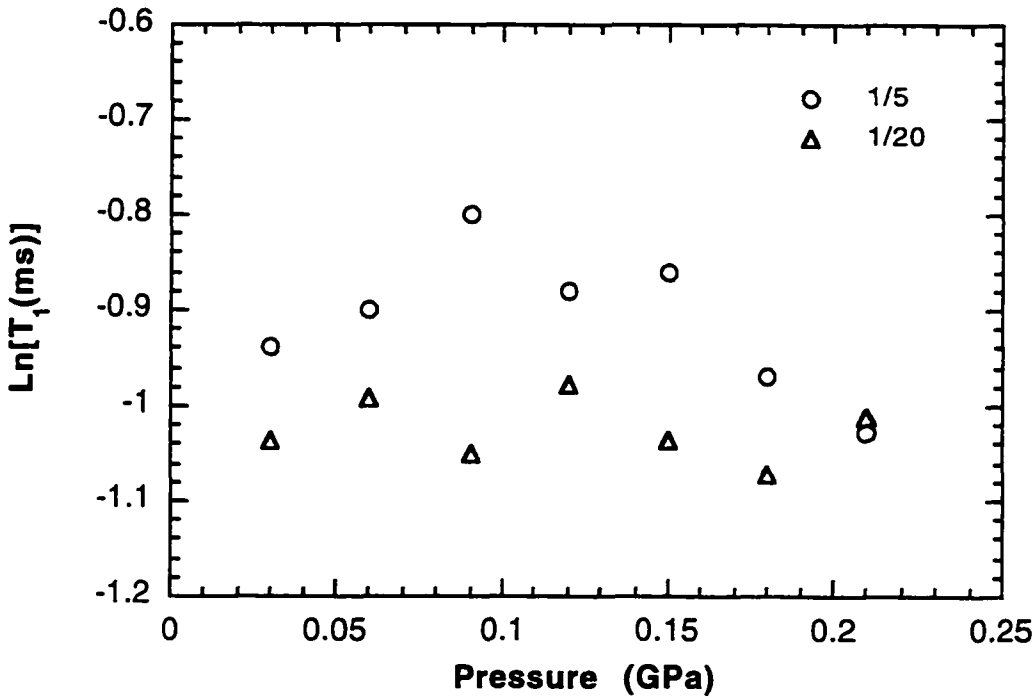

Figure 4.4.9 Proton NMR T_1 *vs.* pressure for various amounts of sulfuric acid in water.

4-4-2. Self-Diffusion Coefficient

The temperature dependence of ^1H self-diffusion coefficients using NMR pulse-gradient spin-echo (PGSE) for various PFSA membranes are studied in this thesis work. All diffusion data in this work are given in Table 4.4.3 and Table 4.4.4. The Arrhenius plots of diffusion coefficients of Nafion 117, Dow Membrane and Nafion 105 exposed to water vapor at elevated temperatures are displayed in Figure 4.4.10-4.4.12. The diffusion coefficients for Nafion 117 at 30°C and 80°C are plotted in Figure 4.4.13 as a function of temperature and water content. The activation energy values for water diffusion in various membranes at various water contents are shown in Table 4.4.5.

Some conclusions from the diffusion data could be summarized as: 1) the diffusion coefficient increases with increasing water content (up to 100% *RH*) at all T's; 2) diffusion coefficient significantly increases with increasing temperature over this temperature range; 3) As see in Figure 4.4.13, a plot of diffuison coefficient of water in Nafion 117 at 30°C and 80°C, over the range of water content λ from 2 to 14, diffusion at 80°C is higher than at 30°C by a factor of 3 to 4; 4) there is a slight variation in activation energy at high water content, but a significant change in activation energy occurs at low water content.

A typical value of the water diffusion coefficient from Figure 4.4.13, for λ=14 in Nafion 117 at 30°C is 6.6×10^{-6} cm^2/s which is similar to the value reported by Zawodzinski (5.8×10^{-6} cm^2/s)[6] and Kreuer's (about 6.5×10^{-6} cm^2/s).[59, 60] This seems not unexpected since all these workers used similar NMR methods, and there should be a reasonable agreement between these measurements.

Table 4.4.3 Water diffusion coefficients from this thesis work in several PFSA membranes at various water contents at elevated temperatures. (D in 10^{-6} cm^2/s)

Membrane	a_w	λ (H_2O/SO_3H)	40°C	50°C	60°C	70°C	90°C	100°C
Dow	1.0	14.0	7.88	20.47	25.28	28.79	34.27	41.32
	0.88	9.8	8.87	16.19	19.61	22.35	28.51	30.20
	0.45	3.3	6.14	14.53	16.93	19.32	26.30	28.02
	0.14	2.0	0.756	0.912	1.28	1.97		
N105	1.0	30.5	16.01	22.02	28.32	37.36	45.22	42.58
	0.88	16.0	13.63	17.60	22.10	29.08	33.43	39.99
	0.45	5.5	8.21	13.28	16.15	14.68	28.01	29.35
	0.14	2.7	7.08	9.04	13.97	16.72		
N117	1.0	14.0	8.74	14.62	15.79	19.49	29.59	33.47
	0.88	9.8	7.38	12.76	16.54	17.99	24.55	28.70
	0.45	3.3	5.64	8.78	11.22	12.37	17.10	21.13
	0.14	2.0	0.434	0.476	0.663	0.874	1.66	1.84

Table 4.4.4 Water diffusion coefficients from this thesis work in Nafion 117 at various water contents at 30°C and 80°C. (D in 10^{-6} cm^2/s)

λ	14.0	13.6	12.2	10.2	8.1	4.6	3.0	2.0
30°C	6.58	5.93	5.46	4.78	3.98	2.58	1.17	0.604
80°C	21.79	20.83	20.74	17.25	13.78	8.96	4.48	1.68

Table 4.4.5 Activation energy for ^1H self-diffusion coefficient in various membranes at various water contents. (activation energies in kcal/mol)

λ (H_2O/SO_3H)	Dow Membrane	Nafion 105	Nafion 117
30.5		3.3	
16.0		3.7	
14.0	3.1		3.7
9.8	3.0		3.7
5.5		4.1	
3.3	3.3		4.0
2.0	6.8		6.7

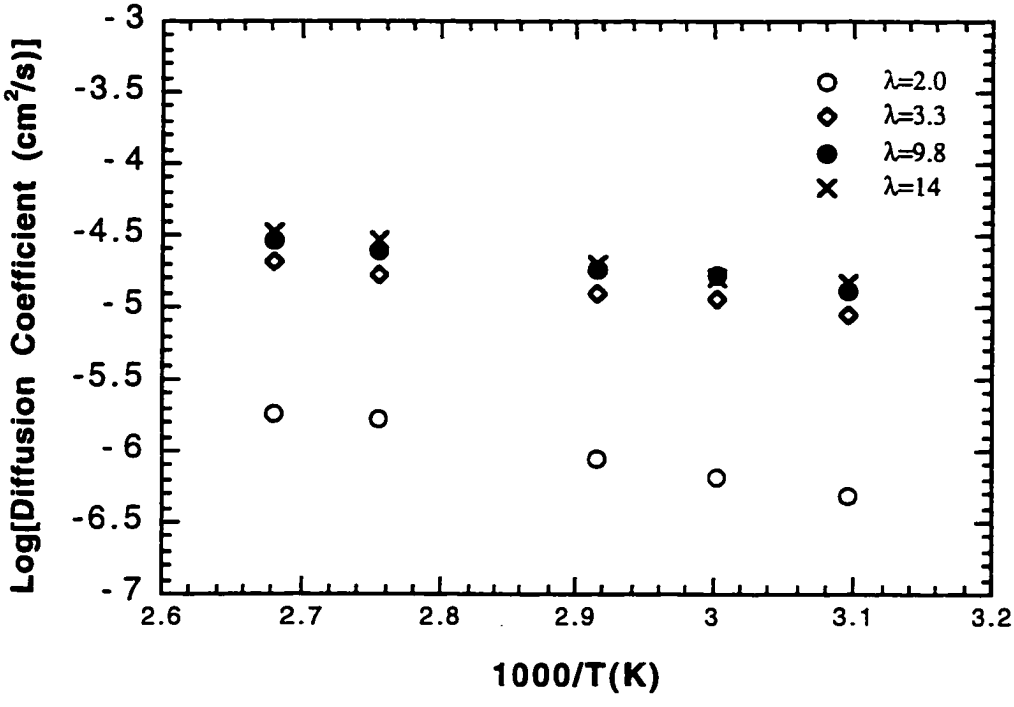

Figure 4.4.10 Arrhenius plot of temperature dependence of diffusion coefficient of Nafion 117 for various water contents.

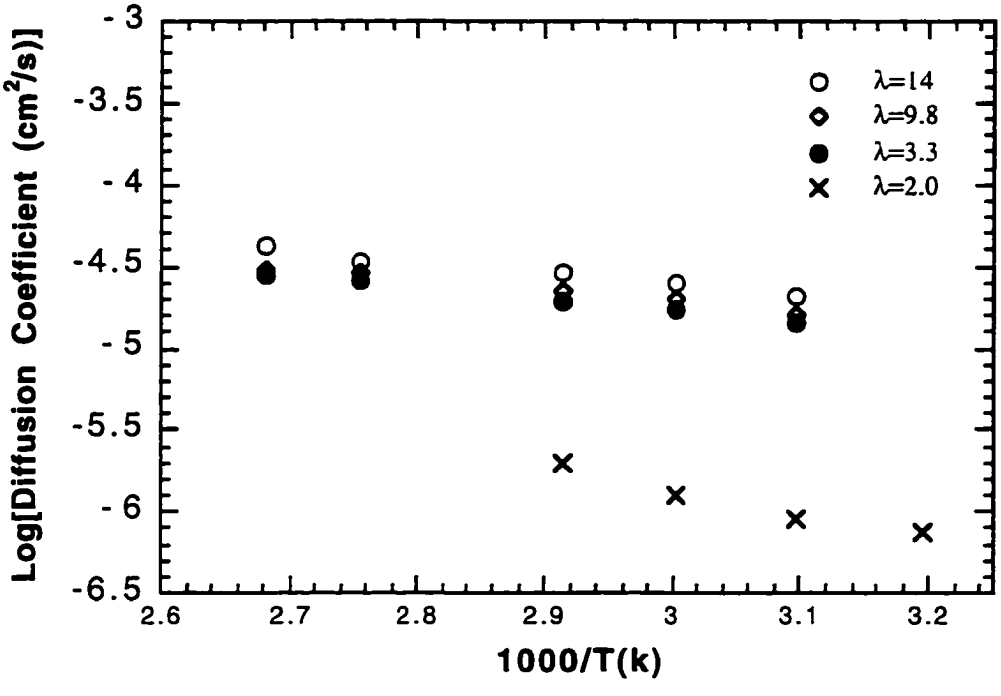

Figure 4.4.11 Arrhenius plot of temperature dependence of diffusion coefficient of Dow Membrane for various water contents.

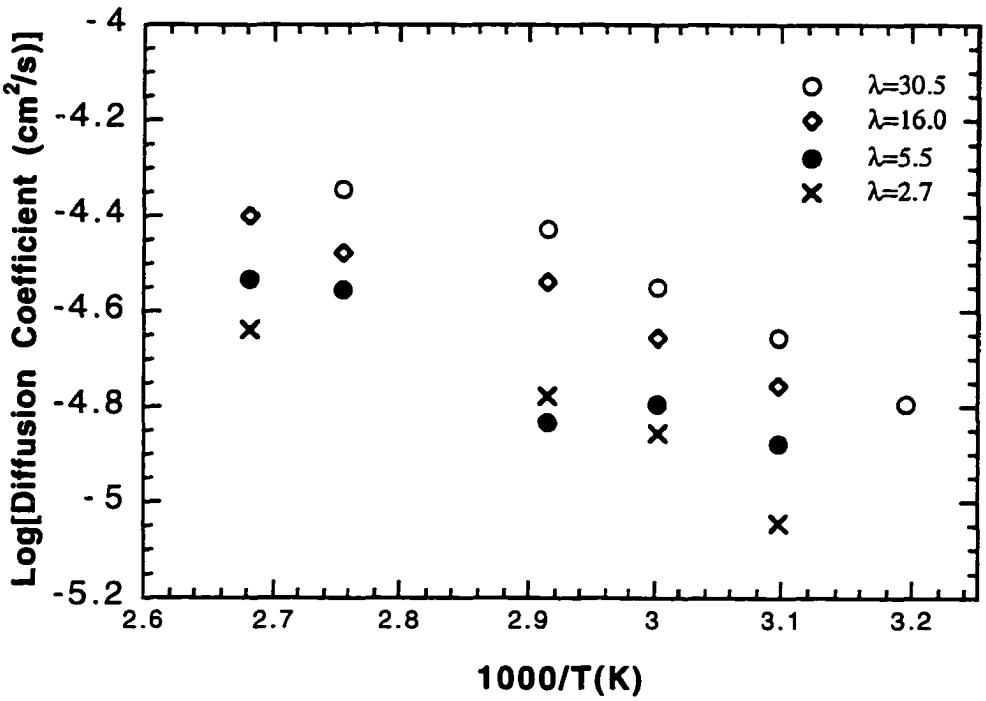

Figure 4.4.12 Arrhenius plot of temperature dependence of diffusion coefficient of Nafion 105 for various water contents.

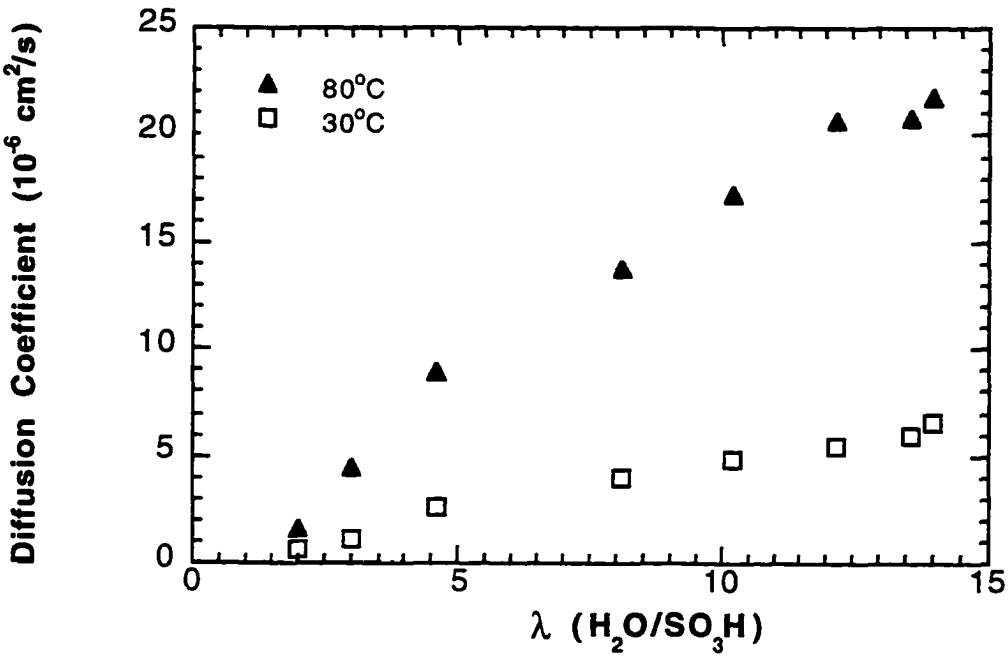

Figure 4.4.13 Water diffusion coefficient for Nafion 117 at 30°C and 80°C.

The water and ion diffusion behavior in the membranes is closely related to the water content in the membrane. The diffusion coefficient of Nafion 117 with λ=14 (100% *RH*) at room temperature, measured by several different groups [6-9, 59, 60] using NMR techniques, is about 6×10^{-6} cm^2/s which is lower than water diffusion in bulk water (about 2.13×10^{-5} cm^2/s).[83] This implies that water in Nafion does not behave exactly as bulk water. In another words, there is a substantial contribution from the ions in fixed sites to lower the water diffusion coefficient. The water content dependence of the activation energy of diffusion coefficient shows that the only significant change occurs at low water content. Such a trend qualitatively agrees with the result reported by Kreuer *et al.*.[59, 60]

In comparison between diffusion and conductivity data, it is interesting that there are similar trends in the conductivity measurements in which there is a significant change in activation energy at lowest water content, and similar activation energy for high water content. (see section 4-2 Figure 4.2.4 and 4.2.6) For liquid water and membranes with high hydration degree, it generally accepted that the Grotthus hopping (definition is deferred to section 1-2-5) is the primary contribution to proton conductivity (See section 4-2). However for low water content in the membranes, the proton transport mechanism related to conduction is still interesting. For the further comparison, the temperature dependence of the activation energy for diffusion and conductivity is plotted in Figure 4.4.14. The activation energies for both diffusion and conductivity increase with decreasing water content. In the region of $\lambda<5$, the activation energies for both diffusion and conductivity fit on a single curve. However, for $\lambda>5$, the activation energy of conductivity drops more steeply than for diffusion. Also notice in Figure 4.4.14 that at high water content, the proton hopping energy barrier is significantly lower

than proton diffusion energy barrier. This result excellently agree with the measurements by Zawodzinski *et al.*,[6] also Kreuer et al.[59, 60] These authors suggested that in the study of amplification factor A ($A=D_\sigma/D_{H2O}$) the proton conductivity of Nafion 117 is correlated with water diffusion for low degrees of hydration. The amplification factor A reaches a maximum value 2.5 at highest water content $\lambda=14$ and a minimum 1 at lowest water content $\lambda=2$. For low hydration membrane the contribution to conductivity is H_3O^+ diffusion corresponding to A=1. With increasing hydration there is an increasing contribution from proton hopping mechanism which leads to an increasing amplification factor.

The activation data in this thesis work gives a unique insight into the proton transport mechanism in Nation membranes. We are able to directly describe the relation between protonic conductivity and diffusion coefficient of Nafion membranes. At the low water content, $\lambda < 5$ the primary transport mechanism of protonic conductivity is the diffusion motion of H_3O^+. For $\lambda > 5$, the proton hopping mechanism start to dominate the contribution to the conductivity.

The interesting results of Fontanella *et al*[64, 65] and author in this thesis work in high pressure conductivity and NMR relaxation measurements (see section 4-4-1) show that the activation volume for high water content $\lambda>5$ is significantly smaller than for $\lambda<5$. These pressure dependence studies seem to suggest that the proton transport mechanism in low water content PFSA membrane is significantly different from that in high water content materials. *Fontanella et al.*[64, 65] point out that for a low water content membrane there is a distinct transport mechanism from that observed in high water content membranes.

It should be noted that self-diffusion coefficients are measured by this method without concentration gradient and water flux. To use Fick's law, it necessary to calculate diffusion coefficients corrected for some thermodynamic factors. In this calculation, we should be aware that the variation of the activity coefficient influences the effective diffusion coefficient in a system with driving force. Since, practically, the fixed SO_3^- groups do not have sufficient diffusional movement due to polymer morphology, this two-component system can be looked at as a "one-component" system in diffusion measurements by ignoring counter charge displacement. Consequently, inter diffusion coefficient obtained by this method can be a very good approximation of self-diffusion coefficient

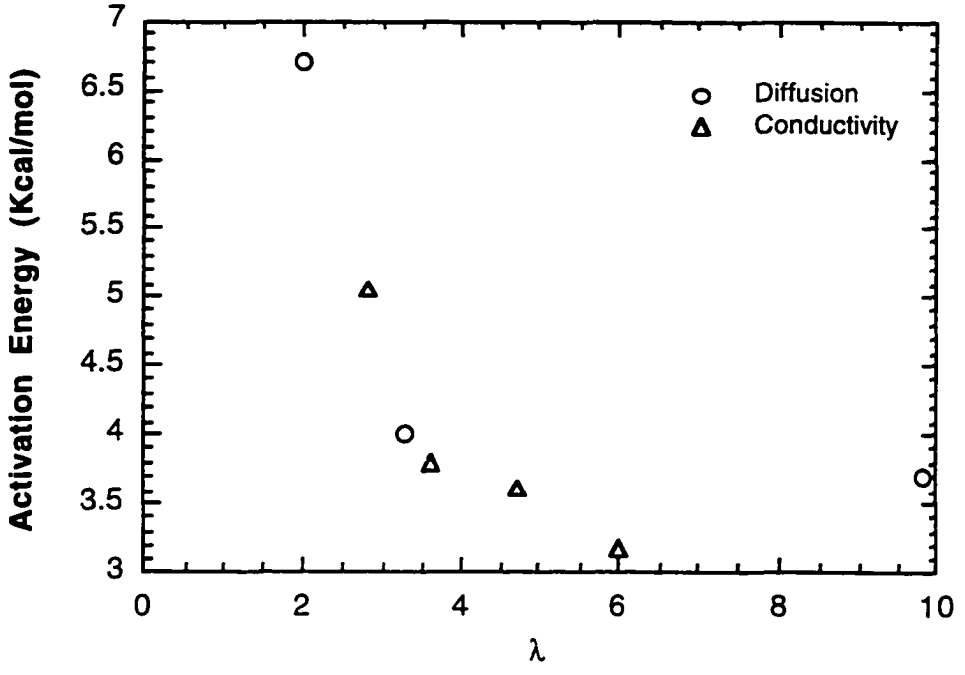

Figure 4.4.14 Comparison of activation energies between diffusion and conductivity as a function of water content.

4-5. Measurements for the Membranes in Contact with Methanol/Water Solutions

In this chapter, proton conductivity, water and methanol diffusion coefficients, and water and methanol spin-lattice relaxation data are presented. All samples are equilibrated with water methanol solution with various methanol concentrations.

Since the focus of transport studies for the direct methanol fuel cell is on the methanol cross-over and developing strategies to minimize its effects,[113] the methanol transport properties through the membrane and its effect were studied by several groups.[109, 113-122] It should be noted that there are to date no methanol permeation data quantitatively consistent with each other. The methanol permeation rate through Nafion 117, based on liquid feed (1M $MeOH/H_2O$ solution), measured by estimating the carbon dioxide evolution rate for the open circuit on the cathode side (thus one can convert CO_2 evolution rate to equivalent current density in the reaction $CH_3OH + H_2O \rightarrow CO_2 + 6H^+ + 6e^-$) are reported in 40 mA/cm^2 at 90°C (Pt-Ru catalyst on the anode), 100 mA/cm^2 at 95°C (Pt alloy catalyst on the anode), and 180 mA/cm^2 at 104°C (Pt-Ru catalyst on the anode), respectively, by Zawodzinski *et al.*,[113-115] Narayanan *et al.*,[116] and Maricle *et al.*[117] Kato *et al.*[120] obtained 250mA/cm^2 for Nafion 125 at 50°C. However, this last study used trimethyl ammonium $(CH_3)_3NH^+$ as the counter ion and the other membrane surface was facing a vacuum in their experiments, therefore their data have little relevance to direct methanol fuel cell application. Ren *et al.*[109] developed a new method to measure the water electro-osmotic drag coefficient in the membrane equilibrated with liquid water methanol mixtures. The drag value 2.4 H_2O/H^+ is reported. This is similar to the case of Nafion 117 equilibrated with water. Maricle *et al.* reported 1.05 $MeOH/H^+$ for methanol drag coefficient in which a stream of hydrogen was introduced into the anode fed with liquid water methanol mixtures. Kauranen and Skou[119] reported methanol diffusion data, 4.9×10^{-6} cm^2/s, for

Nafion 117 membrane in contact with 2.0M sulfuric acid (H_2SO_4) at 60°C using electrochemical method.

4-5-1. Experimental

The membrane used in all the measurements is Nafion 117 (DuPont) in acid form. Its repeat unit equivalent weight is 1100, and thickness is approximately 8 mils in the fully hydrated state. The pretreatment procedures for the membrane samples, and the experiment facilities for protonic conductivity and diffusion coefficient are the same as described in Chapter 3 in this thesis.

Membrane protonic conductivity of Nafion membranes immersed in various methanol water solutions was measured using the same facilities and same method as described in Chapter 3 in this thesis. The conductivities were determined at 70 psi over a range of temperature between 30 °C-150°C. The resistivity of the membrane was measured as the high frequency (10 kHz) impedance of the system. Both real and imaginary components of the impedance were measured and it was determined that the measurement was free of lead inductance effects.

The methanol and water diffusion coefficients were measured using PGSSE (pulsed-gradient stimulated spin-echo) NMR pulse sequence[101] which is described in Chapter 3. Slivers of Nafion 117 membranes of dimensions 7 mm × 25 mm were immersed in different methanol/water solutions for a few days. After blotting up the liquid on the surface of the emersed membranes as quickly as possible, the samples were loaded and then well sealed with parafilm in 10 mm home made NMR glass tube within which the equilibration condition could be maintained. The measurements were carried out using a *Bruker AMX400* spectrometer operating at 400 MHz. Methanol diffusion coefficients were measured at 30°C.

Spin-lattice relaxation times (T_1) measurements were carried out by using the same NMR spectrometer as in the self-diffusion coefficient measurements. The procedures of preparing Nafion 117 membrane samples were similar to what is described in the diffusion measurements. Methanol concentration dependence of spin-lattice relaxation time (T_1) of Nafion 117 membrane at 35°C was determined using inversion recovery which is a common method for measuring spin-lattice relaxation time.

4-5-2. Results and Discussions

Methanol partitioning — Before carrying out conductivity, diffusion and relaxation measurements *etc.*, we have to know the amount of water and methanol uptake into the membrane under certain concentration of water/methanol mixtures and temperature. Methanol uptake into membrane is referred as methanol partitioning through membrane. Table 4.5.1 is the data, previously determined by Zawodzinski *et al.*,[113] of methanol partitioning inside and outside of Nafion 117 membrane at 30°C. Here is a brief description of the experiments probing methanol and water partitioning into the membrane: [113] Membrane samples were immersed in a methanol/water mixture of appropriate composition at room temperature for a few days, and then emmersed and loaded into an NMR tube. The total water plus methanol uptake was determined gravimetrically. The relative amounts of water and methanol absorbed by the membrane from solutions of various compositions were measured by comparing the NMR signal intensities of the water and methanol CH_3 resonances. A *Bruker AMX400* spectrometer operating at 400 MHz was used.

It is clear that at room temperature over a quite wide range of methanol concentration, 0.5-8.0 M (mole), the partitioning of methanol into Nafion 117 membrane is the same as in methanol/water mixtures. It is found that the ratio of

methanol to water concentrations from these measurements is the same inside and outside the membrane. This indicates that methanol does not selectively partition into the membrane exposed to aqueous methanol water solution. These results are consistent with the data that methanol concentrations were evaluated from the electrochemical measurements reported by Zawodzinski *et al.*,[114] in which the membrane porosity was taken into account. The methanol partitioning result does not exactly match Verbrugge's model which predicts partitioning coefficient is 0.80.[120]

Protonic conductivity —It was determined that the protonic conductivity of Nafion 117 membrane over a wider range of methanol concentration from 0.1 to 16 molal and temperature from 30°C to 150°C. Also for the comparison purpose, the protonic conductivity of Nafion membrane with higher equivalent weight (1500 EW) was measured over a range of methanol concentration from 1-6 molal and temperature from 30°C-80°C. The conductivity data, for Nafion 117 and Nafion 1500 EW membrane samples as a function of temperature and methanol concentration are shown in Figure 4.5.1 and Figure 4.5.2. The conductivity significantly increases with increasing temperature and decreases with increasing methanol concentration. In Figure 4.5.1, the conductivity at 30°C for lowest methanol concentration 0.1m is 0.099 S/cm which is the same as the value, 0.1 S/cm , which is the conductivity of Nafion 117 immersed in pure water (λ = 22). The protonic conductivity for highest methanol concentration 16m is significantly low than for membranes immersed in water. It is clear that at such a high methanol concentration the proton hopping (Grotthus hopping) pathways is somehow hindered by methanol molecules. For Nafion 1500EW, in Figure 4.5.2, there is a similar trend to that of Nafion 117. For the methanol concentration of 1m (practical

Table 4.5.1 Methanol partitioning in Nafion 117 membranes at 30°C.

Solution Concentration	Solution $I(CH_3)/H_2O$	Membrane $I(CH_3)/H_2O$
0.5 M	0.014	0.01
1.0 M	0.027	0.03
2.0 M	0.050	0.05
4.0 M	0.110	0.10
8.0 M	0.210	0.19

(From Ref. [113])

concentration in direct methanol fuel cell), conductivities of both Nafion membranes drop about 10%. Accordingly, there is distinct issue in direct methanol fuel cells which differs from that in fuel cells fed with hydrogen. In the latter, the important issue is membrane conductivity, while methanol permeation rate through the membrane is the key point in direct methanol fuel cells.

Noted that in Figure 4.5.1 conductivity at 150°C decrease with increasing methanol concentration is significantly less than at 30°C. This is due to methanol partitioning into the membranes dropping at high temperature. This qualitatively agrees with the data obtained by Zawodzinski *et al.*[114] They found that methanol partitioning inside of membrane for high methanol concentration (1M) drops with

increasing temperature more significantly than for low methanol concentration (0.1M). However, in order to obtain further evidence, the measurements of temperature dependence of methanol partitioning for various methanol concentrations should be extended to higher methanol concentrations.

Figure 4.5.3 and Figure 4.5.4 show the Arrhenius plot illustrating the temperature dependence of the conductivity over the range 30°C-150°C of Nafion 117 membrane immersed in various methanol concentrations and over the range 30°C-80°C of Nafion 1500 EW membrane immersed in methanol/water mixtures. The curves in Figure 4.5.3 are not linear over the whole experimental temperature range. If we prefer to make a linear fit for each curve from which activation energy is yielded as a quantitative observation, the activation energy in Table 4.5.2 increases with increasing methanol concentration. For 0.1m methanol, if the data is fitted over the rage of temperature from 30°C-80°C, the activation energy is 2.2 kcal/mol which is similar to the value of Nafion 117 immersed in water, which, in turn, confirms the data reliability.

It also is noticed this result is consistent with the data reported by Zawodzinski et al.[113] These authors measured the protonic conductivity of Nafion 117 immersed in the water methanol mixtures (0.5-4M) as a function of temperature from 30°C to 80°C. In Figure 4.5.4, the case of Nafion 1500 EW, the activation energy for 1 m methanol concentration is 2.3 which is slight high than that for water and similar to that of Nafion 117(fit from 30°C to 80°C).

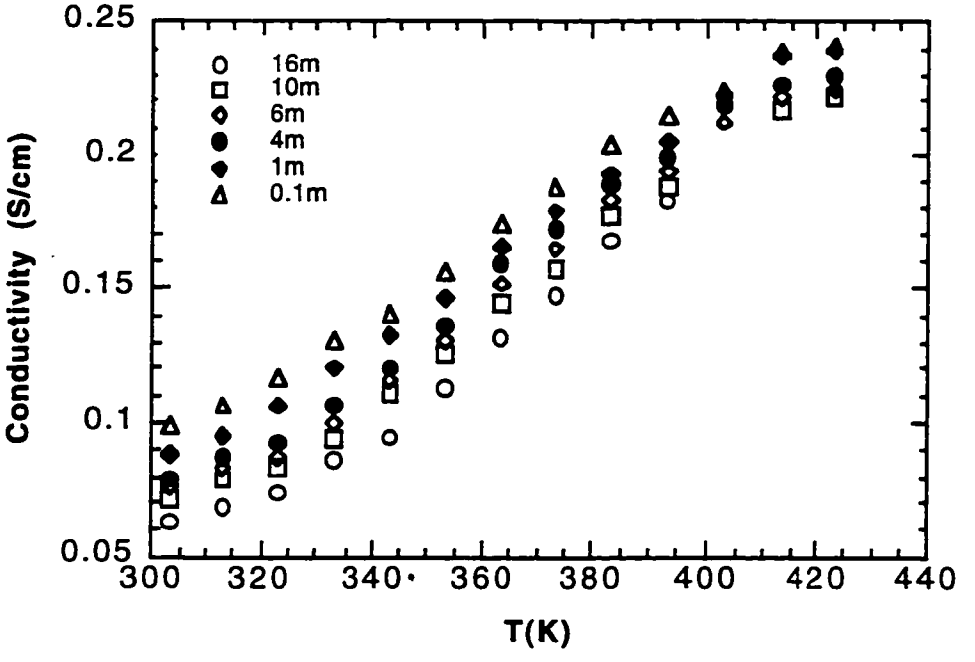

Figure 4.5.1 Conductivity of Nation 117 immersed in several methanol/water solutions at elevated temperatures.

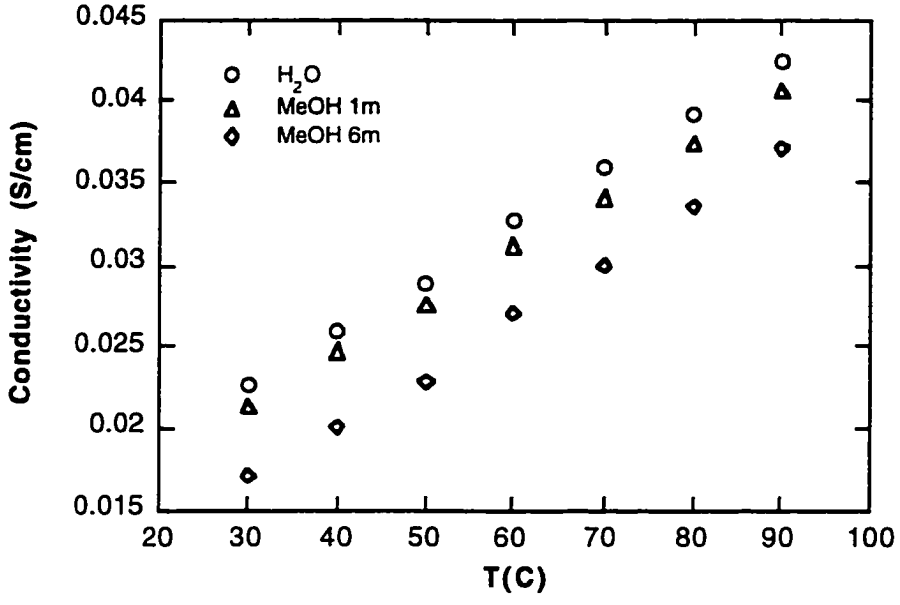

Figure 4.5.2 Conductivity of Nation 1500 EW immersed in several methanol/water solutions at elevated temperatures.

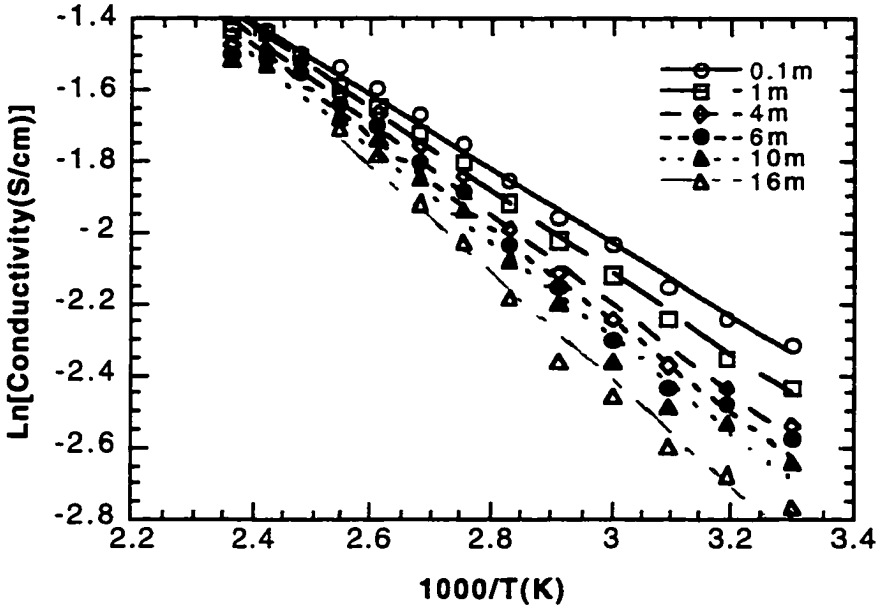

Figure 4.5.3 Arrhenius plot of temperature dependence of Nafion 117 immersed in several methanol water solutions.

Table 4.5.2 Activation energy for immersed Nafion 117 membrane conductivity at elevated temperatures for various methanol concentrations

Methanol Concentration (Molal)	Activation Energy (Kcal/mol)
0.1	2.04
1.0	2.27
4.0	2.50
6.0	2.55
10.0	2.63
16.0	2.96

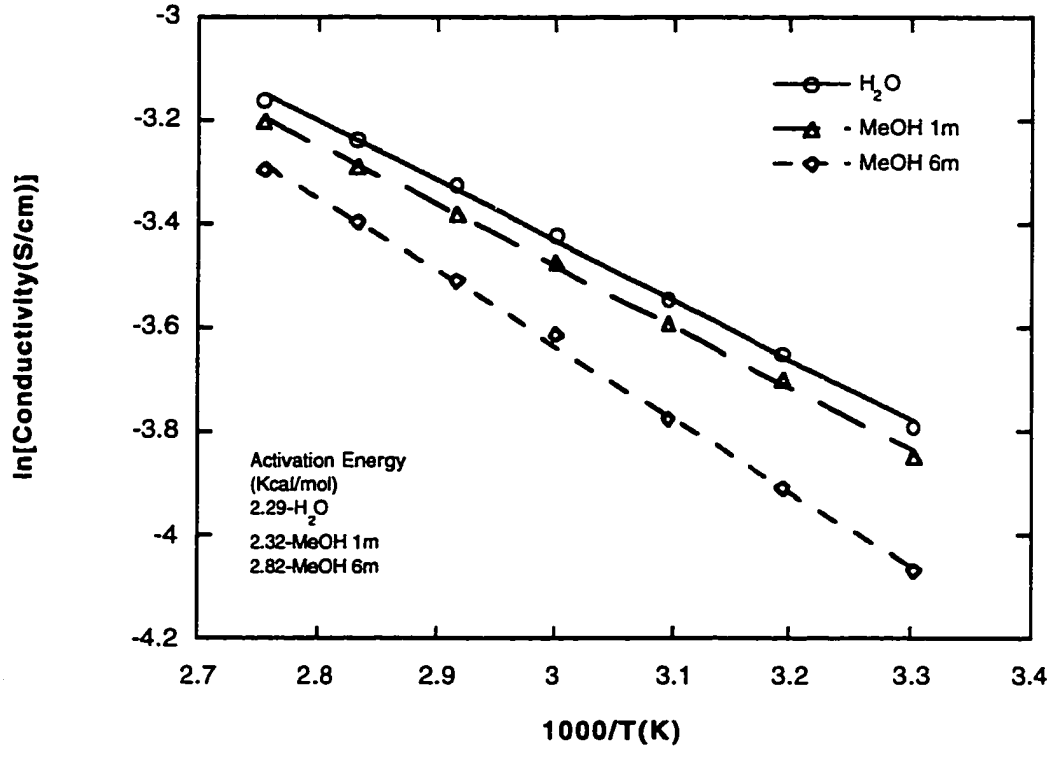

Figure 4.5.4 Arrhenius plot of temperature dependence of Nafion 1500 EW immersed in several methanol water solutions.

Self-diffusion coefficient —Methanol and water diffusion coefficients of Nafion 117 equilibrated with various aqueous methanol solutions (1-16 molal) using pulsed-gradient stimulate spin-echo (PGSSE) NMR pulse sequence are displayed in Figure 4.5.5. At the first glance the diffusion coefficients are independent of methanol concentration in the membrane. The result is similar to the data previously reported by Zawodzinski *et al.* [113] However, diffusion coefficient of methanol in the membrane, 5×10^{-6} cm^2/s from Figure 4.5.5, is slightly lower than previously reported by Zawodzinski *et al.*, 6×10^{-6} cm^2/s, using NMR[113] and electrochemical [114] measurements. It should be noted that in Ref. [113] these authors used a different NMR pulse sequence from this work. It is a little surprising that the methanol and water diffusion coefficients in the membrane are practically independent of methanol concentration in the membrane which contrasts with the results of methanol and water diffusion coefficient in solution.[113] If we estimate methanol cross-over flux through the membrane from these diffusion coefficients, assuming a linear concentration profile of methanol starting at 2m on the anode and dropping to zero on the cathode with the membrane thickness 8 mil, this estimated methanol cross-over equivalent to 46 mA/cm^2 is in the line with the methanol cross-over data, 40 mA/cm^2, shown by Zawodzinski *et al.*[114] The water diffusion in the membrane is constant regardless of methanol concentrations in the membrane. Also there is no good answer regarding this phenomenon. However, the diffusion value, about 7.5×10^{-6} cm^2/s, is similar to the case of membrane equilibrium with 100% *RH* vapor phase at 30°C.

NMR Spin-lattice relaxation times (T_1) — The proton T_1 determined at 35°C for water and methanol in Nafion 117 membranes for various methanol

concentration. In Table 4.5.3, there is no substantial methanol concentration dependence observed. It seems that methanol concentration in the membrane does not strongly affect the local environment of water and methanol molecules. Comparing to ^2H T_1 data of the membrane reported by Chen *et al.*[75], T_1= 0.16s for λ=11 at 23°C, and Zawodzinski *et al.*[7], T_1=0.21s for λ=14 at 30°C, T_1 of the membrane equilibrated with methanol water solution is lower by a factor of 2 than that in D_2O case.

From the conductivity, diffusion coefficient, spin-lattice relaxation measurements, we can see that these data are qualitatively agree with each other. A clear picture shown is that the methanol molecules hinder the motion of the water molecules in the membrane. It implies that there somewhat stronger interaction added in the previous hydrogen bonding networking without the methanol molecules. Therefore, it causes some changes in these transport parameters.

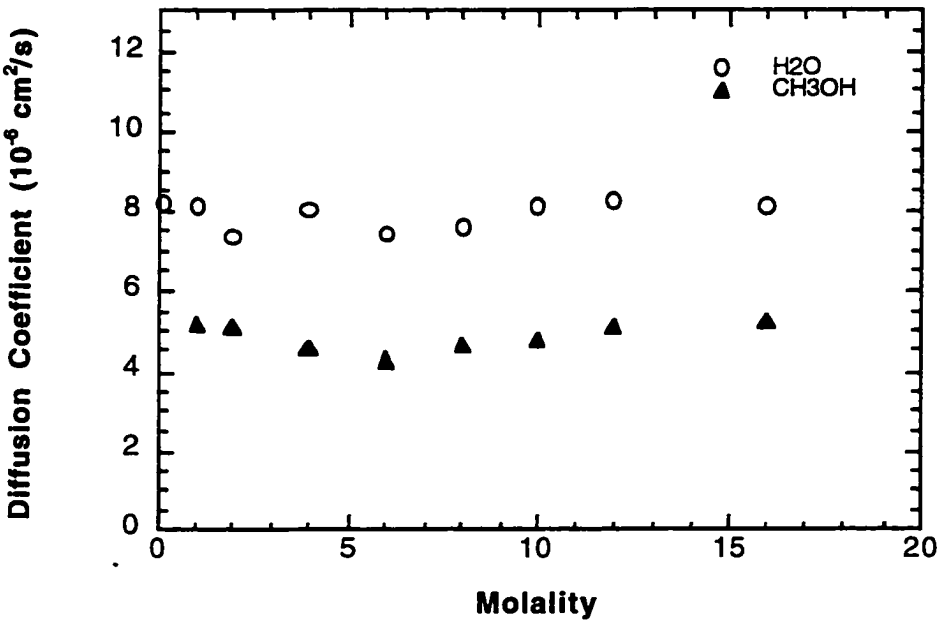

Figure 4.5.5 Diffusion coefficients of Nafion 117 in contact liquid methanol water solution at room temperature.

Table 4.5.3 Spin-Lattice relaxation (T_1) data at T=35°C

Methanol Concentration (Molal)	H_2O T_1 (ms)	MeOH T_1 (ms) (CH_3 peak)
0.1	93.6±0.6	
1.0	83.4±0.3	713±6
4.0	83.7±0.3	732±4
6.0	83.4±0.4	752±3
10.0	83.8±0.4	790±5
16.0	83.9±0.5	786±3

4-6. Conclusions

The water uptake for three Nafion membranes immersed in water at 30°C significantly decreases with increasing equivalent weight. In the case of the PFSA membranes in contact with water vapor phase: 1) the water absorption with various water activities at 80°C exhibit a similar trend to that at 30°C; 2) the water uptakes at both temperatures increase with a steep rise at $a_w \approx 0.75$. 3) the absorption at 80°C is substantially less in the membranes for $a_w > 0.75$. 4) at both temperatures water absorption behavior is typical of weakly cross-linked ion-exchangers.

The protonic conductivity of the PFSA membranes, either immersed in liquid water or exposed to water vapor, substantially increases with increasing temperature. The conductivity is lower for higher equivalent weight. The conductivity for the membranes with the same equivalent weight and different thickness is the same at elevated temperatures. Thus, the measured membrane conductivity is an intrinsic property. For an immersed membrane at a given temperature, the conductivity increases non-linearly with the decrease of equivalent weight. However, the activation energies for the immersed membranes with various equivalent weight are similar. This indicates the proton transport occurs in the similar environment. The activation energies derived from conductivity measurements for the membranes with a fixed water content yields an important conclusion: at low water content, $\lambda<5$, the primary transport mechanism of protonic conductivity is the diffusion motion of H_3O^+ molecules; for $\lambda>5$, the proton hopping mechanism starts to dominate the protonic conductivity.

The electro-osmotic drag coefficient for several partially hydrated membranes at 80°C is a constant, $\xi\approx1$, over the entire range of water activity. This is similar to the observed data at 30°C. Currently, we are not able to successfully explain this phenomenon.

The T_1 measurements of pressure dependence in high pressure ^2H NMR for Nafion membranes shows that the activation volume *vs.* water content exhibits two well-defined regions which are correlated with the two major regions of water sorption from the vapor phase. This suggest that, even for the highest water content, rotational motion is still influenced by polymer. The T_1 relaxation data in high pressure ^{19}F NMR indicate that T_1 is approximately independent of both water content and pressure. This reflects negligible relaxation of the main polymer and pendant chains.

Water diffusion coefficients exhibit significant temperature and water content dependence. There is a relatively slight variation in activation energies, extracted from temperature dependence at high water content. A significant change occurs at low water content. The methanol diffusion coefficient in the membranes at room temperature do not show a significant methanol concentration dependence (1m-16m).

Most of the data mentioned above suggest that there are two water content regions, $\lambda<5$ and $\lambda>5$, in which the transport properties exhibit distinct behavior. However, even at the highest water content, the nature of the water in the membranes is not the same as of bulk water.

The primary contribution of this thesis to science and technology in the studies of ion transport properties in PFSA membranes is an improved understanding of the proton transport properties in PFSA membranes. In particular, it is concluded that the PFSA membrane exhibits two distinct transport mechanisms: at extremely low membrane water content, diffusional motion (with H_3O^+) dominates the proton transport. However, at high membrane water content, proton hopping (Grotthus) mechanism dominates the proton transport mechanism in the membranes.

References

1. Karl Kordesch and Gunter Simader, Fuel Cell and Their Applications, *VCH Verlagsgesellschaft mbH, D-69451 Weinheim, Federal Republic of Germany, 1996.*
2. Leo J.M.J. Blomen & Michael N. Mugerwa, Fuel Cell Systems, *1993 Plenum Press New York.*
3. A.J. Appleby and D.G. Lovering, Fuel Cells, 2nd Grove Symposium '91, *ELSEVIER SEQUOIA S.A. 1992.*
4. U.S. Department of Energy, Office of Fossil Energy, Fuel Cell A Handbook, *May 1988 , Chapter 6.*
5. R.A. Lemons, Fuel Cells for Transportation, *J. Power Sources, 29 (1990) 251-264.*
6. T.A. Zawodzinski Jr., M. Neeman, L.O. Sillerud, and S. Gottesfeld, Determination of water diffusion Coefficients in Perfluorosulfonate Ionomeric Membranes, *J. Phys. Chem. 1991, 95, 6040-6044.*
7. T.A. Zawodzinski Jr., C. Derouin, S. Radzinski, R.J. Sherman, V.T. Smith, T.E. Springer, and S. Gottesfeld, Water Uptake by and Transport Through Nafion 117 Membranes, *J. Electrochem. Soc., Vol. 140, No.4 , 1993, 1041-1047.*
8. T.A. Zawodzinski, Jr., T.E. Springer, F. Uribe and S. Gottesfeld, Characterization of Polymer electrolytes for Fuel Cell Applications, *Solid State Ionics 60 (1993) 199-211.*
9. T.A. Zawodzinski, Jr., T.E. Springer, J. Davey, R. Jestel, C. Lopez, J.Valerio, and S. Gttesfeld, A Comparative Study of Water Uptake by and Transport Through Ionomeric Fuel Cell Membranes, *J. Electrochem. Soc., Vol.140, No.7, 1993, 1981-1985.*

10. T.A. Zawodzinski, Jr., J. Davey, J.Valerio, and S. Gottesfeld, The Water Content Dependence of Electro-Osmotic Drag in Proton-Conducting Polymer Electrolytes, *Electrochimica Acta, Vol.40, No.3, 1995, 297-302.*

11. T.A. Zawodzinski, Jr., M.S. Wilson, J.A. Bett, and S. Gottesfeld, Membrane Electrolyte Issues in Direct Methanol Fuel Cells, *ECS Proceedings, Electrode Materials and Processes for Energy Conversion and Storage, Edi. by S. Srinivasan, D.D. Macdonald, and A.C. Khandkar, Vol. 94-23, 315-325.*

12. W.T. Grubb, Batteries with Solid Ion Exchange Electrolytes, *J. Electrochem. Soc., 106 (1959) 275-278.*

13. W.T. Grubb and L. W. Niedrach, Batteries with Solid Ion-Exchange Membrane Electrolytes, *J. electrochem. Soc., 107 (1960) 131-135.*

14. E.J. Cairns, D.L. Douglas, and L.W. Niedrach, Performance of Fractional Watt Ion Exchange Membrane Fuel Cell, *AIChE J. 7 (1961) 551-558.*

15. H.J.R. Maget, *in Handbook of Fuel Cell Technology, Ed. by Berger, Prentice-Hall, Englewood Cliffs, N. J., 1967, 425.*

16. A. Eisenberg and H.L. Yeager (Eds.), in Perfluorinated Ionomer Membranes, *ACS Symposium Series 180, American Chemical Society, Washington, D.C., (1982).*

17. A. Eisenberg (Ed.), Ions in Polymers, *Advances in Chemistry Series 187, American Chemical Society, Washington, D.C., (1980).*

18. S.P. Rowland (Ed.), Water in Polymers, *ACS Symposium Series 127, American Chemical Society, Washington, D.C., (1982).*

19. R.S. Yeo and Howard L. Yeager, Structural and Transport Properties of Perfluorinated Ion-Exchange Membranes, *in Modern Aspects of Electrochemistry, Ed. by T.G. Linford, 16, 437-504 (1985).*

20. R.S. Yeo and A. Eisenberg, Physical Properties of Perfluorinated Ion-Containing ("Nafion") Polymers, *Polymer Preprints 16 (1975) 104-110.*

21. T.D. Gierke, G.E. Munn, and F.C. Wilson, The Morphology in Nafion Perfluorinated Membrane Products, as Determined by Wide-and Small-Angle X-Ray Studies, *J. Polym. Sci: Polym. Phys. Ed., Vol. 19, 1687-1704 (1981).*

22. A.J. Hopfinger and K.A. Mauritz, Theory of the Structure of Ionomeric Membranes, *in Comprehensive Treatise of Electrochemistry, Ed. by J.O'M. Bockris, G.E. Conway, E. Yeager, and R.E. White, Plenum Press, New York, 1981, Vol. 2, 521-535.*

23. W.Y. Hsu and T.D. Gierke, Elastic Theory for Ionic Clustering in Perfluorinated Ionomers, *Macromolecules 15 (1982) 101-105.*

24. W.H. Koh and H.P. Silverman, Anion Transport in Thin-Channel Cation Exchange Membranes, *J. Membrane Science 13 (1983) 279-290.*

25. B. Rodmacq, J.M.D. Coey, M. Escoubes, E. Roche, R. Duplessix, A. Eisenberg, and M. Pineri, Water Absorption in Neutralized Nafion Membranes, *in Water in Polymers, Ed. by S.P. Rowland, ACS Symposium Series 127, 1980, 487-501.*

26. T .D. Gierke, Ionic Clustering in Nafion Perfluorosulfonic Acid Membranes and Its Relationship to Hydroxyl Rejection and Chlor-Alkali Current EFF, *152nd Meeting of the Electrochemical Soc., Atlanta, 1977, Abstract No.438, J. Electrochem. Soc., Vol.124, No.8, 319C (1977).*

27. M. Falk, An Infrared Study of Water in Perfluorosulfonate (Nafion) Membranes, *Can J. Chem. 58 (1980) 1495-1501.*

28. H.L. Yeager and A. Steck, Cation and Water Diffusion in Nafion Ion Exchange Membranes: Influence of Polymer Structure, *J. Electrochem. Soc. 128, 1981, 1880-1884.*

29. E.J. Roche, M. Pineri, R. Duplessix, and A.M. Levelut, Small-Angle Scattering Studies of Nafion Membranes, *J. Polym. Sci., Polym. Phys. Ed. 19 (1981) 1-11.*

30 M.H. Litt, A Reevaluation of Nafion® Morphology, *190th Meeting of the Electrochemical Soc., San Antonio, 1996, Abstract No.139.*

31. M. Escoubes and M. Pineri Thermodynamic Studies of the Water-Perfluorosulfonated Polymer Interactions, *in Perfluorinated Ionomer Membranes, Ed. by A. Eisenberg, and H.L. Yeager, ACS Symposium Series 180, American Chemical Society Washington, D.C. 1982, 9-23.*

32. F. Volino, M. Pineri an A.J. Dianoux, Water Mobility in a Water-Soaked Nafion Membrane: a High-Resolution Neutron Quasielastic Study, *J. Polym. Sci.: Polym. Phys. Ed., Vol. 20, 481-496.*

33. R. Duplessix, M. Escoubes, B.Rodmacq, F. Volino, E. Roche, A. Eisenberg, and M. Pineri, Water Absorption in Acid Nafion Membranes, *in Water in Polymers, Ed. by S.P. Rowland, ACS Symposium Series 127, ACS Washington, DC, 1980, 469-486.*

34. B. Rodmacq, M. Pineri, J.M.D. Coey, and A. Meagher, Mossbauer-Spectroscopy of Nafion Polyumer Membranes Exchanged with Fe^{2+}, Fe^{3+}, and Eu^{3+}, *J. Polym. Sci. Part B-Polym. Phys., Vol.20, No.4, 603-621 1982.*

35. M. Fujimura, T. Hashimoto, and H. Kawai, Small-Angle Scattering Study of Perfluorinated Ionomer Membranes. 1. Origin of Two Scattering Maxima, *Macromolecules 14 (1981) 1309-1315.*

36. N. Sinvashinsky and G.B. Tanny, The State of Water in Swollen Ionomers Containing Sulfonic Acid Salts, *J. Appl. Polym. Sci. 26 (1981) 2625-2637.*

37. R.S. Yeo and A. Eisenberg, Physical Properties and Supermolecular Structure of Perfluorinated Ion-Containing (Nafion) Polymers, *J. Appl. Polym. Sci. 21 (1977) 875-898.*

38. N.G. Bolyle , J.M.D. Coey, V.J. Mcbrierty, Low-Temperature Behaviour of Water in Nafion membranes, *J. Chem. Phys. Lett. 1982, 86, 16-19.*

39. N.G. Boyle, V.J. McBrierty, and D.C. Douglass, A Study of the Behavior of Water in Nafion membranes, *Macromolecules 1983, 16, 75-80.*

40. K.K. Pushpa, D.Nandan, and R.M. Iyer, Thermodynamics of Water Sorption by Perfluorosulphonate (Nafion 117) and Polystyrene Sulphonate (Dowex 50W) Ion-exchange Resins at 298±1K, *J. Chem. Soc., Faraday Trans 1, 1988, 84 (6), 2047-2056.*

41. A. Steck and H.L. Yeager, Water Sorption and Cation-Exchange Selectivity of a Perfluorosulfonate Ion-Exchange Polymer, *Analytical Chemistry, Vol. 52, No. 8, July 1980, 1215-1218.*

42. S. C. Yeo and A. Eisenberg, Physical Properties and Supermoleclar Structure of Pefluorinated Ion-Containing (Nafion) Polymers, *J. Appl. Polym. Sci., Vol. 21, 875-898 (1977).*

43. M. Fujimura, T. Hashimoto, and H. Kawai, Small-Angle X-Ray Scattering Study of Perfluorinated Ionomer Membranes. 2. Models for Ionic Scattering Maximum, *Macromolecules,1982, 15, 136-144.*

44. T. Hashimoto, M. Fujimura, and H. Kawai, Structure of Sulfonated and Carboxylated Perfluorinated Ionomer Membranes: Small-Angle and Wide-Angle X-Ray Scattering and Light Scattering, *in Perfluorinated Ionomer Membranes, Ed. by A Eisenberg, and H.L. Yeager, ACS Symposium Series 180, ACS Washington, D.C. 1982, 217-248.*

45. N.J. Bunce, S.J. Sondheimer, and C.A. Fyfe, Proton NMR Method for the Quantitative Determination of the Water Content of the Polymeric Fluorosulfonic Acid Nafion-H, *Macromolecules 1986, 19, 333-339.*

46. S.J. Sondheimer, and C.A. Fyfe, Proton NMR Method for the Quantitative Determination of the Water Content of the Polymeric Fluorosulfonic Acid Nafion-H, *Macromolecules 1986, 19, 333-339.*

47. A.B. LaConti, A.R. Fragala, and J.R. Boyack, Solid Polymer Electrolyte Electrochemical Cells: Electrode and Other Materials Considerations, *Electrode Materials and Processes for Energy Conversion and Storage, J. D. E. McIntyre, S. Srinivasan, F. Will, Eds, The Electrochemical Society: Penningon, NJ, 1977, p354-374.*

48. G.A. Eisman, The Physical and Mechanical Properties of a New Perfluorosulfonic Acid Ionomer for Use as a Separator/Membrane in Proton Exchange Processes, *in Diaphragms, Separators, and Ion Exchange membranes (Ed. by J.W. Van Zee, R.E. White, K. Kinoshita and H.S. Burney), PV 86-13, pp. 156-171. The electrochemical Society Softbound Proceedings Series, Pennington, NJ(1986).*

49. R.S. Yeo, *in Transport Processes in Electrochemical Systems, Proc. Vol.82-10, Ed. by R.S. Yeo, ACS Symposium Series 180, p.453, Washington, D.C. (1980)*

50. J.T. Hinatsu, M. Mizuhata, and H. Takenaka, Water uptake of Perfluorosulfonic Acid Membranes from Liquid Water and Water Vapor, *J. Electrochem. Soc. Vol.141, 1493-1498 (1994).*

51. K. Broka, P. Ekdunge, Oxygen and Hydrogen Permeation Properties and Water Uptake of Nafion 117 Membrane and Recast Film for PEM Fuel Cell, *J. Appl. Electrochem. 27 (1997) 117-123.*

52. A. Sen, K.E. Leach , and R.D. Varjian, Determination of Water Content and Resistivity of Perfluorosulfonic Acid Fuel Cell Membranes, *not published.*

53. J.J. Fontanella, M.G. McLin, and M.C. Wintersgill, Electrical Impedance Studies of Acid Form Nafion® Membranes, *Solid State Ionics, 66 (1993) 1-4.*

54. B.D. Cahan and J.S. Wainright, AC Impedance Investigations of Proton Conduction in NafionTM, *J. Electrochem. Soc., Vol.140, No. 12 (1993) L185-L186.*

55. P.C. Rieke and N.E. Vanderborgh, Temperature Dependence of Water Content and Proton Conductivity in Polyperfluorosulfonic Acid Membrane, *J. Membrane Sci., 32 (1987) 313-328.*

56. Z. Cai, C. Liu, and C.R. Martin, Measuring Conductivities of Highly Conductive Membranes, *J. Electrochem. Soc., Vol.136, No.11, 1989, 3356-3361.*

57. C. Gavach, G. Pamboutzoglou, M. Nedyalkov, and G. Pourcelly, AC Impedance Investigation of the Kinetics of Ion Transport in Nafion Perfluorosulfonic Membranes, *J. Membrane Sci., 45 (1989) 37-53.*

58. M.W. Verbrugge, R.F. Hill, Analysis of Promising Perfluorosulfonic Acid Membranes for Fuel-Cell Electrolytes, *J. Electrochem. Soc., Vol.137, No.12, 1990, 3770-3777.*

59. K.D. Kreuer, T. Dippel, W. Meyer and J. Maier, Nafion Membranes: Molecular Diffusion, Proton Conductivity and Proton Conduction Mechanism, *Mat. Res. Soc. Symp. Proc. 293, 273-282 (1993).*

60. K.D. Kreuer, T. Dippel, and J. Maier, Membrane Materials for PEM-Fuel-Cells: A Microstructural Approach, *Electrochemical Society Poceedings Vol.95-23, 241-246.*

61 M.G. McLin, M.C. Wintersgill, J.J. Fontanella, R.S. Chen, J.P. Jayakody, and S.G. Greenbaum, High Pressure Studies of Hydrated Nafion Membranes: Dielectric Relaxation and Deuteron NMR, *Solid State Ionics 60 (1993) 137-140.*

62. J.J. Fontanella, M.G. McLin, and M.C. Wintersgill, Electrical Relaxation in *in Situ* Dried acid-Form Nafion, *J. Polym. Sci.: Part B: Polym. Phys., Vol.32, 501-507 (1994).*

63. R.S. Chen, P.E. Stallworth, S.G. Greenbaum, J.J. Fontanella, and M.C. Wintersgill, High Pressure NMR and Electrical Conductivity Studies in Acid Form Nafion Membranes, *Electrochimica Acta, Vol.40, No.3, 309-313, 1995.*

64. J.J. Fontanella, M.C. Wintersgill, R.S. Chen, Y. Wu, and S. G. Greenbaum, Charge Transport and Water Molecular Motion in Variable Molecuar Weight Nafion Membranes: High Pressure Electrical Conductivity and NMR, *Electrochimica Acta, Vol.40, No.13-14, 2321-2326, 1995.*

65. J.J. Fontanella, C.A. Edmondson, M.C. Wintersgill, Y. Wu and S.G. Greenbaum, High-Pressure Electrical Conductivity and NMR Studies in Variable Equivalent Weight Nafion Membranes, *Macromolecules 1996, 29, 4944-4951.*

66. B.R. Breslau and I.F. Miller, A Hydrodynamic Model for Electroosmosis, *Ind. Eng. Chem. Fundam., Vol. 10, No.4, 1971, 554-565.*

67. T. Okada, S.K. Ratjke and H. Hanche-Olsen, Water Transport in Cation Exchange Membranes, *J. Memb. Sci., 66 (1992) 179-192.*

68. G. Xie and T. Okada, Water Transport Behavior in Nafion 117 Membranes, *J. Electrochem. Soc., Vol.142, No.9 (1995) 3057-3062*

69. Y. Fujita, *Ph.D. Thesis, kyoto University.*

70. T. Fuller and J. Newman, Experimental Determination of the Transport Number of Water in Nafion 117 Membrane, *J. Electrochem. Soc. 139, 1332-1337 (1992).*

71. F. Helfferich, Ion Exchange, *p412, McGraw Hill Book Company, Inc., New York, 1962.*

72. High Pressure NMR *Ed. by J. Jonas et al , Springer-VerlagBerlin Heidelberg 1991.*

73. J.H. Walton, M.J. Lizak, M.S. Conradi, T. Gullion, and J. Schaefer, Hydrostatic Pressure Dependence of Molecular Motions in Polycarbonates, *Macromolecules, 23, 416 (1990) 416-422.*

74. Nan-I Liu and J. Jonas, High Pressure NMR Study of Molecular Motions and Glass Transition in Several elastomers, *J. Magn. Reson. 18, 444 (1975).*

75. R.S. Chen, J.P. Jayakody, S.G. Greenbaum, Y.S. Pak, G. Xu, M.G. McLin, and J.J. Fontanella, Studies of Water in Nafion Membranes, Using Deuteron and Oxygen-17 Nuclear Magnetic Resonance, and Dielectric Relaxation Techniques, *J. Electrochem. Soc., Vol.140, No.4, 1993, 889-895.*

76. L.W. Jelinski, *in High-Resolution NMR Spectroscopy of Synthetic Polymers in Bulk,Ed. by L. Komoroski, Chap. 10, VCH Publisher, New York (1986).*

77. H.W. Spiess, Molecular Dynamics of Solid Polymers as Revealed by Deuteron NMR, *Colloid and Polymer Sci. 261, 193-209 (1983).*

78. H.W. Spiess, Deuteron NMR-A New Tool for Studying Chain Mobility and Orientation in Polymers, *in Characterization of Polymers in the Solid State I, Edi. by H.H. Kausch, and H.G. Zachmann, Apringer-Verlag Berlin Heidelberg 1985 22-58.*

79. A. Abragam, The Principles of Nuclear Magnetism, *Oxford University Press, Oxford (1961).*

80. J.H. Wang, Self-diffusion and Structure of Liquid Water. II. Measurement of Self-diffusion of Liquid Wate with O^{18} as Tracer, *J. Phys. Chem. (1951) 4181-4183.*

81. M.W. Verbrugge and R.F. Hill, Ion and Solvent Transport in Ion-Exchange Membranes-2. A Radiotracer Study of the Sulfuric-Acid, Nafion-117 System,*J. Electrochem. Soc., Vol. 137, No.3, 1990, 893-899.*

82. H.R. Zelsmann and M. Pineri, Water Self-Diffusion Coefficient Determination in an Ion Exchange Membrane by Opticl Measurement, *J. Appl. Polym. Sci., 41, 1673-1684 (1990).*

83. J.H. Simpson and H.Y. Carr, Diffusion and Nuclear Spin Relaxation in Water Diffusion and Nuclear Spin Relaxation in Water, *Phys. Rev., 111, 1201-1202 (1958).*

84. R.C.T. Slade, J. Barker, and J.H. Strange, Protonic Conduction and ^{1}H Self-Diffusion in Nafion Film Studied by AC Conductivity and Pulsed Fiels Gradient NMR Techniques, *Solid State Ionics 35 (1989) 11-15.*

85. M.W. Verbrugge and R.F. Hill, Experimental and Theoretical Investigation of Perfluorosulfonic Acid Membranes Equilibrated with Aqueous Sulfuric Acid Solutions, *J. Phys. Chem. 1988, 92, 6778-6783.*

86. M.W. Verbrugge and R.F. Hill, Ion and Solvent Transport in Ion-Exchange Membranes-1. A Macrohomogeneous Mathematical Model, *J. Electrochem. Soc., Vol. 137, No.3, 1990, 886-893.*

87. H. L. Yeager and B. Kipling, Ionic Diffusion and Ion Clustering in a Perfluorosulfonate Ion-Exchange membrane, *J. Phys. Chem., Vol.83, No.14, 1979, 1836-1839.*

88. H. L. Yeager, B. O'Dell, and Z. Twardowski, Transport Properties of Nafion Membranes in Concentrated Solution Environments, *J. Electrochem. Soc.: Electrochemical Science and Technology, 1982, Vol.19, No.1, 85-89.*

89. W. Smyrl and J. Newman, *J. Phys. Chem., 72, 298 (1968).*

90. Allen J. Bard and Larry R. Faulkner, Electrochemical Methods: Fundamentals and Applications, *Section 2.3, John Wiley & Sons, Inc. 1980.*

91. F. Bloch, W.W. Hansen, and M.E. Packard, Nuclear Induction, *Phys. Rev. 69, 127 (1946).*

92. E.M. Purcell, H.C. Torrey, and R.V. Pound, Resonance Absorption by Nuclear Magnetic Monments in a Solid, *Phys. Rev. 69, 37-38 (1946).*

93. I.J. Lowe and R.E. Norberg, Free-Inductino Decays in Solids, *Phys. Rev. 107 46-61 (1957)*

94. R.R. Ernst and W.A. Anderson, Application of Fourier Trandsform Spectroscopy to Magnetic Resonance, *The Review of Scientific Instruments, Vol.37, No.1 (1966) 93-102.*

95. R.R. Ernst, Sensitivity Enhancement in Magnetic Resonance. I. Analysis of the Method of Time Average, *The Review of Scientific Instruments, Vol.36, No.12 (1965) 93-102.*

96. D. Brinkmann, Solid-State Studies at High Pressure, *in High Pressure NMR, Chapter 1, Ed. by J. Jonas, Springer-Verlag Berlin Heidelberg 1991.*

97. E.L. Hahn, Spin Echoes, *Phys Rev. 80, 580-594 (1950).*

98. H.Y. Carr, Effects of Diffusion on Free Precession in Nuclear Magnetic Resonance Experiments, *Phys. Rev. 94, 630-638 (1954).*

99. D.W. McCall, D.C. Douglass and E.W. Anderson, *Ber. Bunsenges, Phys. Chem. 67, 366 (1963).*

100. E.O. Stejskal and J.E. Tanner, Spin Diffusion Measurements: Spin Echoes in the Presence of a Time-Dependent Field Gradient, *J. Phys. Chem. Vol.42, 288-292 (1965).*

101. J.E. Tanner, Use of the Stimulated Echo in NMR Diffusion Studies, *J. Chem. Phys. Vol.52, 2523-2526 (1970).*

102. D.E. Woessner, Effects of Diffusion in Nuclear Magnetic Resonance Spin-Echo Experiments, *J. Chem. Phys. Vol.34, 2057-2061 (1961).*

103. T.A. Zawodzinski, Jr., S. Gottesfeld, S. Shoichet, and T.J. Mccarthy, The Contact-Angle between Water and The Surface of Perfluorosulfonic Acid Membranes, *J. Appl. Electrochem., Vol.23, No.1, 86-88 1993.*

104. R. Chen, Ph.D. Thesis, Nuclear Magnetic Resonance Studies of Water in Perfluorinated Ion Exchange Membranes, *The City University of New York, 1994.*

105. M. Escoubes, and M. Pineri, Water Absorption Studies of Carboxilic And Sulfonic Ionomers:Correlations with their microstructure, *in Structure and Properties of Ionomers, Ed. By M. Pineri, and A. Eisenberg, D. Reidel Pulbishing Company, Dordrecht, Holland (1987), 341-359.*

106. F. Helferrich, Ion Exchange, *Chapter 5, McGraw-Hill, New York (1962).*

107. P. Schroeder, *Z. Phys. Chem. 45 (1903) 75.*

108. P.W. Atkins, Physical Chemistry, *5th Edition, W.H. Freeman and Company, New York 1994.*

109. X. Ren, W. Henderson, and S. Gottesfeld, Electro-Osmotic Drag of Water in Ionomeric Membranes: New Measurements Employing a Direct Methanol Fuel Cell, *J. Electrochem. Soc., Vol.144, No.9, L267-L270 1997.*

110. T.E. Spirnger, T.A. Zawodzinski, Jr., and S. Gottesfeld, Polymer Electrolyte Fuel-Cell Model, *J. Electrochem. Soc., Vol.138, No.8, 2334-2342 1991.*

111. Jacob N. Israelachvili, Intermolecular and Surface Forces, *Second Edition, Academic Press, Harcourt Brace & Company, Publishers, 1991, Section 4.5.*

112. Jacob N. Israelachvili, Intermolecular and Surface Forces, *Second Edition, Academic Press, Harcourt Brace & Company, Publishers, 1991, Chapter 3 and 12.*

113. T.A. Zawodzinski, Jr., M.S. Wilson, J.A. Bett, and S. Gottesfed, Membrane Electrolyte Issues in Direct Methanol Fuel Cell, *in Electrode Materials and Processes for Energy Conversion and Storage, Ed. by S. Srinivasan, D.D. Macdonald, and A.C. Khandkar, ECS Proceedings Vol.94-23, 315-325.*

114. X. Ren, T.A. Zawodzinski, Jr., R. Uribe, H. Dai, and S. Gottesfeld, Methanol Cross-over in Direct Methanol Fuel Cells, *in Proton Conducting Membrane Fuel Cells I, ECS Proceedings Vol.95-23, 284-293.*

115. X. Ren, T.E. Springer, T.A. Zawodzinski, Jr., and S. Gottesfeld, Methanol Transport through Nafion Membranes Electroosmotic Drag Effects on Potential Step Measurements, *submitted to the J. Electrochem. Soc. 1996.*

116. S.R. Narayanan, E. Vamos, S. Surampudi, H. Frank and G. Halpert, Implications of Fuel Crossover in Direct Methanol Fuel Cells, *Extended Abstracts of the Electrochemical Society, Fall 1993 Meeting, Vol.93-1, Abstract No.73, 126, 1993.*

117. D.L. Maricle, B.L. Murach, L.L. Van Dine, Direct Methanol Fuel Cell Stack Development, *Extended Abstracts of the Electrochemical Society, Spring 1994 Meeting, Vol.94-1, Abstract No.35, 58, 1994.*

118. D. Nandan, H. Mohan, and R.M. Iyer, Methanol and Water Uptake, Densities, Equivalental Volumes and Thicknesses of Several Uni- and Divalent Ionic Perfluorosulfonate Exchange Membranes (Nafion 117) and Their Methanol-Water Fractionation Behavior at 298K, *J. Membrane Sci. 71 (1992) 69-80.*

119. P.S. Kauranen, and E. Skou, Methanol Permeability in Perfluorosulfonate Proton Exchange Membranes at Elevated Temperaures, *J. Appl. Electrochem. 26 (1996) 909-917.*

120. M.W. Verbrugge, Methanol Diffusion in Perfluorinated Ion-Exchange Membranes, *J. Electrochem. Soc., Vol.136, No.2, 417-423 (1989).*

121. R. Savinell, E. Yeager, D. Tryk, U. Landau, J. Wainright, D. Weng, K. Lux, M. Litt, and C. Roger, A Polymer Electrlyte for Operation at Temperatures up to 200°C, *J. Electrochem. Soc. Vol.141, 1994, L46-L48.*

122. S. Kato, K. Nagahama, H. Noritomi and H. Asai, Permeation Rates of Aqueous Alcohol Solutions in Pervaporation Through Nafion Membranes, *J. Membrane Sci. 72 (1992) 31-41.*